PHOTOELECTROCHEMICAL PROCESSES AT THE INTERFACE BETWEEN TWO IMMISCIBLE ELECTROLYTE SOLUTIONS.

ALAN R. BROWN

PhD THESIS

UNIVERSITY OF EDINBURGH

1992

For my parents.

Solitary and withdrawn with nothing to occupy me save my hopeless but, as far as I am concerned, indispensible little investigations, that is how I live; yet in my distant isolation I have not lost sight of my people, news often penetrates to me, and now and then I even let news of myself reach them.

Franz Kafka "Investigations of a Dog."

ii

Declaration.

Except where specific reference is made to other sources, the work presented in this thesis is the original work of the author. It has not been submitted, in part or in whole, for any other degree. Certain of the results have been published elsewhere.

Acknowledg̷ements.

Abstract

This thesis is devoted to the photoelectrochemical characterisation of the interface between two immiscible electrolyte solutions, and a number of novel phenomena are reported.

Photoinitiated ion transfer is reported to occur in systems containing tetraarylborates or tetraarylarsonium salts in the organic layer. This effect is ascribed to the photochemical production of derivatives of these ions, these photoproducts being more hydrophilic than the parent ions. A mathematical analysis is presented, from which the lifetimes and quantum yield of charge carriers may be determined by curve fitting with real photocurrent-time transients. The tetrakis(pentafluorophenyl)borate ($TPFB^-$) anion is shown not to show such activity at the liquid/liquid interface.

A new technique is presented by which the ion transfer reactions of electrogenerated ionic species may be examined. This is made possible by the use of a supporting electrolyte which was both highly hydrophobic and also resistant to oxidation and reduction. The ferricenium and di-n-butylferricenium cations and the radical anion of tetracyanoquinodimethane were generated in this manner, and their transfer studied by cyclic voltammetry. The transfer potential of the $[Ru(bpy)_3]^{3+}$ ion across the water/1,2-dichloroethane interface was determined through the approach of synthesis and isolation. The data for the ferricenium cation are brought to bear on the heterogeneous oxidation of ferrocene by hexacyanoferrate(III).

The phenomena of photosensitised ion transfer at the liquid/liquid interface is presented. This takes place as a result of the homogeneous reaction of the luminescent state of the $[Ru(bpy)_3]^{2+}$ ion with tetraaryl borate anions. The reductive quenching process, followed by back electron transfer gives rise to an ionic species more hydrophilic

than the parent borate, and thus to an ion transfer current. Again, the TPFB⁻ anion is shown not to generate such signals, which resistance is ascribed to the extreme oxidation potential for this ion.

Photocurrents are described which may be assigned to the heterogeneous photoanation of the $[Ru(bpy)_3]^{2+}$ ion by halide ions in the aqueous phase. This signal may be avoided by the use of the non-coordinating sulphate ion in place of the halide. Further results are presented showing that an ion transfer signal may be generated using cerium(IV)sulphate in the aqueous phase. This is ascribed to the oxidation of the luminescent state of the $[Ru(bpy)_3]^{2+}$ ion, either by a hetero- or homogeneous route.

Photoinitiated electron transfer across the water/ 1,2-dichloroethane interface is demonstrated, using tetracyanoquinodimethane in the organic phase to quench, through a heterogeneous oxidative reaction, the excited state of the $[Ru(bpy)_3]^{2+}$ ion. The transfer potentials of all the reactants and products being known, ion transfer following electron transfer may be neglected for this system.

List of Abbreviations.

Roman Alphabet.

A	Electrode area.
BTPPA	Bis(triphenylphosphoranylidene)ammonium.
c	Concentration.
D	Diffusion coefficient.
1,2-DCE	1,2-dichloroethane.
E	Electrical potential.
E^0	Standard electrode potential.
$E^{0\prime}$	Formal electrode potential.
$E_{1/2}$	Half wave potential.
F	Faraday's constant.
G	Gibb's energy.
I	Current density.
k	Rate constant.
NHE	Nernst hydrogen electrode.
R	Universal gas constant
T	Absolute temperature.
TBA	Tetrabutylammonium.
TMA	Tetramethylammonium.
TPAs	Tetraphenylarsonium.
TPB	Tetraphenylborate.
TPFB	Tetrakis(pentafluorophenyl)borate.
UV-Vis.	Ultraviolet-visible.
z	Charge number.

Greek Alphabet.

φ	Galvani potential.
ψ	Quantum yield.
μ	Chemical potential.
ν	Linear potential sweep rate.

Certain other infrequently used abbreviations are defined where they first occur in the text.

Table of Contents.

Chapter One.   Introduction.

Chapter Two.   Photoinitiated Ion Transfer at the ITIES.

Chapter Six. Photoinitiated Electron Transfer Across the Interface Between Two Immiscible Electrolyte Solutions.

List of Figures.

Chapter One.

Chapter Two.

Chapter Three.

Chapter Four.

Chapter Six.

List of Tables.

CHAPTER ONE

Introduction

The 1970's were a time of political unrest in those regions of the world on which the West relied for supplies of oil , and this social turmoil prompted research into systems capable of converting sunlight into electrical energy. The fundamental problem in all such systems is that of restricting the recombination of charges separated by the action of light , and many arrangements have been proposed for this purpose , including thin films [1] , zeolites [2] and micellar assemblies [3]. Some workers in the field of charge transfer at the liquid / liquid interface , a discipline raised from obscurity at the end of the the 1960's , recognised an opportunity to expand the field and proposed the interface between two immiscible electrolyte solutions (the ITIES) as a means towards this end [4]. From here stems the motivation for such work as has been reported on photoelectrochemistry at the ITIES , although perhaps of late some work has been carried out for its own sake.

Section 1.1   Historical Background to the ITIES.

The first report of electrochemical investigation of charge transfer at the ITIES is that of Nernst and Riesenfeld [5]. They passed current through a water / phenol / water system , containing coloured inorganic electrolytes , with the aim of obtaining information about transport numbers in organic solvents. The field developed from here when a parallel was drawn by Cremer [6] between the ITIES and biological bilayer membranes. Interest consequently spread to the origins of the potential

differences in such cells [7,8]. As the 1940's approached , attention focused on the distribution of potential across the interface and indeed to the structure of the interface itself [10,11] , and these have remained fruitful research topics to this day.

As hinted at previously a renaissance of the field in the late 1960's took place with the announcement by Gavach and co-workers [12] that the ITIES could , by suitable choice of electrolytes , be made polarisable. This discovery allowed the full blossoming of the field as direct comparisons could now be drawn between classical redox electrochemistry and electrochemistry at the ITIES. Such comparison led naturally to the adoption of the techniques developed for redox electrochemical systems , allowing full congress between the two domains.

Section 1.2   Comparison of the ITIES with the Solid Electrode / Electrolyte Solution Interface.

Casual inspection of the results of an experiment on the ITIES would cause few surprises to the classical electrochemist , however there are some important differences that must be borne in mind.

Section 1.2.1   Charge Transfer

There are three basic modes of charge transfer across the ITIES , described briefly below.

Section 1.2.1.1   Ion Transfer

Most of the early work on the ITIES centred on ion transfer , a phenomenon without real parallel in classical redox electrochemistry. Under this regime ions are transfered from one phase to the other under the influence of the applied potential difference , whole and unchanged

save for their solvation shells. Perhaps the closest analogous process in redox electrochemistry lies in reduction of metal ions at a mercury drop. A liquid / liquid interface is of course present , but the metal ion must be reduced at the mercury surface before it diffuses into the bulk of the drop.

Section 1.2.1.2   Electron Transfer

Classically electrons are transfered to or removed from a species in solution using a metallic or semiconducting electrode. Electron transfer at the ITIES is analogous with the exception that two redox couples are involved , one in each phase , electrons being transfered from one couple across the interface to the other.

Figure 1.2.1.1   Electron Transfer at the ITIES

$$Ox(1) \qquad Red(1)$$
$$Phase\ 1$$
$$Ox(2) \qquad Red(2) \qquad Phase\ 2$$
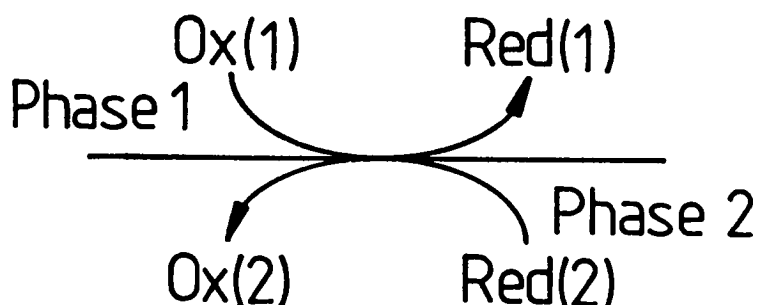
Section 1.2.1.3   Facilitated Ion Transfer

This phenomenon is similar to ion transfer in that an ion is transfered across the interface without undergoing any change in its oxidation state. This process is facilitated by coordination of the transfering ion by a ligand in the phase to which it is to be transported. To date this process has been limited to the transfer of cations , the ligand generally being an organic polyether or polythioether. The exact mechanism of the process is the subject of much contention.

Section 1.2.2   Potential Scales

One of the real divides between classical and liquid / liquid electrochemistry is the choice of a scale on which to measure potentials. For a redox reaction at a metallic electrode;

$$O + e^- \rightleftharpoons R$$
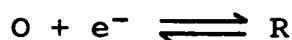
at equilibrium

$$\mu_O + \mu_{e^-} = \mu_R$$

The electrochemical potential of an electron in the electrode is not a measurable quantity , but the difference between this and the electrochemical potential of an electron in the vacuum is. This is then taken as the basis of the vacuum scale of potential , in which the potential of an electrode is expressed relative to the potential of an electron in an infinitely distant vacuum. Since an electron is at lower energy in almost all materials than the vacuum , the electrochemical potential of the electron in most metals is a negative quantity. For practical reasons however , in the time of Nernst , electron electrochemical potentials were not measureable , and an alternative approach was required. One particular redox reaction was chosen , somewhat arbitrarily , to have by definition a free energy change of zero.

$$1/2 \ H_2 \rightleftharpoons H^+ + e^- \qquad \Delta G = 0$$
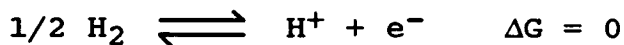
By relating the potential of any other reaction to the potential for this reaction , there was then no need to consider the electrochemical potential of the electron.

The hydrogen electrode was taken as a standard against which others were compared. Because of the danger involved in using gaseous dihydrogen , this electrode is rarely used , and is replaced by others such as the saturated calomel electrode. The potentials of these electrodes against the NHE are well known.

The introduction of non aqueous solvents has led to the problems in defining electrode potentials. The commonest approach has been to rely on an extrathermodynamic assumption. It is common practice to refer potentials to the electrode potential for some "well behaved" couple for instance ferrocene / ferricenium on the assumption that the nature of the solvent does not affect the electrode potential for that couple.

In the field of liquid /liquid electrochemistry the measured quantity is the absolute potential difference between two phases. The zero for potential difference between two phases in contact is known as the potential of zero charge or pzc. This is a directly measureable quantity , using the streaming electrolyte electrode [13]. The use of pzc values however is not without contention and there is another approach , using the TATB assumption due to Grundwald [14]. This extrathermodynamic assumption is used in the following way.

It is possible , experimentally , to measure the free energy of partition of a salt MX between two phases α and β , denoted by

$$\Delta G^{O\alpha\to\beta}_{tr,MX} = \Delta G^{O\alpha\to\beta}_{tr,M} + \Delta G^{O\alpha\to\beta}_{tr,X}$$

In order to obtain information about individual ions the TATB assumption is brought to bear , involving the assumption that the free energies of transfer of the $TPAs^{+}$ and TPB^{-} ions are equal. This assumption rests in turn on the supposed similarity , apart from overall charge , of the two ions , and may be represented by

5

$$\Delta G^{\circ \alpha \to \beta}_{tr,TPAs^+} = \Delta G^{\circ \alpha \to \beta}_{tr,TPB^-} = 0.5 \Delta G^{\circ \alpha \to \beta}_{tr,TPAsTPB}$$

Knowing then the free energy of partition of TPAsTPB between the two phases , the free energy of partition of another ion i may be measured. This procedure fails on closer inspection due to the differences between the TPAs and TPB ions [15]. Although they share a number of different characteristics such as S_4 symmetry , they are quite different in others such as size , and the fact that they are of opposite charge is not trivial. Nevertheless the TATB assumption provides a useful first approximation.

Section 1.2.3   Mass Transport

The three main types of mass transport are common to both fields as they are primarily properties of the solutions involved.

Section 1.2.3.1   Diffusion.

Diffusion is the movement of a species down its concentration gradient and takes place whenever such a gradient is formed. It is the mass transport regime of prime importance in electrochemical experiments , since electrolysis at an electrode or at the ITIES depletes or enhances the concentrations of electroactive species in solution. Diffusion is then set into motion , always contributing to and in some cases limiting the current which may be passed. Diffusion is described mathematically by Fick's first and second laws of linear diffusion. The first law is:

$$-J_{(x,t)} = D_i[\delta c_{i(x,t)}/\delta x]$$

6

where $-J_{(x,t)}$ is the flux , that is the number of moles of electroactive species i to pass a given location per second per cm^2 of area normal to the axis of diffusion , $c_{i(x,t)}$ is the concentration of i at a displacement x and a time t. From this it follows that:

$$\delta c_{i(x,t)}/\delta t = D_i[\delta^2 c_{i(x,t)}/\delta x^2]$$

and this is Fick's second law of diffusion.

Section 1.2.3.2   Migration.

This is the motion of charged particles under the influence of a potential gradient or electric field. By this method is the largest part of of the current passed in the bulk solution of an electrochemical cell. In order that migration of the electroactive species should play as small a part as possible in the overall regime of charge transport , an inert electrolyte , usually in large excess, is commonly added to any solution employed.

Section 1.2.3.3   Convection.

The displacement of species in solution by mechanical forces is known as convection. These forces may arise through a number of sources , including temperature gradients , deliberate and accidental mechanical agitation.

Section 1.2.4   Solvents and Supporting Electrolytes

The characteristics of solvents and supporting electrolytes in classical redox electrochemical situations have been well reviewed elsewhere [17].

Section 1.2.4.1   Solvents for the ITIES

Koryta *et al* [18] have suggested the following three points which must be taken into account in the selection of organic solvents for work on the ITIES.

(i)   The solvent should be genuinely immiscible with water , that is the solubility of the solvent in water , and *vice versa* , should be low.

(ii)   The solvent should be sufficiently polar to ensure adequate conductivity of solutions through dissociation of dissolved electrolyte.

(iii)   The density of the solvent must be sufficiently different from that of water to ensure that it either floats or sinks , thus producing a mechanically stable interface.

The solvents previously tested for suitability to form an ITIES in conjunction with water have been listed elsewhere [15].

Section 1.2.4.2   Electrolytes for the ITIES

The electrolytes for work on the ITIES fall into two categories. Firstly salts composed of two hydrophobic ions , used as electrolytes for the organic phase. In the second instance salts composed of two hydrophilic ions are used in the aqueous phase. Depending on their individual free energies of transfer or partition , the transfer of at least two of these ions will determine the limit of the window of polarisation of the ITIES.

Section 1.3   Electrochemical Techniques for the ITIES.

Heyrovsky's dropping mercury electrode [33] (DME) inspired Koryta's three electrode dropping electrolyte apparatus [19] (see figure 1.3.1) in which the drop of

Figure 1.3.1. Dropping Electrolyte Electrode Used by Kihara.

1. Dropping electrode 2. Ag/AgBr reference electrode. 3. Nitrobenzene electrolyte solution. 4. Platinum electrode. 5. Insulated lead for reference electrode. 6. Counter electrode. 7. Aqueous electrolyte solution.
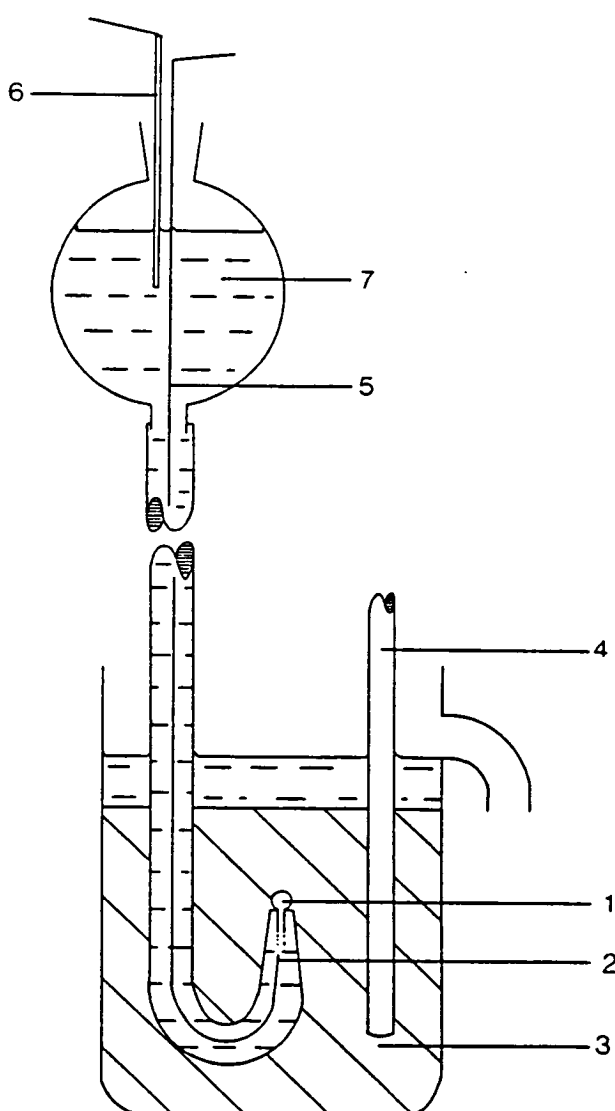
organic phase is intended to mimic the mercury drop of the DME. This apparatus was used to investigate the transfer of TMA^+ across the water / nitrobenzene interface , but results were poor due to the low conductivity of the nitrobenzene solution used compared to that of liquid mercury. This led to a large ohmic drop which distorted the resulting polarograms.

Classical electrochemical techniques became transposable only with the introduction in the early 1980's of the four electrode potentiostat and associated ohmic drop compensation circuits by Samec *et al* [20].

Section 1.3.1   Cyclic Voltammetry.

This potential sweep reversal technique was one of the first to be applied at the ITIES using the new generation of four electrode potentiostats [21]. It has been shown that for reversible ion transfer the properties of the cyclic voltammograms produced are similar to those for reversible electron transfer at a metal electrode [22]. The full implications of this statement may be summarised by noting that the Randles-Sevcik relationship

$$i_p = 0.4463nFAc^*(nF/RT)^{1/2}D^{1/2}v^{1/2}A$$

holds in both cases. Cyclic voltammetry has also been extended to electron transfer [26] and facilitated ion transfer [27] at the ITIES.

Section 1.3.2   Potential Step Chronoamperometry.

Successful application of this technique to the ITIES has been demonstrated [23] and again transposition of the theory developed for classical systems is appropriate . For reversible ion or electron transfer the current – time relationship is that predicted by the Cotterel Equation.

Section 1.3.3   Other Techniques.

Most techniques developed for classical electrochemistry have been adapted to the ITIES field. They include polarography [22], differential pulse stripping voltammetry [24], a.c. voltammetry [25], chronopotentiometry [26] and microelectrode techniques [23].

Section 1.4   Tris(2,2'-bibyridine-N,N')-ruthenium (II).

The literature concerning this ion , conveniently denoted as $[Ru(bpy)_3]^{2+}$, is epic in proportion and a comprehensive review would be quite outside the remit of this work. Some idea of the extent of the field may be gained by considering that this species has , in the form of its various salts , found applications as diverse as an oxidometric indicator [29] ,a catalyst for the exotic Belousov-Zhabotinsky reaction [30] and a detoxification agent for chemical warfare agents [31]. Primarily however the interest in this complex stems from the discovery in 1959 [32] of intense luminescence from an excited state with a lifetime in the microsecond range in solution , at room temperature. The suggestion [33] that this luminescent state undergoes electron transfer quenching

Figure 1.4.1   Electron transfer quenching of $[Ru(bpy)_3]^{2+*}$

$$[Ru(bpy)_3]^{2+} \xrightarrow{\text{h}\nu} [Ru(bpy)_3]^{2+*}$$

$$[Ru(bpy)_3]^{2+*} + [Co(NH_3)_5Br]^{2+} + 5H^+ \longrightarrow$$

$$[Ru(bpy)_3]^{3+} + Co^{2+} + 5NH_4^+ + Br^-$$
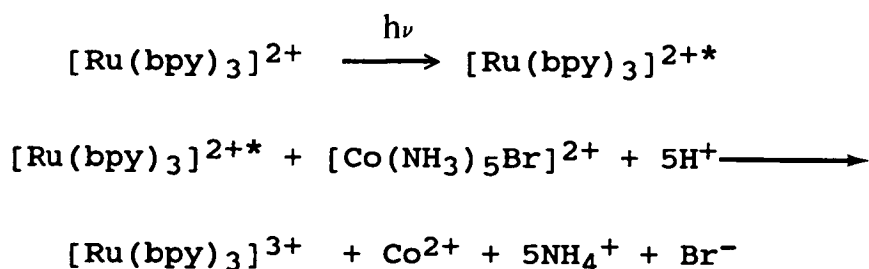
with some cobalt complexes led to myriad investigations intended to elucidate both the exact nature of the emitting state and also the variety of possible quenching systems.

Section 1.4.1   The Luminescent State of $Ru(bpy)_3^{2+}$

Controversy has raged and will no doubt continue as to the exact nature of the luminescent state of the $[Ru(bpy)_3]^{2+}$ ion , frequently denoted as $[Ru(bpy)_3]^{2+*}$. The initial report of the luminescence [32], a short communication , reports the fact of the luminescence without any thorough analysis of the nature of the emitting state , other than the use of the term "fluorescence" to describe the emission , which was assigned as charge transfer in character. The use of the term fluorescence implies that the emitting state is of the same spin multiplicity as the ground state , and so the luminescent state was assigned as the lowest singlet charge transfer (CT) state.

One of the authors of this paper , however , in his PhD thesis reputedly [34] refers to the emission as phosphorescence , thus assigning the luminescent state as having triplet or higher multiplicity , and foreshadowing some of the confusion on the subject which was to follow. Porter and Schlafer [35] subsequently assigned the emission to $d^* \to d$ phosphorescence and Crosby *et al* to $d^* \to d$ fluorescence [36] , but the current view began to form with the work of Lytle and Hercules [34]. They proposed that in order to fully rationalise their spectroscopic data it was necessary to assign the luminescence as originating from the transition:

$$[\text{core}](t_{2g})^5(\pi^*)^1 \to [\text{core}](t_{2g})^6(\pi^*)^0$$
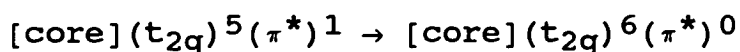
where π^* represents a molecular orbital approximating

12

to the LUMO of the bipyridyl moeity. Little issue has been taken with this assignment since and attention has focused on the degree to which the promoted electron is localized on any one ligand.

The electron ion parent model [36,37] introduced the concept of spin-orbit coupling to the debate , an effect which results in a blurring of the rigid singlet / triplet division due to the influence of the heavy ruthenium ion in the complex. The conclusion was also reached that the π^* orbital into which the electron was promoted spanned all three bipyridyl (bpy) ligands. It was , however , discovered [38] that the selection rules apparently in operation in the luminescence spectrum were inconsistent with an excited state having the same symmetry as the ground state as required by the electron ion parent model.

The death knell sounded for the fully delocalised model of the excited electron in $[Ru(bpy)_3]^{2+*}$ with the observation of bands in the electronic spectrum of the excited state [39], which in combination with spectroelectrochemical data it was possible to assign as being due to intraligand transitions within a coordinated $(bpy)^-$ ligand. It seems likely therefore that the luminescent state $[Ru(bpy)]^{2+*}$ may be formulated , at least on the vibrational timescale , as:

$$[(bpy)_2Ru^{III}(bpy)^-]^{2+*}$$
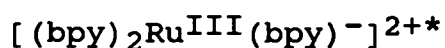
Section 1.4.2 Redox Properties of the Luminescent State.

It has been known since the early 1970's [40] that the excited states of some organic molecules show enhanced redox activity compared to the ground state of the same molecule. That this is so may be rationalised on the basis that in the process of excitation by light an electron is moved into an orbital with a different spatial

13

distribution from the one in which it originated , thus leaving behind a positive "hole" as a centre for the oxidation of another molecule , and also making the promoted electron more available for capture.

These arguments apply particularly well to $[Ru(bpy)]^{2+*}$ as formulated in the previous section , and indeed enhancement of both the oxidative and reductive potentials have been found compared to the ground state ion [41]. The effect has been quantified by Meyer *et al* [42] and is summarised in Figure 1.4.2.1.

Figure 1.4.2.1 Selected Redox Potentials for the $[Ru(bpy)_3]^{2+}$ System, in Water , after Meyer [43].

$E^{0'}$,V   Couple

1.26 ───────────────── $[Ru(bpy)_3]^{3+/2+}$

0.84 ───────┬───────── $[Ru(bpy)_3]^{2+*/+}$

   +hν +hν

-0.84 ───────┴───────── $[Ru(bpy)_3]^{3+/2+*}$

-1.26 ───────────────── $[Ru(bpy)_3]^{2+/+}$
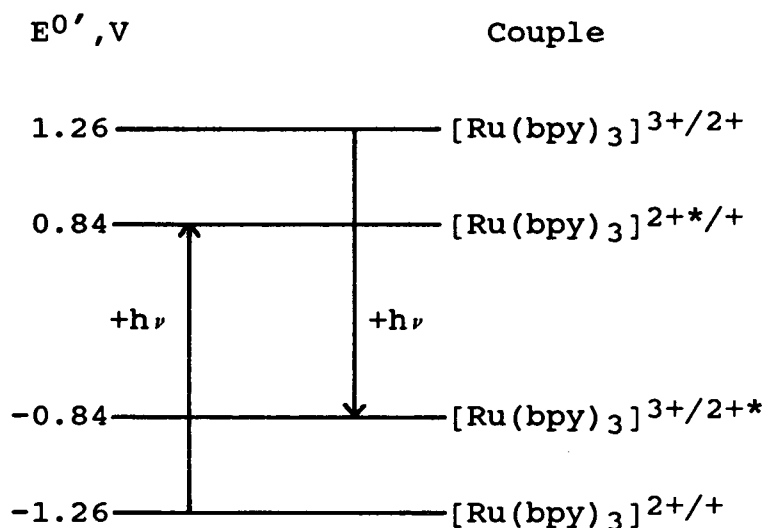
Thus it can be seen that the excited state of the complex is both a more powerful oxidizing and reducing agent than the ground state by 2.1V.

Section 1.4.3   Photochemistry of $[Ru(bpy)_3]^{2+}$

The field of synthetic organic photochemistry has for many years taken advantage of the fact that the excited states of molecules tend to be amenable to reactions and rearrangements which would appear unlikely in the ground

state. This phenomenon may be explained on the grounds of coupling between the potential energy surfaces of the excited state and those of a range of molecules of lower energy , including the ground state. An excited state molecule , seeking to minimize its free energy , has a number of avenues available , one of which is to undergo chemical change. The product of such a reaction is most likely to be a molecule for which the potential energy surface shows a maximum at those coordinates for which the the excited state surface shows a minimum , thus allowing coupling to take place. The practical result of this is that strained and exotic molecules often result from photochemical reactions. Coincidental in explaining the widespread use of $[Ru(bpy)_3]^{2+}$ as a photosensitizer , along with the redox properties outlined in Section 1.4.2. , is its apparent resistance to photochemically driven rearrangement or decomposition.

Whilst this resistance is very real [44] , it is not however absolute and both photoracemization [45] and photoanation [46] have been reported for the complex in solution.

Figure 1.4.3.1 Photoracemization of $[Ru(bpy)_3]^{2+}$

$\bigcirc\!\!\smile\!\!\bigcirc$ = 2,2' Bipyridyl
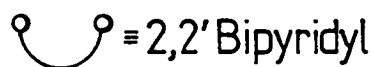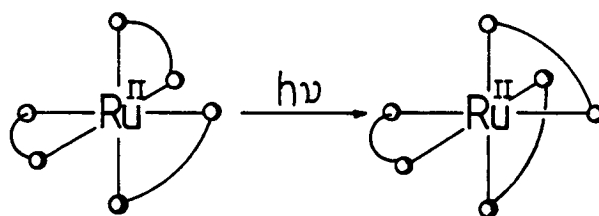
A five coordinate intermediate has been proposed in the photoanation of the complex

Figure 1.4.3.3   Photoanation of [Ru(bpy)$_3$]$^{2+}$

$$\xrightarrow[2Cl^-]{h\nu}$$
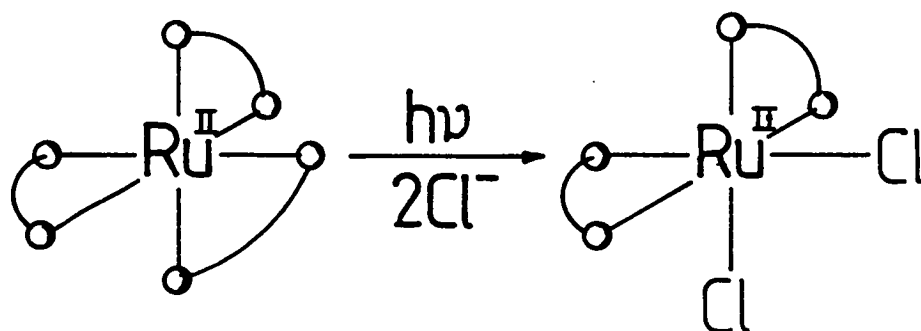
Figure 1.4.3.2 Five Coordinate Intermediate in the Photolysis of $[Ru(bpy)_3]^{2+}$
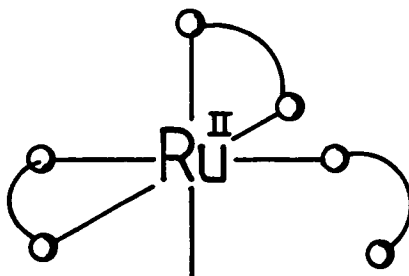
Section 1.4.4. Applications of The Luminescent State of $[Ru(bpy)_3]^{2+}$ to Photoinitiated Charge Transfer.

The basis of most photoelectrochemical systems for the conversion of sunlight into useful electrical energy is the efficient separation of the component molecules of a charge transfer complex formed through the action of light.This is illustrated in Figure 1.4.4.1. , where D is a donor , A an acceptor molecule , D^* an excited state of D.

Figure 1.4.4.1 Formation of a Photoinitiated Charge Transfer Complex.

$$D \xrightarrow{h\nu} D^* \qquad 1.$$

$$D^* + A \longrightarrow [D^+ A^-] \qquad 2.$$

$$[D^+ A^-] \longrightarrow D^+ + A^- \qquad 3.$$

$$[D^+ A^-] \longrightarrow D + A \qquad 4.$$
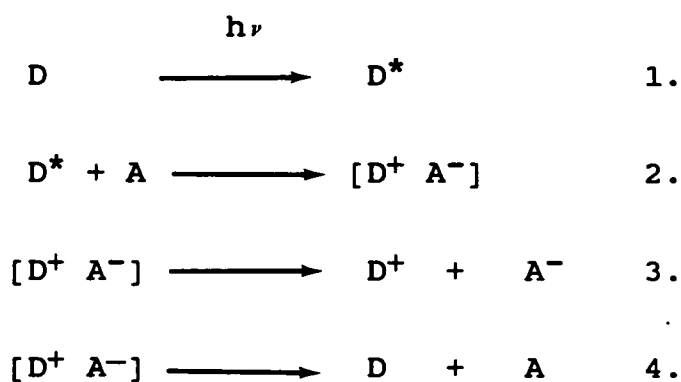
The rationale behind much of the work carried out on $[Ru(bpy)_3]^{2+}$, formally at any rate , has been to design systems in which this ion takes the place of D in figure 1.4.4.1. , and in which reaction 4. is minimized to form a practical photoelectrochemical solar energy conversion device. Although figure 1.4.4.1 shows D to have been oxidatively quenched , this is not necessarily so and for $[Ru(bpy)_3]^{2+*}$ three distinct types of quenching are possible.

(i) Reductive quenching involves the quenching of the luminescent state by an easily oxidized species so:

$$[Ru(bpy)_3]^{2+*} + Q \longrightarrow [Ru(bpy)_3]^{+} + Q^{+}$$
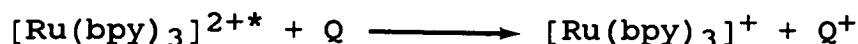
(ii) Oxidative quenching is similar but involves collision of the excited state with an easily reduced species:

$$[Ru(bpy)_3]^{2+*} + Q \longrightarrow [Ru(bpy)_3]^{3+} + Q^{-}$$

(iii) Energy transfer quenching , favoured when the absorption spectrum of the quenching species overlaps with the emmission spectrum of the luminescent state , results in the generation of an excited state of the quencher , Q^*.

$$[Ru(bpy)_3]^{2+*} + Q \longrightarrow [Ru(bpy)_3]^{2+} + Q^*$$

Section 1.4.4.1 A Sacrificial System Designed to Seperate the Products of Photoinitiated Electron Transfer Reactions of Tris-diimino Ruthenium(II) Complexes in Bulk Solution.

One of the simplest means employed to restrict back reaction is typified in the system used by Meyer [47]. Here a sacrificial electron donor is used to scavenge the oxidized form of the ruthenium complex , in competition

with the straightforward back reaction. The quencher used to perform the quenching process was methylviologen , also known as paraquat (PQ^{2+}):

Figure 1.4.4.2   Structure of Methylviologen.
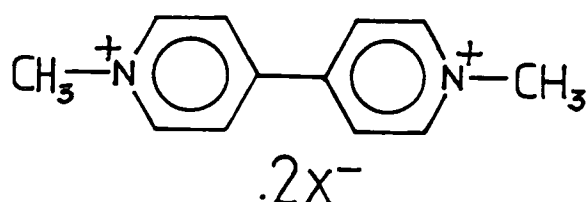
That a permanent build-up of the photoproduct , methylviologen radical cation , takes place is due to the fact that the scavenger used , a tertiary amine , decomposes irreversibly on oxidation. This leaves the radical cation no suitable source of electrons , and a net reaction is obliged to take place:

$$[Ru(bpy)_3]^{2+} \xrightarrow{h\nu} [Ru(bpy)_3]^{2+*}$$

$$[Ru(bpy)_3]^{2+*} + PQ^{2+} \longrightarrow [Ru(bpy)_3]^{3+} + PQ^{+}$$

$$[Ru(bpy)_3]^{3+} + R_3N \longrightarrow [Ru(bpy)_3]^{2+} + R_3N^{+}$$

$$R_3N^{+} \longrightarrow \text{Decomp. Prods.}$$

Overall Reaction: $R_3N + PQ^{2+} \xrightarrow{h\nu} PQ^{+} + \text{Decomp. Prods.}$
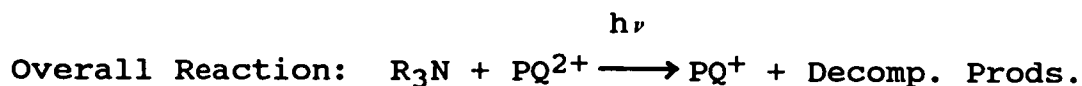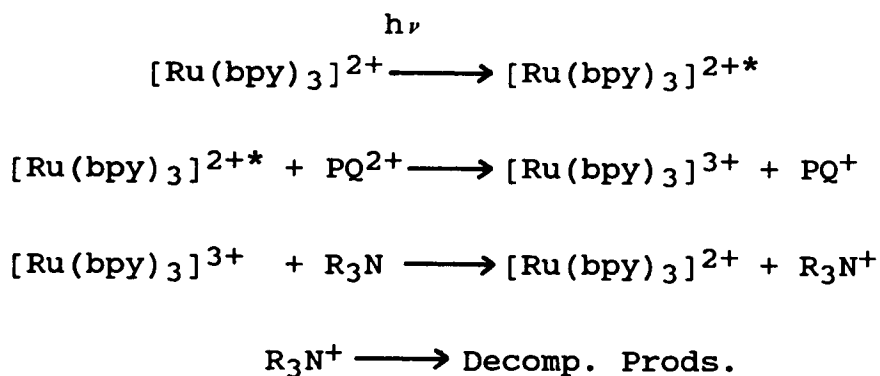
In terms of a practical energy conversion system this system is of course untenable due to the consumption of tertiary amine. A similar *caveat* applies to any system employing a sacrificial scavenger , which is to say ,

almost all of the systems reported to date , despite the various elegant techniques employed to separate the photoproducts.

Section 1.4.4.2   Solid State Charge Separation Devices.

One particularly elegant method for inhibiting back reaction is the use of quenchers and sensitisers restricted to the surface of inert porous solid substrates such as zeolites [48] and Vycor glass [49]. In the work of Shi and Gafney [Ru(bpy)$_3$]$^{2+}$ and PQ^{2+} are adsorbed onto porous glass and the photoreaction takes place not through collision but through photoionization of the ruthenium complex. The detached electron is free to roam the glass surface [50] , and may eventually reduce one of the adsorbed quencher ions.

Semiconductors   may also be used to quench the excited states of dye molecules , and a number of photosensitized semiconductor systems have been proposed. The dye involved may be a salt of [Ru(bpy)$_3$]$^{2+}$ [51,52] or some organic dye , as in the work of Tsubomura *et al*[58] In this case a sintered disc of zinc oxide was treated with the dye rose bengal , forming an adsorbed dye layer on the semiconductor. The electrolyte solution used was an aqueous solution of potassium iodide and iodine , the operation of the cell then being summarised in figure 1.4.4.3.

20

Figure 1.4.4.3.   A Sensitized Semiconductor.

Semiconductor   Dye   Solution   Count. Elec.
                Layer
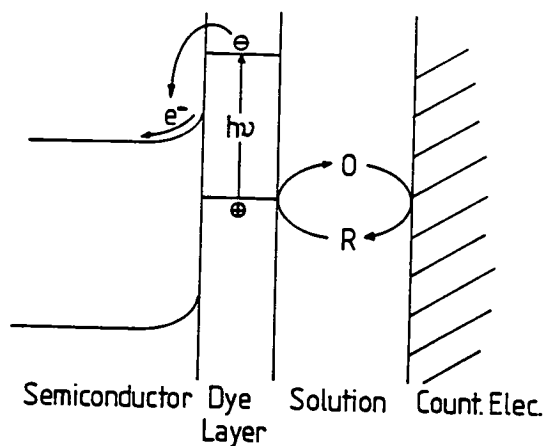
In the above figure incident radiation excites the adsorbed dye molecule , raising an electron to a level where its transfer into the conduction band of the semiconductor is spontaeous. The operation of the device then relies on "band bending" at the semiconductor electrolyte interface. The distortion of the conduction band within the space charge region at the electrode surface is used to separate the electron from the positive "hole" left in the now oxidised dye molecule , thus preventing recombination. The redox couple in the aqueous phase is then used to recycle the oxidised dye to its reduced form , available for repeat reaction. This process leads to the generation of a net current in the external circuit

Section 1.4.4.3   Microemulsions and Lipid Vesicles as Charge Separation Devices.

The common factor between these two types of assembly is the presence of a water / oil boundary which may be used to separate charge transfer photoproducts on the basis of their hydrophobicities or hydrophilicities. Microemulsions are formed by the dispersion of an oil in water , a water continuous emulsion , or water in oil , an

21

oil continuous emulsion. The emulsion is stabilised by the use of a surfactant , which may be anionic, cationic or neutral. Vesicles and microvesicles are prepared from dispersions of a variety of lipids in water , as illustrated in figure 1.4.4.3.

Figure 1.4.4.4. Schematic Structure of a Vesicle.
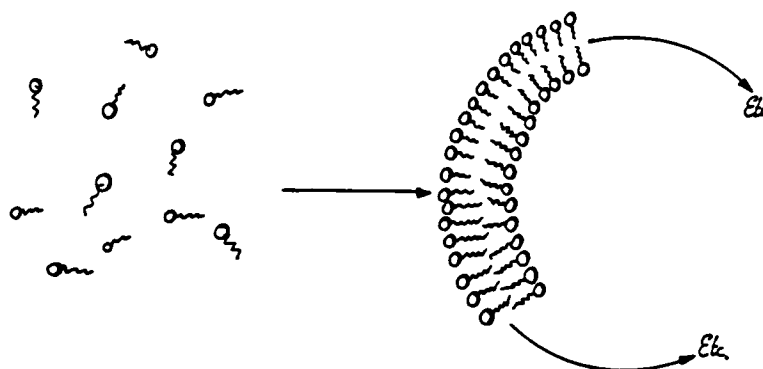
There are many published papers reporting the use of such systems for photochemical purposes [53,54,55]. Although there are technical differences between the two types of structure stemming from the fact that a vesicle has both an external and an internal water / oil boundary , the overall photoreactions reported for such systems are very similar and may be typified by figure 1.4.4.4:

Figure 1.4.4.5. Typical Photoreaction Scheme for Microemulsions and Vesicle Dispersions.
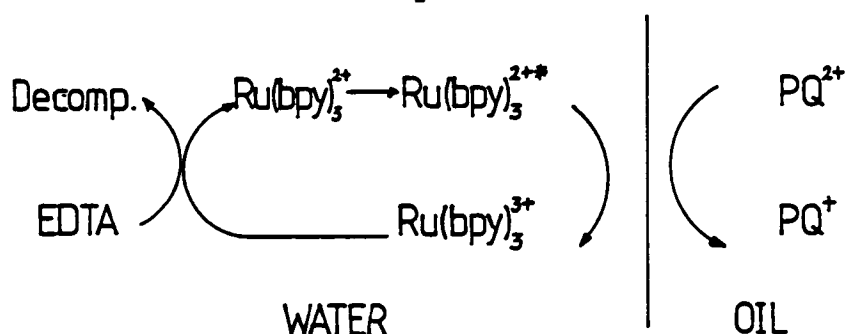
The quenchers used to generate these photoreactions are almost without exception alkyl viologens , and a variety of sacrificial electron donors have been employed

, for instance disodium ethylenediaminotetraacetate [55]. To date no such system has been reported to generate a net photoreaction without the use of a sacrificial electron donor , and so , considering the amount of work which has been performed , this approach must be called into question , other than as a model for biological systems.

Section 1.4.4.4.   The ITIES as a Charge Separation Device

The ITIES is similar to microemulsion systems in that it may be possible to separate photoproducts on the basis of their hydrophobicities , but it has the considerable potential advantage that a sacrificial electron source may not be necessary. In its stead the counter electrodes placed in each phase can act as both sources and sinks of electrons , thus driving a current round an external circuit.

Photocurrents claimed to be the result of photoinitiated charge transfer at the ITIES have been reported [56,]. The paper by Maracek et al describes a photocurrent in a system comprising $[Ru(bpy)_3]^{2+}$ in benzonitrile solution and a quencher in the aqueous phase. It is known that many small aromatic molecules , quench the luminescent state of the metal complex with high efficiency [57,42] and so this publication must be held in suspicion.

There are also reasons why the situation described in the work of Thompson et al [4] may not be as simple as claimed , and these complications will be dealt with in the main body of this thesis.

References.

1. C.L. Renschler and L.R. Faulkner, Faraday Discuss. Chem. Soc., 70 (1980) 311

2. P.K. Dutla and J.A. Incavo, J. Phys Chem., 92 (1987) 4443

3. S.A. Alkaitis, G. Beck and M. Gratzel, J. Am. Chem. Soc., 97(1975)5723

4. F.L. Thomson, L.J. Yellowlees and H.H.Girault, J. Chem. Soc., Chem. Commun., (1988)1574

5. W. Nernst and E.H.Riesenfield, Ann. Phys. 8(1902)600

6. M. Cremer, Z. Biol., 47(1906)562

7. B. Beutner, Trans. Am. Electrochem. Soc., 21(1912)219

8. E.Baur, Z. Elektrochem., 24(1918)100

10. E.J.W. Verwey and K.F. Niesson, Philos. Mag., 28(1939)435

11. M. Kahlweit and H. Strenlow, Z. Elektrochem., 58(1954)658

12. C. Gavach, T.Mlodnika and J.Guastalla, C.R.Acad.Sci.,C266(1968)1196

13. H.H. Girault and D.J. Schifrin, Electrochim. Acta, 31(1986)1341

14. E. Grundwald, G. Baughman and G. Kohnstam, J. Amer. Chem. Soc., 82(1960)5801

15. Y. Shao, PhD Thesis, University of Edinburgh, 1991

17. Charles K. Mann, Nonaqueous Solvents for Electrochemical Use, Publisher and date not available.

18. J. Koryta and P. Vanysek, in Gerischer and C.W. Tobias (Eds.) Advances in Electrochemistry and Electrochemical Engineering, Vol. 12, J. Wiley and Sons, New York, 1981, p113

19.J. Koryta, P.Vanysek and M. Brezina, J. Electroanal. Chem.67(1976)263

20. Z. Samec, V. Maracek and J. Weber, J.Electroanal. Chem. 100(1979)841

21. Z. Samec, V. Maracek, J. Koryta and M.W. Khalil, J. Electroanal. Chem, 83(1977)393

22. D. Homolka and V. Maracek, J. Electroanal. Chem. 112(1980)91

23. G. Taylor and H.H. Girault, J. Electroanal. Chem. 208(1986)179

24. V. Maracek and Z. Samec, Anal. Lett. 14(B15)(1981)1241

25. M. Senda, T. Kakutani, T. Osakai and T. Ohkouchi, Proc. 1st. Bioelectroanal. Symp., Matrafured, 1986

27. A. Hofmanoua, L.Q. Hung and M.W. Khalil, J. Electroanal. Chem, 135(1982)257

29. A.J. Nutten, Mettallurgia 42(1950)271

30. R. Gyenge, E. Koros, K. Toth and E. Pengor, Anal. Chim. Acta., 98(2)(1978)385

31. R.A. Kenley, Proc. Int. Symp. Prot. Against Chem. Warf. Agents, (1983)161

32. J.P. Paris and W.W. Brandt, J Amer. Chem. Soc., 81(1959)5001

33. H.D. Gafney and A.W. Adamson J. Amer. Chem. Soc., 94(1972)8238

34. F.E. Lytle and D.M. Hercules J. Amer. Chem. Soc., 91:2(1969)253

35. G.B. Porter and H.L. Schlafer, Ber. Bunsenges. Physik. Chem., 68(1964)316

36. R.W. Harrigan , G.D. Hager and G.A. Crosby, Chem. Phys. Lett., 21(1973)487

37. R.W. Harrigan and G.A. Crosby, J. Chem. Phys., 59(1973)3468.

38. A.Ceulemans and L.G.Vanquickenborne, J. Amer. Chem. Soc., 103(1981)2238.

39. L.J. Yellowlees, Ph.D. Thesis, University of Edinburgh (1983).

40. D. Rehm and A. Weller, Ber. Bunsenges. Physik. Chem., 73(1969)834.

41. C. Creutz and N. Sutin, J. Amer. Chem. Soc., 98(1976)6384

42. C.R. Bock, J.A. Connor, A.R. Guttierez, T.J. Meyer , D.J. Whitten, B.P. Sullivan and J.K. Nagel, J. Amer. Chem. Soc., 101(1979)4815

43. T.J. Meyer, Prog. Inorg. Chem. 30(1983)389

44. K.W.S. Chan and K.D. Cook, J. Amer. Chem. Soc., 104(1982)5031

45. G.B. Porter and R.H.Sparks, J.Photochem., 13(1980)123

46. R.J.Crutchley and A.P.B. Le·ver, J. Amer. Chem. Soc., 102(1980)7128

47. T.J. Meyer, Acc. Chem. Res., 11(3)(1978)94

49. W. Shei and H.G. Gafney, J. Amer. Chem. Soc., 109(1987)1582

50. T. Kennelly, H.D. Gafney and M.J. Braun, J. Amer. Chem. Soc., 107(1985)4431

51. W.D.K. Clark and N. Sutin, J. Amer. Chem. Soc., 99:14(1977)4676

52. A. Hamnett, M.P. Dare-Edwards , R.D. Wright , K.R. Seddon and J.B. Goodenough, J. Chem. Phys. 83:25(1979)3260

53. C.A. Jones, L.E. Weaner and R.A. Mackay, J. Phys. Chem. 84(1980)1495

54. S.S. Atik and J.K. Thomas, J. Amer. Chem. Soc., 103:25(1981)7404

55. I.Willner, W. Ford, J.W. Otvos and M. Calvin, Nature 280(1979)823

56. V. Maracek, A.H. De Armond and M.K. De Armond, J. Amer. Chem. Soc. 111:7(1989)2561

57. R.Ballardini, G. Varani, M.T. Indelli, F. Scandola and V. Balzini, J. Amer. Chem. Soc., 100(1978)7219

58. H. Tsubomura, M. Matsumura, Y. Nomura and T. Amamiya, Nature, 261(1976)402.

CHAPTER TWO

Photoinitiated Ion Transfer at the ITIES.

Section 2.1   Introduction.

Despite the wealth of data collected on the study of charge transfer at the liquid / liquid interface , these processes are , in comparison to charge transfer at solid electrodes , only poorly understood. The basic processes are known though ,and there is general agreement on suitable systems and experimental techniques. There is unfortunately no such happy concord in the field of photoelectrochemistry at the ITIES , and indeed no substantial body of relevant literature. A brief overview of the research reported will perhaps serve to demonstrate the turbidity of thought on the subject.

In 1979 Calvin *et al* [55] reported the net generation of the radical monocation of 1,1'-hexadecyl-4,4' -bipyridinium in an oil continuous water / toluene microemulsion , using $[Ru(bpy)_3]^{2+}$ as a sensitizer for photoinitiated charge transfer. This system was the inspiration for the work of Girault *et al* [4]. Using a two electrode configuration these workers reported a photocurrent at a non-polarisable toluene / water interface , the toluene being mounted as a thin film on a platinum gauze electrode. The sensitizer again was $[Ru(bpy)_3]^{2+}$, in the form of its chloride salt , in the aqueous phase , and the quencher heptyl viologen , as the tetraphenyl borate salt , in the organic film.

Maracek *et al* [56] were the first to claim a photocurrent as photoinitiated charge transfer using a conventional four electrode arrangement (see section 2.2).

Their use of air saturated solutions and a virtually non-polarisable interface taken alone cast their claim in some doubt. The same authors [59] also report photoinduced potential shifts at the ITIES.

Kuzmin [60] has reported the use of a porphyrin species as a photosensitizer to generate ion transfer currents at the water / 1,2-DCE interface , together with a mathematical analysis of the process. It was Samec , however , who first observed photoinitiated ion transfer at the ITIES and this process is discussed in section 2.2.

Section 2.2   Photoinitiated ion transfer at the ITIES.

It is of prime importance in any attempt to measure photoelectrochemical events at the ITIES that only one component of the entire system should be photochemically active under the conditions employed. Solvents , supporting electrolytes and any quenchers used should not , of themselves , show any photochemical activity.

The most commonly used organic phase supporting electrolyte in early studies of the ITIES was tetra n-butylammonium tetraphenyl borate (TBATPB) , and tetraphenyl arsonium tetraphenyl borate (TPAsTPB) has also been used. The use of the TPAs$^+$ ion has been reported in photoelectrochemical systems [56] in the form of its 7,8,9,10,11,12-hexabromo-hexahydro-1-carba-closo-undecaborate(1-) salt (TPAsCBB). It was whilst testing these tetraaryl ions for photoelectrochemical activity , under visible and UV irradiation , at the ITIES that Samec was able to demonstrate a photocurrent in the system shown in figure 2.2.1

Figure 2.2.1 The Cell Used by Samec to Demonstrate Photoinitiated Ion Transfer.

Ag/AgCl/ TBACl (1mmoldm^{-3})(aq)/ TBATPB (DCE)
// LiCl (10mmoldm^{-3})(aq) /AgCl/Ag'
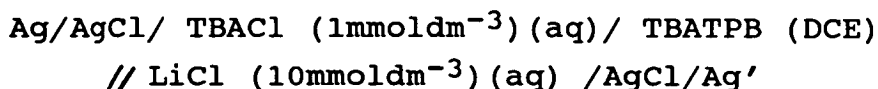
Cell 2.1

It is the refinement and extension of the original work carried out in Edinburgh by Samec that forms the basis of this chapter. Results attributable to the Czeck investigator are duly reported.

Section 2.3 Experimental Procedure.

Figure 2.3.1. shows the form of a typical cell used for the investigation of a large planar ITIES. The body of the cell contains the aqueous layer , floating on top of the organic layer. All experiments reported in this thesis employ 1,2-dichloroethane (1,2-DCE) as the organic solvent.

There were three main differences between the experimental apparatus of Samec and that used subsequently. Firstly a liquid filled light pipe was used to direct the output of the xenon arc lamp down towards the cell. This was done because ultraviolet radiation was required and the reflection characteristics of the glass mirror previously employed were in some doubt. An interference filter was used to select the appropriate band from the output of the lamp , and a purpose built battery operated low noise combined potentiostat/zerostat was used in place of the potentiostat with external zerostat. In addition all solutions used were saturated with argon prior to assembly of the interface.

The interface between water and 1,2-DCE was assembled in an all glass four electrode cell , of active area 2.5

Figure 2.3.1.   A Typical Four Electrode Cell.
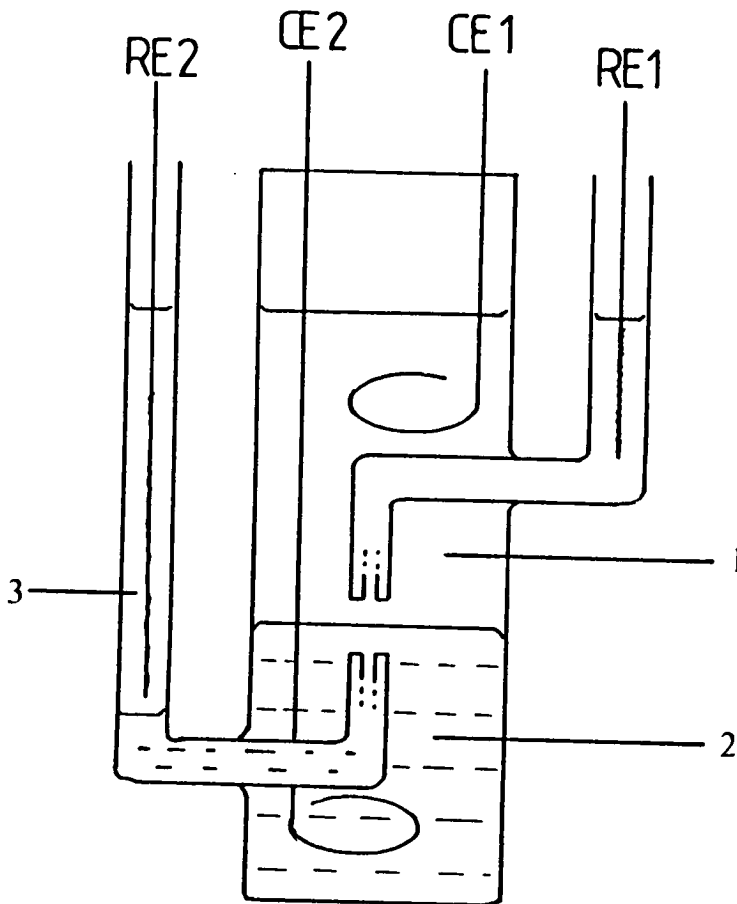
CE1 and CE2 platinum wire electrodes. RE1 and RE2 silver/silver halide or sulphate electrodes. 1. Aqueous electrolyte solution. 2. Organic electrolyte solution. 3. Aqueous solution for organic reference electrode.

Figure 2.3.2. Block Diagram of the Apparatus Used.

31
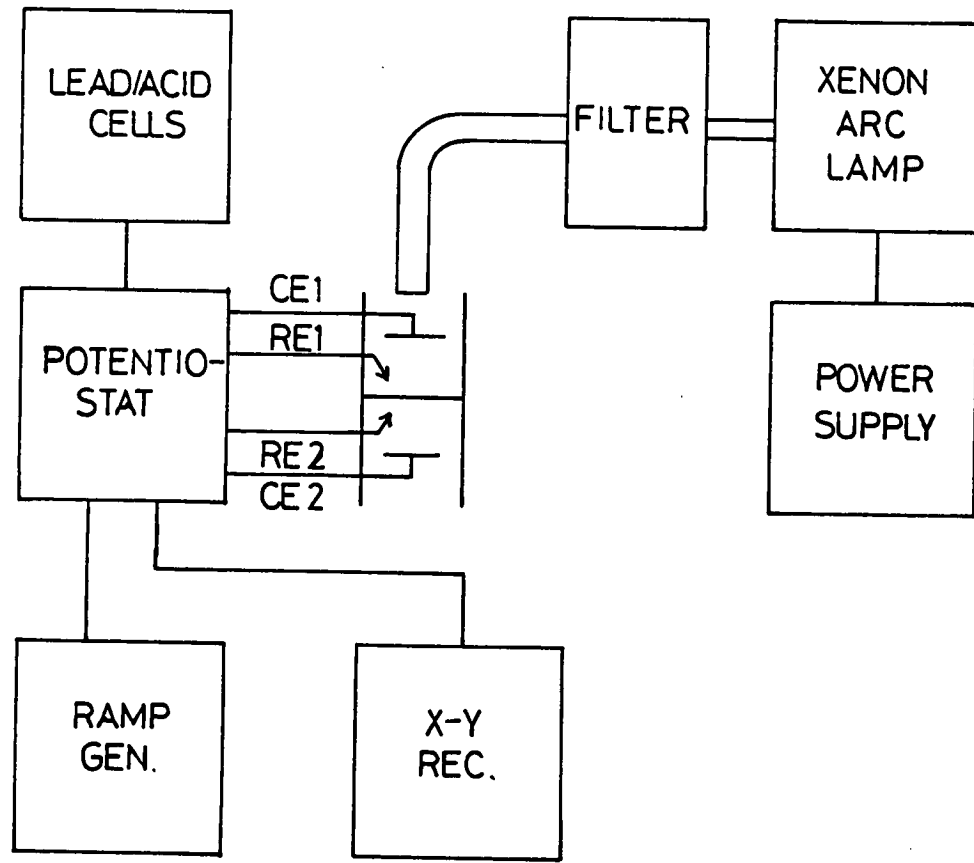
cm^2 (see figure 2.3.1) ,the inside surface of which was previously made hydrophilic by the action of a dilute aqueous solution of sodium hydroxide. The solutions used were saturated with argon gas , previously saturated with the vapour of the solvent to be employed by passage through a sintered bubbler immersed in that solvent. This solvent saturated argon was passed through the solutions *via* a narrow Teflon tube for twenty minutes , after which time the cell , previously filled with argon gas was filled using argon filled Pasteur pipettes.

It was found that a thin layer of 1,2-DCE tended to float on top of the aqueous layer which was LiCl (10 mM) unless otherwise stated , and in order that this thin layer did not affect results by blocking light directed from above the cell , argon was passed gently through the aqueous phase thus ensuring the return of this thin organic layer to its proper resting place in the bottom half of the cell.

The potential E = ψ (Ag) - ψ (Ag') was controlled by means of a purpose built battery driven four electrode potentiostat. Both reference electrodes were shrouded with black PVC tubing. The limits of polarisability of each system studied were determined by cyclic voltammetry prior to any other measurement. A typical voltammogram is shown in figure 2.4.1. All potentials reported here are quoted as oil *versus* water , on a scale on which the standard potential of transfer of the tetramethylammonium ion between water and 1,2-DCE is 160 mV [68]. Tetramethyl ammonium sulphate was therefore added to the aqueous layer , in a predetermined quantity , at the end of each experiment as an internal reference , its potential of transfer being determined by cyclic voltammetry. All currents corresponding to passage of negative charge from organic to aqueous phase or positive charge in the opposite direction were conventionally regarded as positive. Positive feedback ohmic drop compensation was

applied for the cyclic voltammograms recorded , the correct amount being determined by gradually increasing the compensation until the potentiostat output went into oscillation. The maximum value of compensation which did not drive the system into oscillation was then applied. Ohmic drop compensation was not applied during the measurements of photocurrent - time transients.

Light from the xenon arc source was brought to the cell *via* a liquid light pipe (Applied Photophysics) , the end of which was brought as close as possible to the top of the aqueous layer. The light was wavelength selected by means of an interference filter (Applied Photophysics UXX 35-2823) with maximum transmittance of 15% at a wavelength of 264.2 nm. All other experimental conditions were as described previously [61]. A block diagram of the apparatus used is shown in figure 2.3.2.

Section 2.4   Results.

The limits of polarisability for each system studied were determined by cyclic voltammetry (See Chapter 4) and a typical cyclic voltammogram is shown in figure 2.4.1. When the cell was assembled as shown in figure 2.2.1 and illuminated from above by light from the xenon arc source , current was observed to pass in the direction corresponding to the flow either of negatively charged species from organic to aqueous phase , or of positively charged species transferring in the opposite direction. The photocurrent-time transient took the general form shown in figure 2.4.2. A similar signal was observed upon irradiation of a cell where TPAs CBB replaced TBA TPB , with the important distinction that the current was passed in the opposite direction.

Figure 2.4.2. Typical Photocurrent-Time Transient for Cell 2.1.
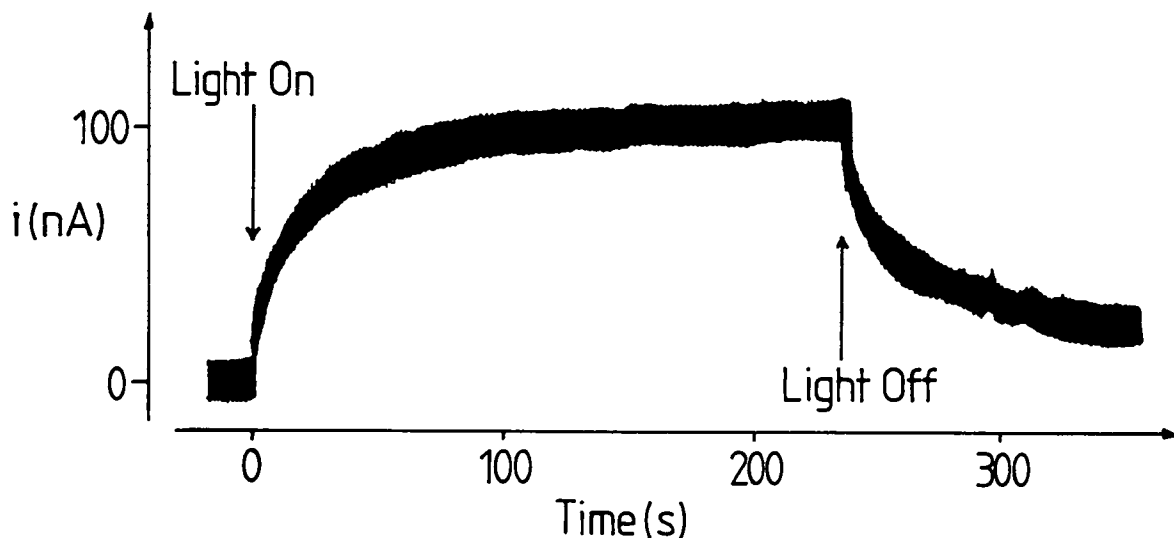
Figures 2.4.3. and 2.4.4. show the effect of the intensity of the incident radiation on the initial slope and limiting photocurrent , i_{lim} (see section 2.5.). Figure 2.4.5. shows the variation of the limiting photocurrent with the wavelength of light used. The potential dependance of the initial slope and i_{lim} are shown in figures 2.4.6. and 2.4.7. Figures 2.4.8. and 2.4.9. show the effect of TPB^- concentration on i_{lim} and the initial slope. The results presented on the following pages ,   are original with the exception of those in figures 2.4.5 to 2.4.7. These are due to Samec.

Figure 2.4.1. Typical Cyclic Voltammogram for Cell 2.1.
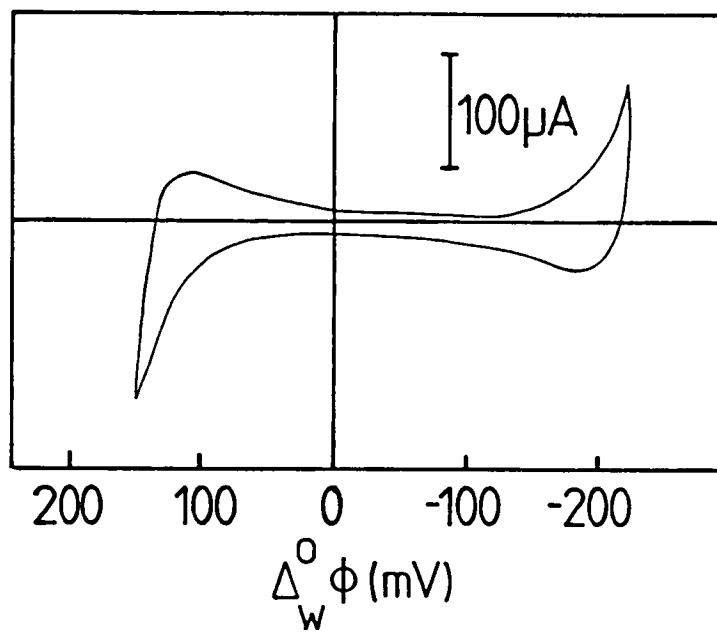
Figure 2.4.3. Variation of the Initial Slope of the Photocurrent
for cell 2.1 with Light Intensity.
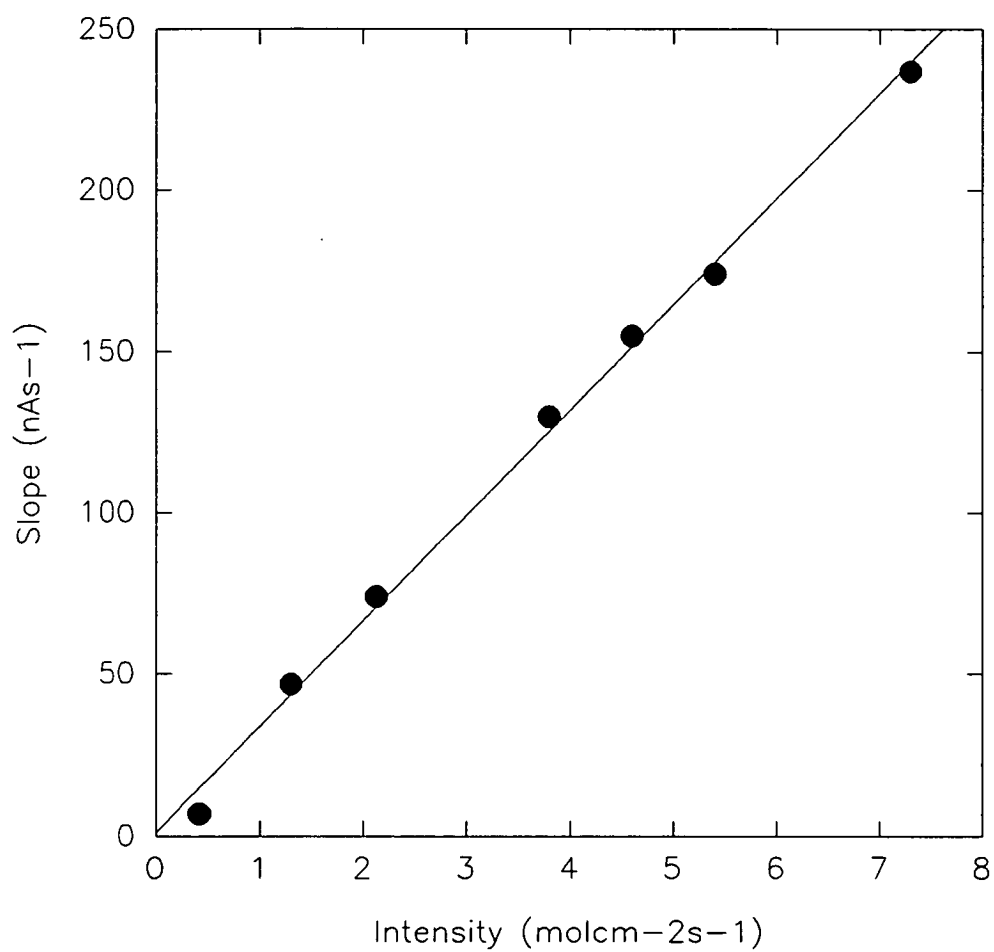
Figure 2.4.4. Variation of Limiting Photocurrent for Cell 2.1
with Light Intensity.
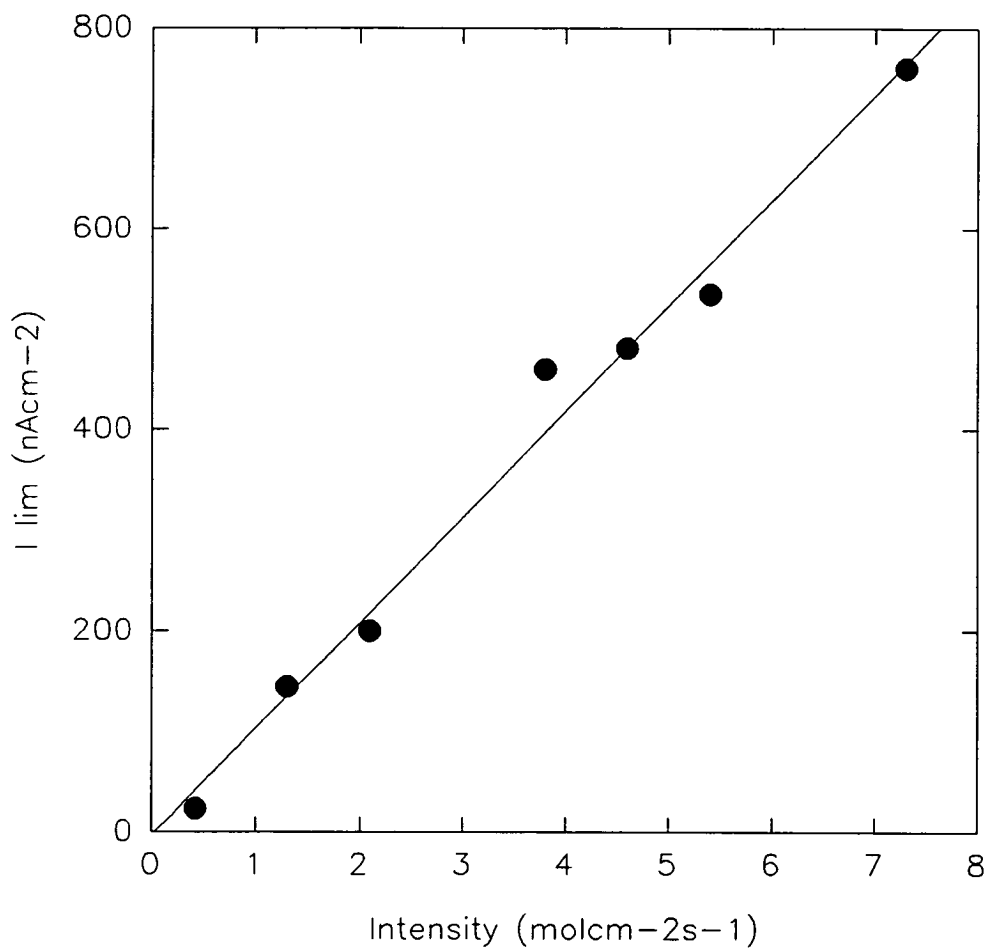
Figure 2.4.5. Action Spectrum for the TPB⁻ Photocurrent , 10 mmoldm^{-3} LiCl, 10 mmoldm^{-3} TBATPB.
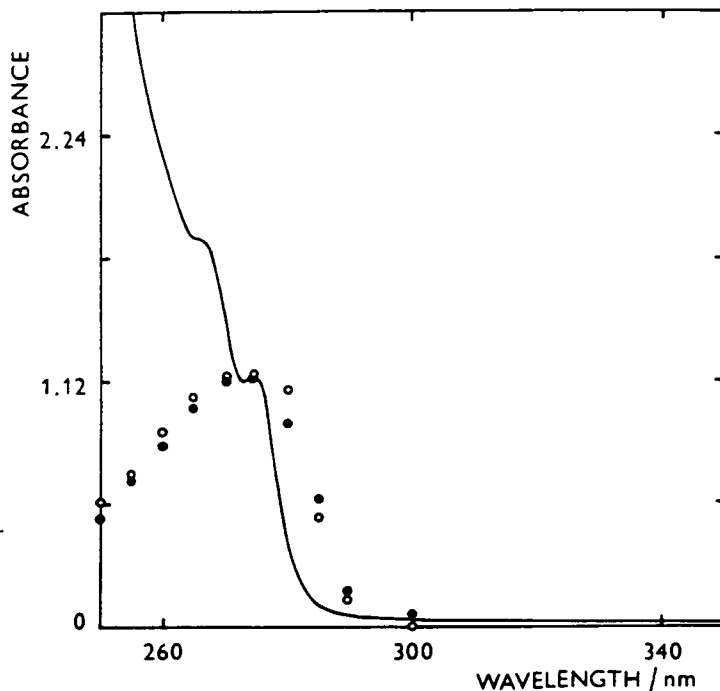
Figure 2.4.6. Variation of the Initial Slope ,s, with Applied Interfacial Potential Difference.
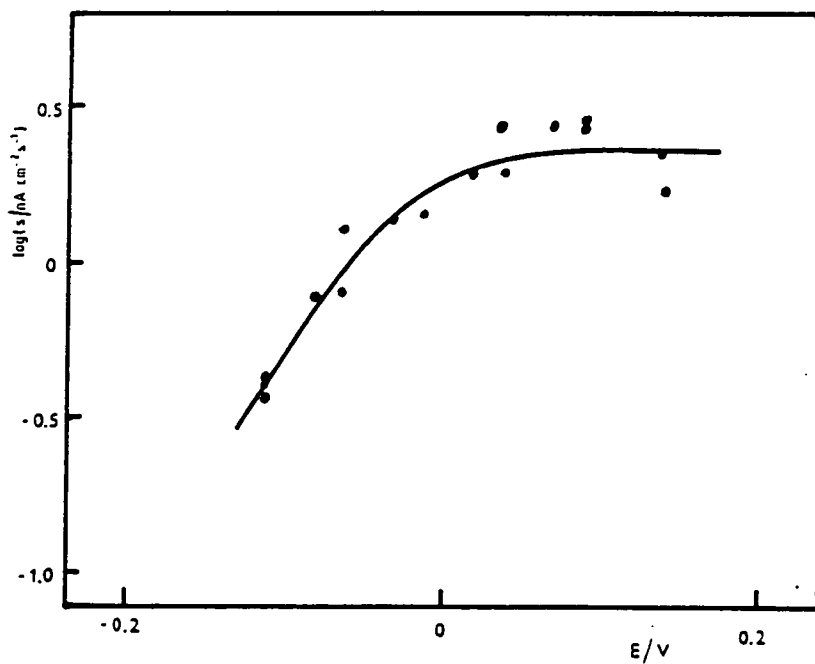
Figure 2.4.7.   Variation of Limiting Photocurrent for
Cell 2.1 with Interfacial Potential Difference.
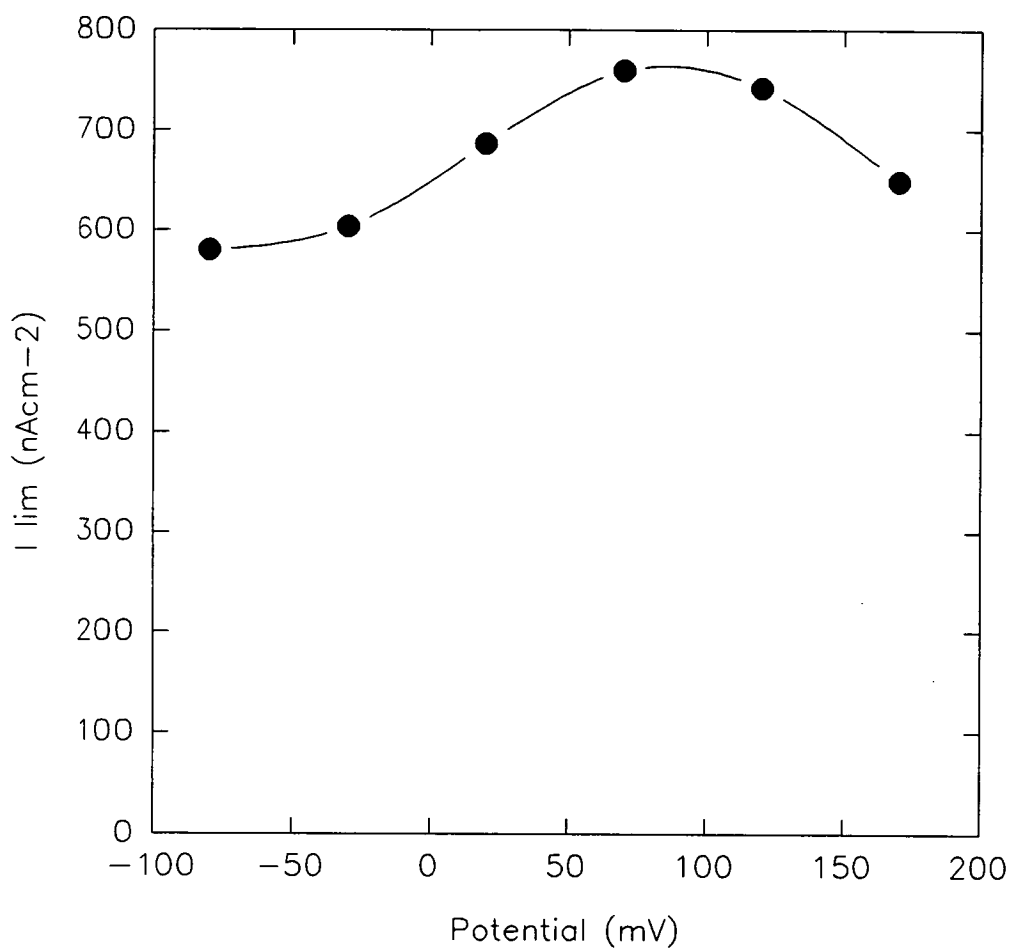
Figure 2.4.8. Variation of Initial Slope of the Photocurrent for Cell 2.1 with Concentration of Tetraphenylborate.
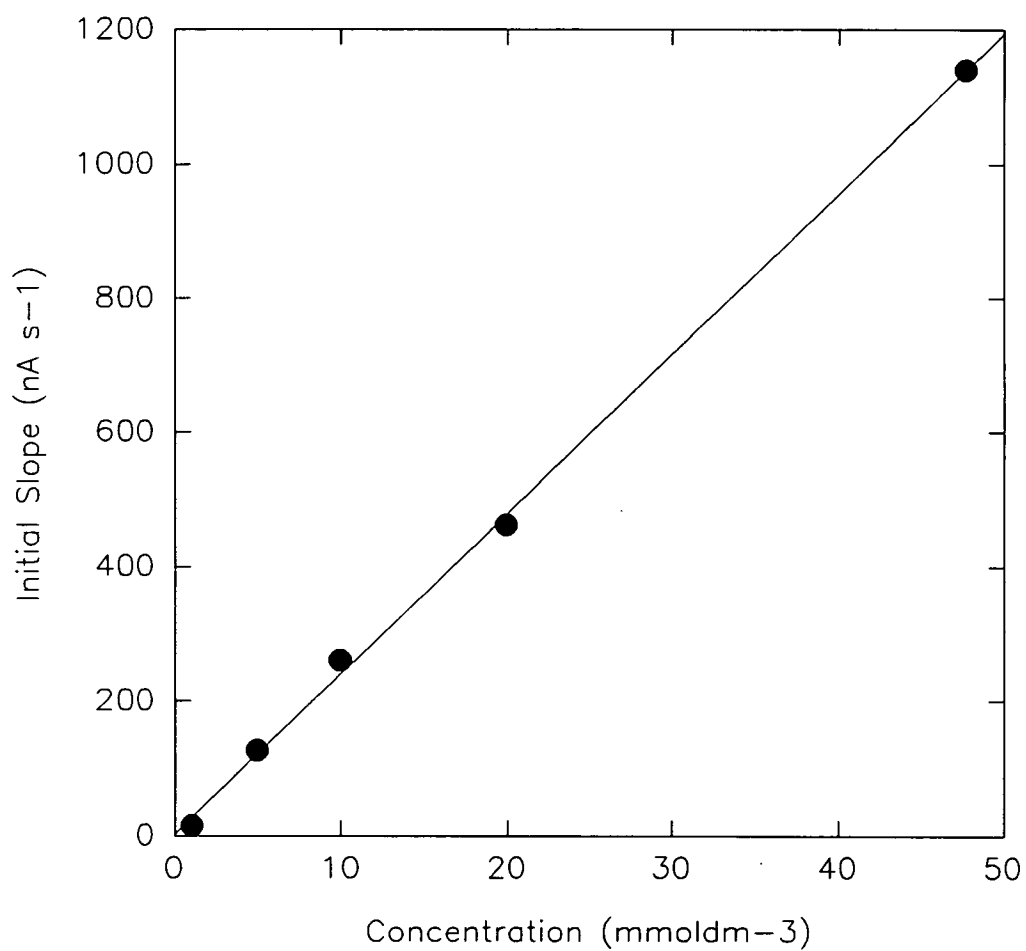
Figure 2.4.8.   Variation of the Limiting Photocurrent
for Cell 2.1 with Tetraphenylborate Concentration.
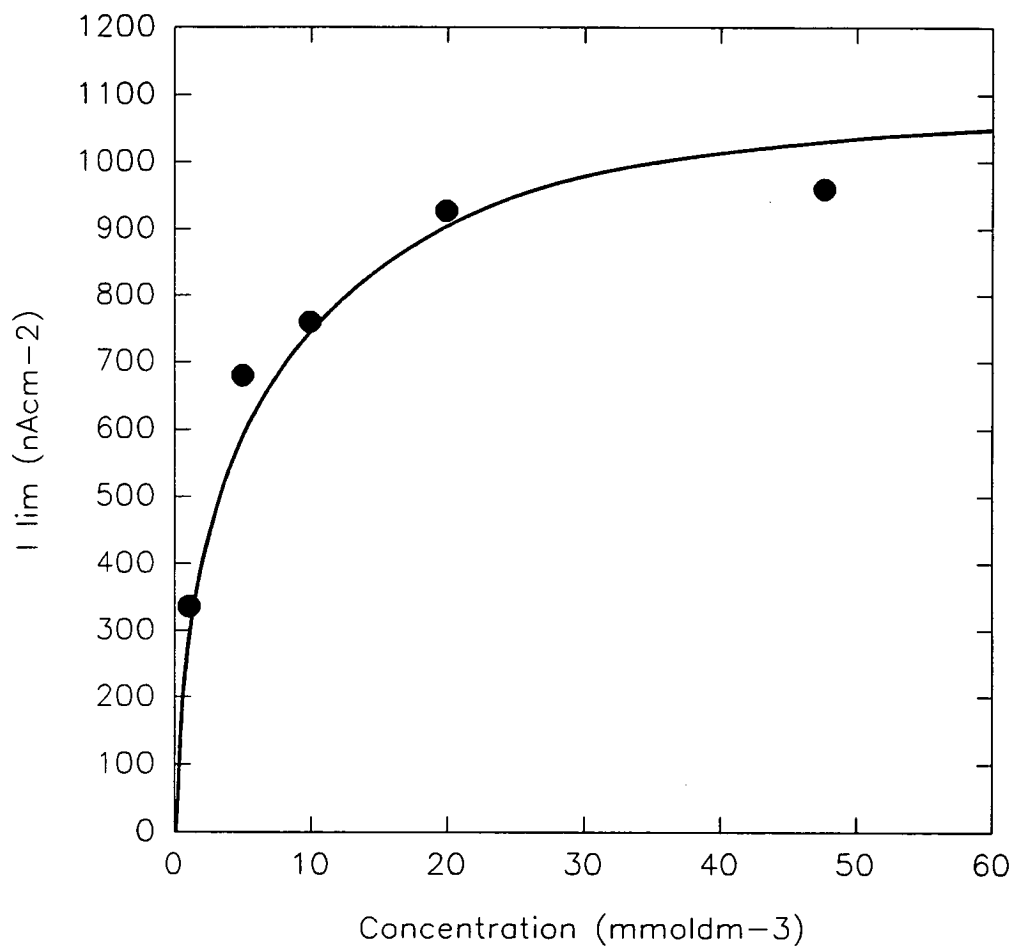
Considerable effort was directed towards attempts to measure the lifetime of the lowest triplet excited state of the TPB⁻ ion under various conditions using flash photolysis. These attempts all failed. The teraphenylborate ion behaves spectroscopically as four independent benzene rings [71] , and this analogy may explain these difficulties. The first triplet-triplet transition of benzene is obscured by the first singlet-singlet transitions [72] , which makes conventional flash photolysis measurements difficult , and a similar argument may apply to tetraphenylborate.

Section 2.5 Discussion

In general , for each photocurrent-time transient obtained two measurements were made. These were the slope , s , of the transient at the commencement of illumination , and the limiting value of the current i_{lim}. The derivation of these parameters is demonstrated in figure 2.5.1.

Figure 2.5.1 Analysis of Photocurrent-Time Transients.
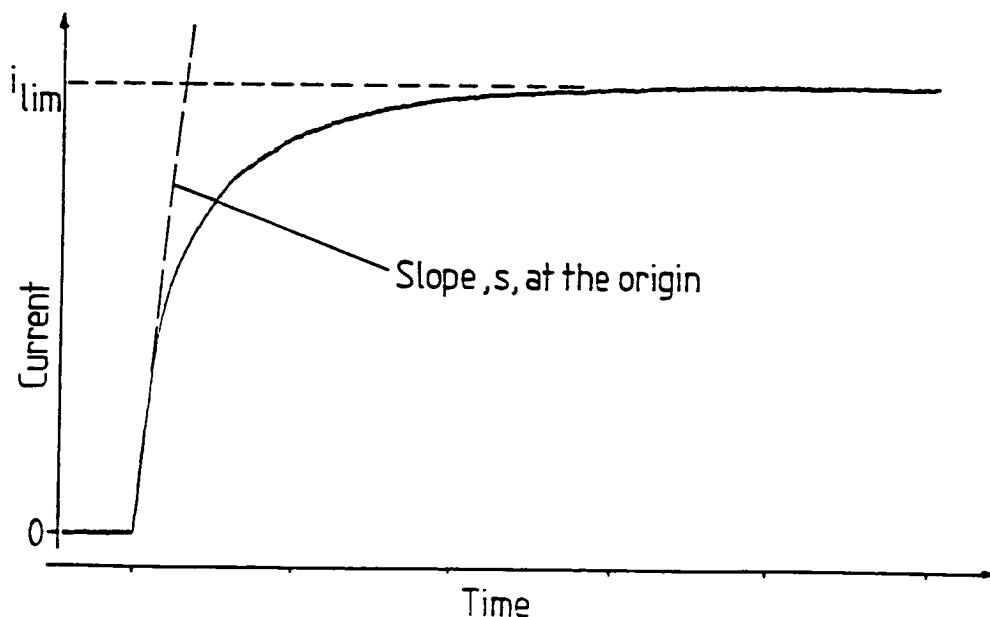
The magnitude of the photocurrent was found to be independent of both the concentration and the nature of the aqueous supporting electrolyte used. HCl could be substituted for LiCl , and the concentration of LiCl could be increased tenfold without producing significant change in the photocurrent recorded. Saturation of both phases with argon also produced no change in the photocurrent , although this procedure was undertaken for all experiments performed by the author on the grounds of the known non-innocence of dioxygen in photochemical and electrochemical systems.

From figures 2.4.3 and 2.4.4 it can be seen that both the initial slope and the limiting photocurrent depend linearly on the intensity of the incident radiation. It can be inferred from this fact with reasonable certainty that , whatever process is involved in the generation of the photocurrent , this process is uniphotonic. One quantum of light only is required to drive a charge carrier across the interface. This is quite reasonable as biphotonic processes are generally only observed experimentally with intense laser or synchrotron radiation.

Figure 2.4.5 shows the action spectrum of the process , as measured for an organic layer composed of TBA TPB (10mM) in 1,2-DCE. This is a plot of i_{lim} , corrected for lamp output , against the wavelength of the incident radiation. From the electronic absorption spectrum underlying this action spectrum , it can be seen that the photocurrent strongly correlates with the generation of electronically excited states of the TPB^- anion. That the action spectrum appears to lead the absorption spectrum to the low wavelength side is probably due to the high bandwidth of the monochromator . With both entrance and exit slits set to seven millimetres the term monochromator is perhaps not appropriate , the bandwidth being quite large , however this measure was necessary to allow

sufficient light to reach the cell.

Given that the composition of the aqueous phase made no apparent difference to the photocurrent , it seemed unlikely that any species in that phase was contributing to the photoinitiated process . That is to say that the photochemistry involved was located exclusively in the organic layer , and that some product of the photochemical process , bearing a negative charge , subsequently crossed the interface. The scheme proposed for the analysis of the photocurrents is shown in figure 2.5.2.

Figure 2.5.2.   Scheme for the Analysis of Photoinitiated Ion Transfer.

$h\nu$

G $\longrightarrow$ E

Diffusion $\longleftarrow$ X $\longrightarrow$ Transfer

k'

k_f

Y

1,2-DCE   Water
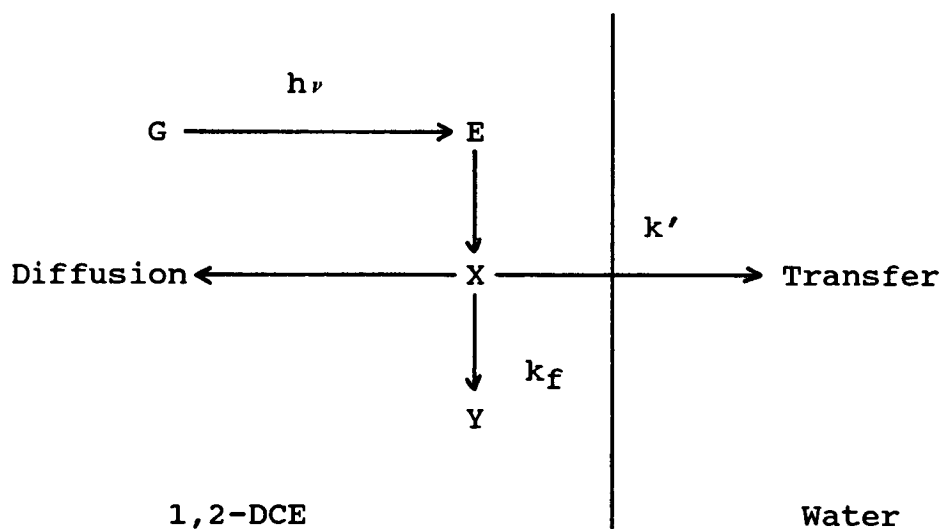
The process is postulated to be initiated by the absorption of one quantum of UV light by a TPB$^-$ ion in its ground state , G , to produce that ion's first singlet excited state S_1. There are a number of routes open to this excited ion for deactivation. Radiative or non radiative decay will lead to the ground state ion , intersystem crossing will lead to the lowest triplet excited state. E in the above figure may be either or both of the lowest singlet and triplet excited states.

The energy of the lowest triplet state was determined

by ultraviolet-visible (UV-Vis) spectroscopy in iodoethane where the external heavy atom effect [63] allows direct population of T_1 from S_1. Radiative decay of S_1 in tetraaryl borates is well known [63].

Both S_1 and T_1 may fragment or rearrange under the influence of those factors outlined in section 1.4.3 This then leaves open the question of the identity of the crossing species X in figure 2.5.2. The possibility must be considered that TPB$^-$ ions in either S_1 or T_1 states cross the interface , as must the possibility that ions forming part of the chain of photochemical decomposition are responsible for the observed current. The TPB$^-$ ion is known to have a rich photochemistry [64-66].

The approach chosen to identify or at least narrow down the possible identities for the transferring species X was mathematical in nature. It was hoped that , by modelling the process outlined in figure 2.5.2 and subsequent fitting of the equation generated to the experimental results by parameter optimisation , some information might be gained about the ion transfer process and about k_f , the rate constant for deactivation of X to a non crossing species Y , in particular. This non crossing species may be G or another ion. If the species X were to be a TPB$^-$ ion in S_1 then k_f would be around 10^8 s^{-1} as time resolved laser induced fluorescence experiments indicated a lifetime for the first singlet excited state of under 10 ns. If T_1 were involved then k_f should be 10^5 s^{-1} as most organic triplet states are collisionally quenched in solution. It seemed unlikely from the outset that ions in S_1 or T_1 states were directly involved in the photocurrent production as a residual photocurrent may be observed tens of seconds after the cessation of illumination.

With reference to figure 2.5.2 the equations determining the concentrations of G,E and X : c_G , c_E , and c_X respectively are ;

$$c_{G(x,t)} = G_0 = \text{a constant} \qquad \text{Eqn. 2.5.1}$$

$$c_{E(x,t)} = A \exp(-ax) \qquad \text{Eqn. 2.5.2}$$

$$\delta c_{X(x,t)}/\delta t = D \left[\delta^2 c_{X(x,t)}/\delta x^2\right] + A\exp(-ax) - kc_{X(x,t)}$$

$$\text{Eqn. 2.5.3}$$

where $A = \psi \epsilon G_0 I_0$,such that ψ is the quantum yield for production of E , ϵ is the extinction coefficient of G , x is displacement normal to the interface , D is the diffusion coefficient of X and a is $\log_{10} \epsilon G_0$. By assuming a steady state concentration of the primary excited state E in the photochemical process
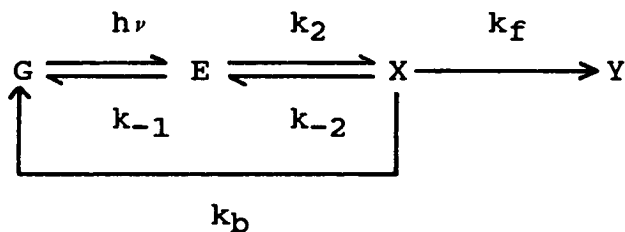
then the constant k is given by $k_f + k_b + k_{-1}k_{-2}/(k_{-1}+k_2)$ and ψ is equal to $k_2/(k_{-2}+k_{-1})$.

Using these boundary conditions an expression was derived for the current density at a time t after the commencement of illumination of the interface

$$I_{(t)} = [nFADk'/k'-Da].[-(a/B)[1-\exp(-Bt)\text{erfc}(a(Dt)^{1/2}]$$

$$-(k'/CD)[1-\exp(Ct)\ \text{erfc}(k'(t/D)^{1/2})]$$

$$+(k/D)^{1/2}[B^{-1} + C^{-1}]\text{erf}(kt)^{1/2}]$$

$$\text{Eqn. 2.5.4}$$

where $B = k - Da^2$, $C = (k'^2 / D) - k$, n is the stoichiometric charge of X , k' is the heterogeneous rate constant for ion transfer of X, and F is Faraday's constant. This equation is similar to that reported by Hamnett et al [52] to describe the diffusion of $[Ru(bpy)_3]^{2+*}$ to a semiconductor electrode. Application of equation 2.5.4 to the situation at t = infinity leads to:

$$i_{lim} = nFAk' / [(a + (k/D)^{1/2}(k' + (kD)^{1/2})] \quad \text{Eqn. 2.5.5.}$$

Section 2.5.1   The General behaviour of Equation 2.5.4.

Two computer programs were written to calculate equations 2.5.4 as a function of time and 2.5.5 as a function of concentration of G numerically (See Appendix 1.). Figures 2.5.3 to 2.5.5 show the behaviour of the curve calculated for equation 2.5.4 with variation of the three variables k , ψ and k'. These are the variables found to be necessary in quantifying the effect described here and yet whose experimental determination was not achieved. It was the purpose of this mathematical modelling procedure to throw up some reasonable value for one or more of these three crucial factors.

The general form of the calculated current-time profiles may be seen to be satisfyingly similar to those obtained in the laboratory. The curve rises steeply from the origin and reaches a plateau value , although of course it never ceases to rise on a microscopic scale. The curve calculated for equation 2.5.5 also mimics the general form of the experimental results presented in figure 2.4.8. The two factors on which it was decided to base a heuristic attempt to optimise the fit between the calculated and measured current-time profiles were the time taken to reach a plateau value of current and the value of that plateau current itself. The choice of these

Figure 2.5.3. Behaviour of Equation 2.5.4. with variation of k.
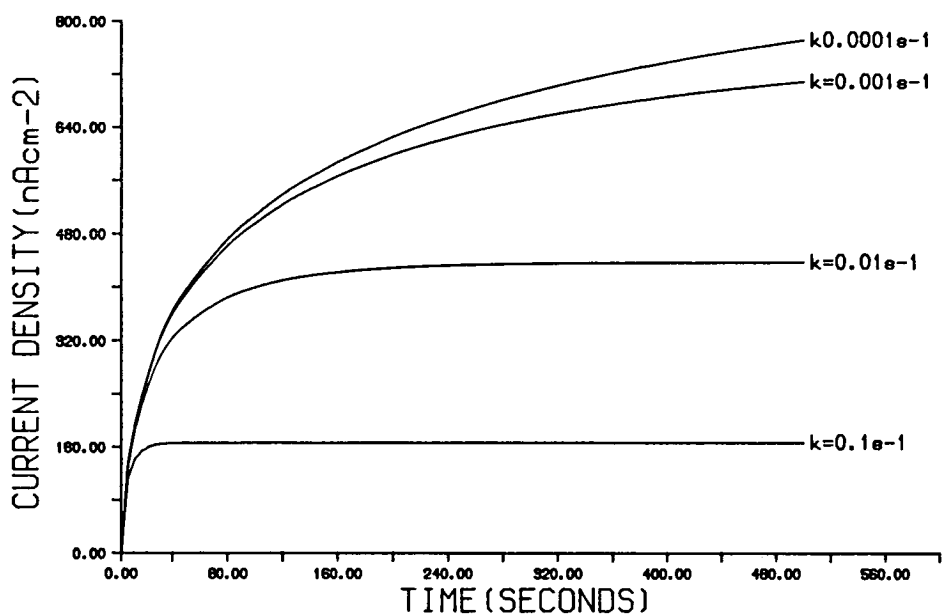
Figure 2.5.4. Behaviour of Equation 2.5.4. with variation of ψ.
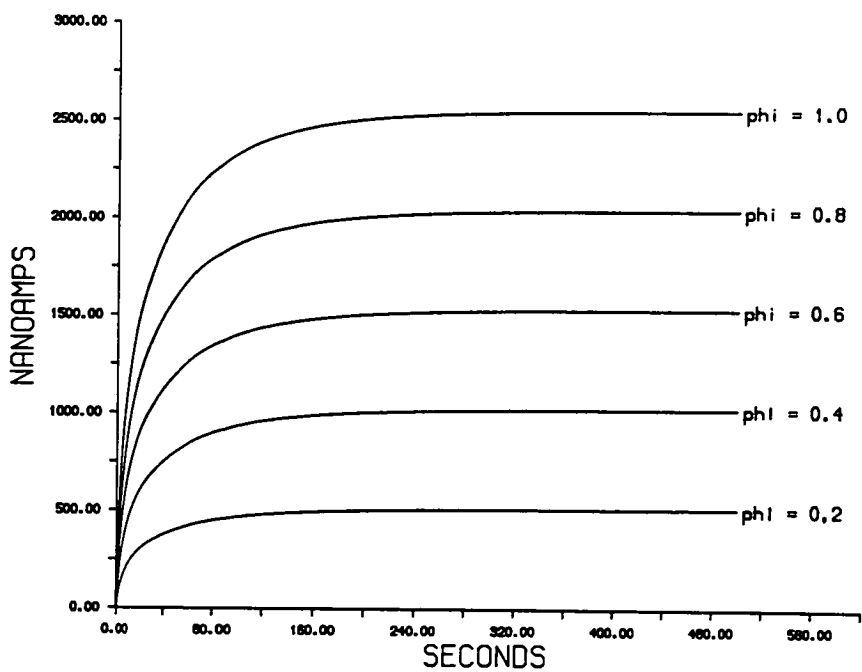
Figure 2.5.5. Behaviour of Equation 2.5.4. with variation of k'.
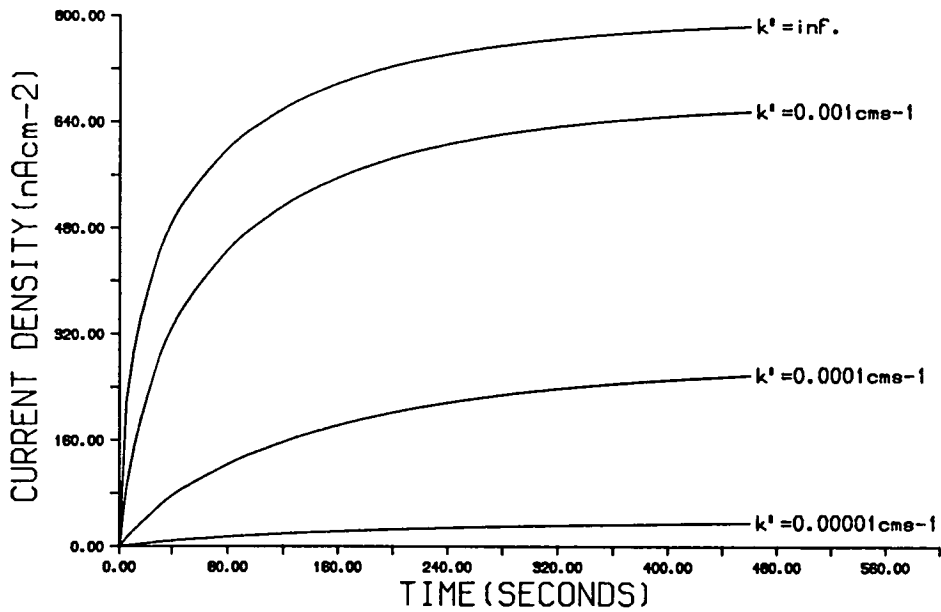
Figure 2.5.6. Experimental and Theoretical Photocurrent-Time Transients for 9.94 mmoldm^{-3} TBATPB.
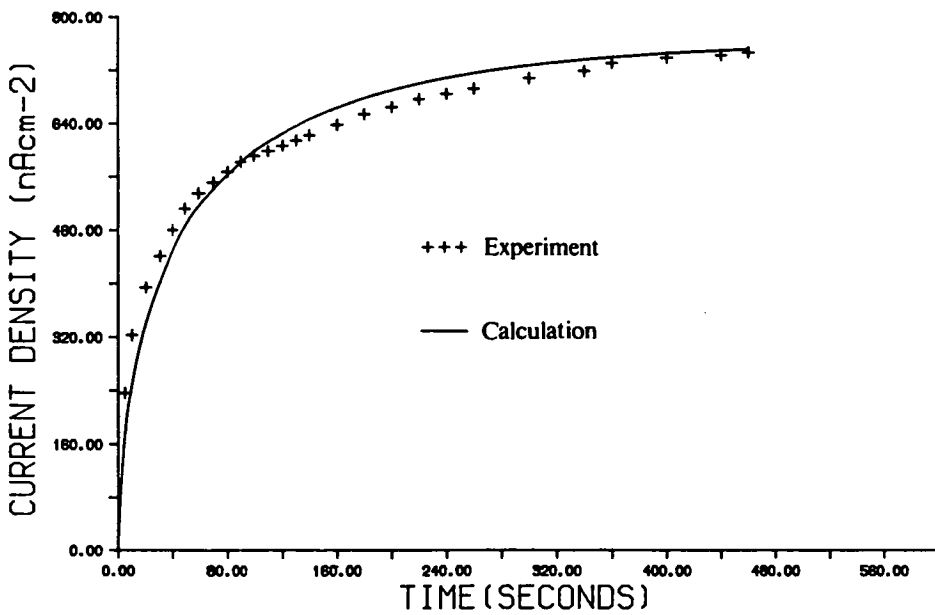
Figure 2.5.7. Experimental and Theoretical Variation of
i_{lim} with Concentration of TBATPB.
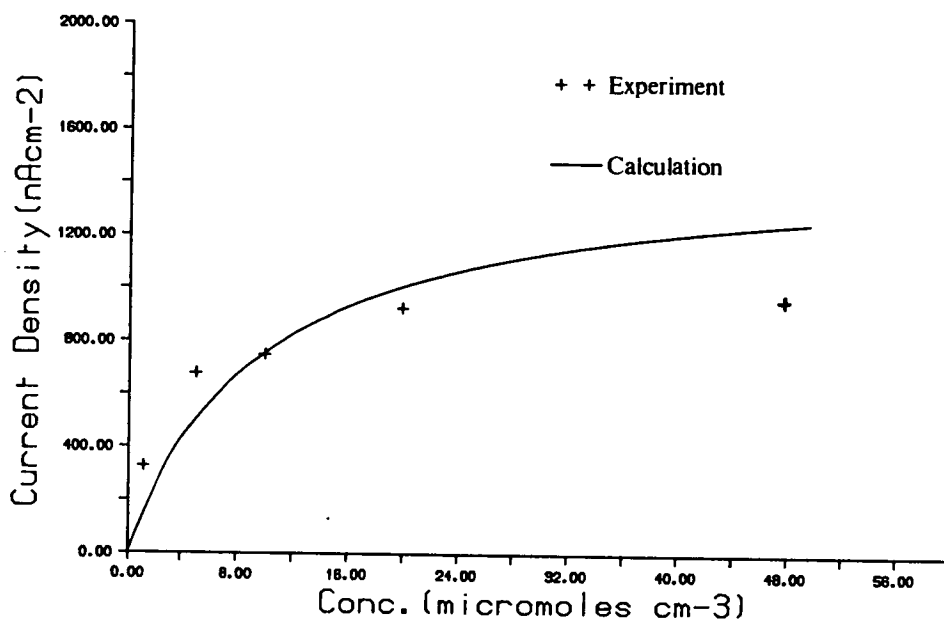
factors is justified by the discovery , illustrated in figures 2.5.3 to 2.5.5 , that the time taken to reach a plateau or pseudo steady state value of current depends only on k , and that ψ and k' then act as multipliers on the curve , the shape of which is dictated by k.

The value of the decay rate constant , k , of X appeared to represent both the most useful piece of information in the characterisation of X and also the factor most amenable to determination through the optimisation process. It was decided then to choose a reasonable value for k' and determine the quantum efficiency for the production of X.

Figure 2.5.6 shows the result of this optimisation process for equation 2.5.4 as applied to photolysis of an organic layer composed of a solution of TBATPB (9.94mM) in 1,2-DCE. This method led to values for k and ψ of $0.0035s^{-1}$ and 0.22 respectively. Figure 2.5.7 demonstrates the transposition of these values to equation 2.5.5 , and the superimposition of the resulting curve on the data also shown in figure 2.4.8. No two values of k and ψ could be found which gave an exact fit for all the experimental data , but the variation in one or both of these factors required to give reasonable fit for the experimental data was in the order of 15%. Considering the simplicity of the model employed and the possible complexities of the photochemical processes involved , such harmony between theory and experiment , even given the wide latitude of the optimisation process , is satisfactory.

It was hoped to gain some insight into the chemical nature of X from the values of k and ψ derived. Time resolved laser induced fluorescence points to the population of an initial excited state with k_{-1} around 10^8 s^{-1}. It seems unlikely that k_{-2} could play a large part in the deactivation of X , considering the short lifetime of E . It is suggested that this deactivation takes place to some stable species , and that this decay takes place with

a rate constant of around 0.0035 s^{-1}. It follows then that TPB$^-$ ions in excited states S$_1$ or T$_1$ are not the charge carriers , as the lifetimes of these species are far too short to account for the currents observed , either in profile or in magnitude. In order to approach more closely the goal of identifying X , recourse must be taken to the known photochemistry of the TPB$^-$ ion in an attempt to locate some ionic intermediate in the photolysis pathways to which a lifetime in the order of hundreds of seconds might be ascribed.

Section 2.5.2   The Photochemistry of the TPB$^-$ Ion in Relation to the Observed Photocurrents.

The photochemistry of the TPB$^-$ anion has been previously studied [64-66]. There is common agreement throughout these publications that in the presence of dissolved dioxygen , photolysis of tetraphenyl borate containing solutions leads to diphenyl borinate (Ph$_2$BO$^-$) formation. This is of limited use in identifying X , as the experiments were carried out in argon saturated solutions.

The work of Wilkey and Schuster [66] reports the ultraviolet photolysis of tetraalkylammonium tetraphenylborates in the degassed aprotic solvents acetonitrile and tetrahydrofuran , probably the most similar conditions reported to those employed here. They investigated the final photoproducts of irradiation of TPB$^-$ using nuclear magnetic resonance (NMR) and UV-Vis. spectroscopy. The conclusion was reached that a single boron containing product resulted , and that this species comprised an anionic four-coordinate boron atom. Isotope labelling experiments led to the conclusion that this species had the structure shown in figure 2.5.8.

Figure2.5.8. Proposed Structure of the Final Photoproduct of TPB⁻.
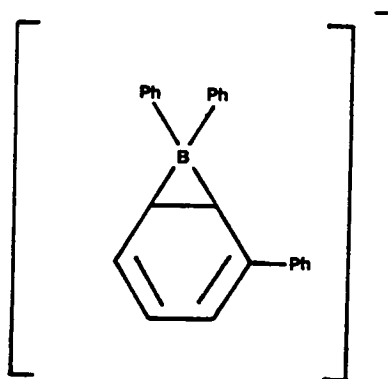
This species (I) was found to be indefinitely stable in the sealed photolysis cell used , however it was reported that all attempts at isolation of this compound failed , and this tends to point towards some instability of I , presumably towards aerial oxidation.

Wilkey and co-workers also proposed the formation of a biradical intermediate (Species II in figure 2.5.9.) between the TPB⁻ ion and I.

Figure 2.5.9. Proposed Biradical Intermediate in the Photolysis of TPB⁻.
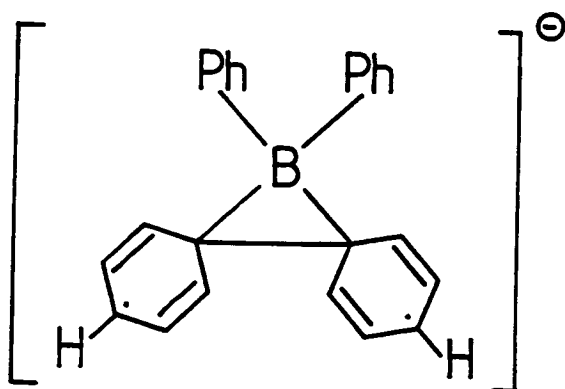
It is quite conceivable that I or II may be more hydrophilic than tetraphenylborate itself and thus liable to cross the interface.

The mathematical analysis previously presented does not allow for the possibility that more than one species contributes to the photocurrent. No allowance is made either for the possibility that some stable hydrophilic photoproduct may also contribute to the flow of charge across the interface. It may , however , be concluded with reasonable certainty that the observed current is not exclusively due to the transfer of a stable photoproduct as i_{lim} should then be equal to nFA/a , that is to say it should be independant of the concentration of the ground state. This of course was found not to be the case. The possibility is left open then that diphenyl borinate , which would undoubtedly be more hydrophilic and so more disposed to transfer than TPB^- itself , is being produced in these experiments. The argon saturated solutions employed will still contain some dioxygen , but the fact that saturation of the the solutions with air makes little difference to the photocurrent recorded suggests that this contribution to the whole is minimal.

The variation of the plateau current with the applied potential difference is small (figure 2.4.7.) , rising only gently towards more negative potentials before tailing off at extreme negative potentials. This low linkage between i_{lim} and potential difference suggests that the transfer of X is fast at all potentials investigated and that the formal potential for partition of X lies outwith the range of potentials amenable to study here. This is not surprising , as TBATPB provides quite a small window of polarisation , due to the similar free energies of partition of these two ions between water and 1,2-DCE [68].

Although species I was found to be stable under an inert atmosphere , the conditions for a liquid / liquid

experiment may be sufficiently different to lend some instability to this compound. Species II remains a contender as do certain other bridged borate species. In order to gain some insight into the possible involvement of these bridged species which have been postulated in the photochemistry of TPB⁻ [65] it was decided to synthesise a TPB⁻ analogue for which bridging was blocked for all phenyl carbon atoms other than those at the the *ipso* positions. To this end the tetrakis(pentafluorophenyl)-borate (TPFB⁻) ion was synthesised (See Appendix 2.) in the form of its TBA salt.

Figure 2.5.10. The TPFB⁻ Ion.
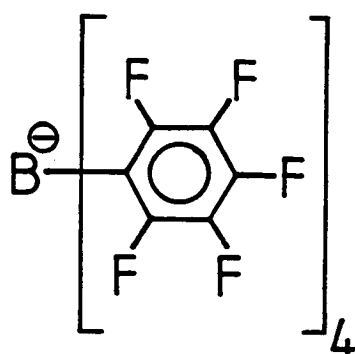
When TBATPFB takes the place of TBATPB in the experiments described here , no photocurrent is observed. This lack of photoelectrochemical activity cannot be assigned to the TPFB⁻ ions failure to absorb UV radiation as demonstrated in figure 2.5.11. Nor , unfortunately can it be said to be due to failure to form bridged intermediates. Whilst it is unlikely that such intermediates form , due to the high C-F bond strength , in the event that they did form , their free energies of partition might well be too high to observe transfer. Figure 2.5.12. shows the cyclic voltammogram for the cell:

Figure 2.5.11. UV-Vis. Spectra of_A_TBATPB and_B_TBATPFB.
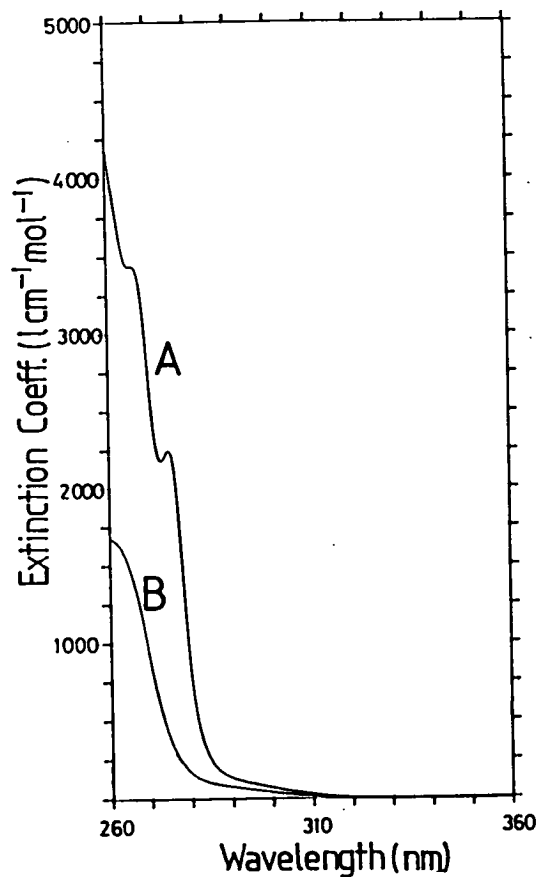
Figure 2.5.12. Typical Cyclic Voltammogram for Cell 2.2.
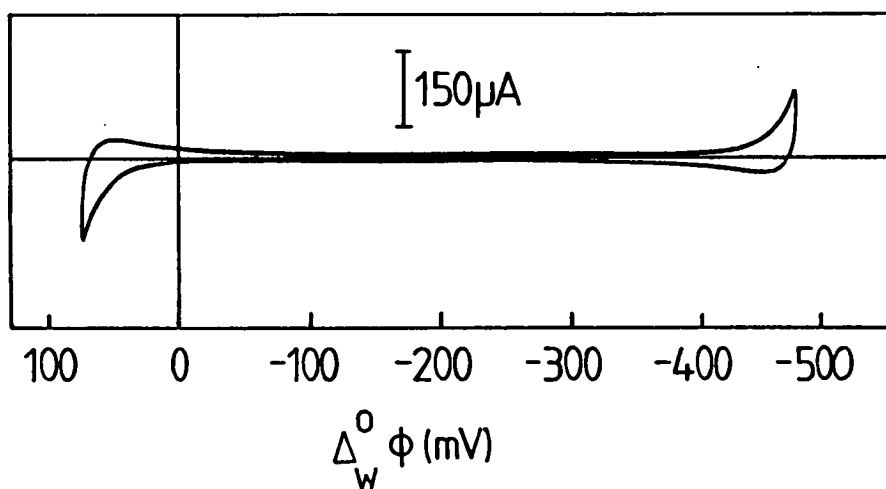
Ag/AgCl/1mM TBACl/10mM TBATPFB // 10 mM LiCl/AgCl/Ag'
(aq)   (1,2-DCE)   (aq)

Cell 2.2

the window is no longer limited at the negative end
by transfer of the tetraaryl species but by transfer of
the lithium cation from the aqueous layer. The free energy
of partition of the $TPFB^-$ ion is therefore not known , but
is almost certain to be large and positive. Addition of
one chlorine atom to the 4-position of each phenyl ring of
TPB^- to form the $TPBCl^-$ ion renders this species
sufficiently hydrophobic [69] that its free energy of
partition is also not amenable to determination by cyclic
voltammetry at the ITIES. Nonetheless a photocurrent
similar to that described for the TPB^- ion may be observed
for the $TPBCl^-$ ion [61]. Addition of five fluorine atoms
per phenyl ring to TPB^- would almost certainly render even
a bridged or otherwise tortured variant of the $TPFB^-$ ion
too hydrophobic to cross the water / 1,2-DCE interface. It
would be possible , by means of an NMR experiment , to
determine wether the $TPFB^-$ ion undergoes photochemical
change , but the outcome of such an experiment would have
little bearing on the present investigation. It would
always be possible to ascribe the lack of
photoelectrochemical activity of this ion to the extreme
hydrophobicity of the photochemical daughter products of
this ion rather than to their structural characteristics.

Section 2.6   Conclusion.

Mathematical analysis of the phenomenon of
photoinitiated ion transfer at the ITIES has ruled out
some of the more far fetched possible explanations for the
effect , but perhaps not surprisingly failed to turn up

any hard evidence as to the real nature of X. At best one can point to conventional photochemical investigations and pick out candidate ions that seem to fit the bill. The key to identifying X may well lie in the discovery of some common link in the photochemical behaviour of tetraaryl borates and tetraaryl arsonium ions , both of which exhibit photoinitiated ion transfer behaviour at the ITIES.

It has though demonstrated that some long lived ionic intermediate is involved in the production of the photocurrent , and that tetraphenyl borates should preferably not be at all involved in photoelectrochemical systems , and should certainly not be subject to UV irradiation. The TPFB$^-$ ion has been shown to be a suitable substitute both in enlarging the window of polarisation and in reducing background photocurrents.

References.

59. V. Maracek , A.H. De Armond , M.K. De Armond, J. Electroanal. Chem. 261(1989)287.

60. N.A. Kotov and M.G. Kuzmin, J. Electroanal. Chem., 285(1990)223

61. Z. Samec , A.R. Brown , L.J. Yellowlees and H.H. Girault, J. Electroanal. Chem., 288(1990)245.

62. M. Kasha, J. Chem. Phys., 20(1952)71.

63. M. Gouterman and P. Sayer, J. Mol. Spec., 53(1974)319.

64. J.L.R. Williams , J.C. Doty , P.J. Grisdale , R. Searle , T.H. Regan , G.P. Happ and D.P. Maier, J. Amer. Chem. Soc. 89:20(1967)5153.

65. J.J. Eisch , K. Tamao and R.J. Wilcsek, J. Amer. Chem. Soc. 97:4(1975)895.

66. J.D. Wilkey and G.B. Schuster, J. Org. Chem., 52:11(1987)2117.

67. A. Weissberger ,E.S. Proskauer ,J.A. Riddick and E.E. Toops Jnr., Organic Solvents 2nd. Edn., Interscience Publishers Inc.(1955).

68. T. Wandlowski , V. Maracek and Z.Samec, Electrochim. Acta., 35(1990)1173.

69. Y.Shao , A.A. Stewart and H.H. Girault, J. Chem. Soc. Faraday Trans., 87(16)(1991)2593.

CHAPTER THREE

On the Determination of the Potentials of Transfer of Species Produced in Electron Transfer Reactions.

Section 3.1   Introduction.

Electron transfer reactions at the ITIES have attracted considerable interest from both a theoretical and a practical standpoint. This attention has been justified in part at least by the desire to model heterogeneous electron transfer in biological systems , such as the mitochondrial electron transfer chain.

Figure 1.2.1.1 shows schematically the form of an electron transfer reaction at the ITIES. The first instance of such a reaction was demonstrated by Samec *et al* [70] , using the hexacyanoferrate(II/III) couple in the aqueous phase and the (bis(η^5-cyclopentadienyl)) iron(II/III) (ferrocene / ferricenium) couple in nitrobenzene or 1,2-DCE. The analysis of the data from this system was however complicated by the ionisation of the ferrocene in the organic phase. Because ferrocene itself is uncharged its transfer across the ITIES is not accompanied by passage of current through the external circuit of the potentiostat. Subsequent to electron transfer however , the ferricenium ion is generated , and the possibility arises that this cation may cross the interface and so give rise to an ion transfer current. These same workers prepared ferricenium salts [71] by means of chemical oxidation and studied the ion transfer reactions of these at the water / nitrobenzene and water / 1,2-DCE interfaces , but themselves admitted that the situation was complicated by the presence of partially hydrophobic ions such as tetrafluoroborate. They instead

used tetraphenylborate as a counter ion , a species which unfortunately reacts with the ferricenium ion. The potential of transfer across the water / nitrobenzene interface is reported , but that for the water 1,2-DCE interface is not , presumably due to the instability in this solvent of the ferricenium ion in the presence of tetraphenylborate.

There have been two approaches taken to the circumvention of the problem of ion transfer subsequent to electron transfer. Geblewicz and Schiffrin *et al* [72,73] discarded ferrocene altogether , employing instead a lutetium phthalocyanine macrocyclic complex , expressing the belief that this compound , in its various oxidation states would be resistant to transfer to the aqueous phase. These workers went on to measure the rate constant for electron transfer by a.c. impedance techniques. Kihara *et al* [74] on the other hand employed a dropping electrolyte electrode , similar in principle to that depicted in figure 1.3.1. , to study electron transfer reactions. Using this arrangement , where the ITIES is constantly renewed with the birth of each drop , it was hoped that following ion transfer reactions would not be significant on the timescale of the drop time.

Similar problems also arise in those systems intended to demonstrate photoinitiated electron transfer at the ITIES. In order to claim the measurement of pure , undiluted electron transfer currents it is necessary to know the potentials of transfer of all the species present , both initially and in the aftermath of any putative electron transfer step. This problem has not been addressed with any formality by any of the workers in the field to date. The most rigorous so far may perhaps be summed up in the quote "...the aqueous photoproduct $[Ru(bpy)_3]^{3+}$ is more hydrophilic than the aqueous reactant $[Ru(bpy)_3]^{2+}$..." [4] , a claim for which no evidence or justification is presented. The work of Marecek [59] also

fails to take into account following ion transfer reactions. $[Ru(bpy)_3]^{3+}$ is claimed to have been generated in the oil phase at extreme oil positive potentials , but no mention is made of the possible tranfer of this species to the aqueous phase.

Section 3.2   Determination of the Transfer Potential of an Ion Between Two Immiscible Liquids.

Charge transfer is possible at a metal electrode / solution interface if the electrode potential is greater than the equilibrium oxidation potential of any electroactive species present , or lower than the relevant reduction potential. A similar formalism is possible at the ITIES , where cation transfer will take place from from organic to aqueous phase should the applied interfacial potential difference be greater than the equilibrium potential for transfer of this species. Similarly anion transfer will take place should the applied potential difference be less than that for transfer of that ion. The equilibrium potential for partition of one ion across the ITIES is given by;

$$\Delta_W^O \varphi = -\Delta G_{tr,ion}^{O \to W} / z_i F + [RT/z_i F] \ln (a_{i(o)}/a_{i(w)})$$

Equation 3.2.1

where the subscripts o and w refer to the organic and aqueous phases respectively, $\Delta G_{tr,ion}^{O \to W}$ is the standard free energy of transfer of the ion i from organic to aqueous phase and a_i is the activity of the species i in the specified phase.

The term $-\Delta G_{tr,ion}^{O \to W}/zF$ may also be written as $\Delta_W^O \varphi_{ion}^O$, the standard potential of transfer of the ion i between the two solvents , on a scale constructed on a chosen extrathermodynamic assumption (see section 1.2.2).

Substitution of this term into equation 3.2.1 yields the Nernst-Donnan equation , whose relation to the Nernst equation is clear.

For simple , reversible ion transfer across the ITIES then those techniques employed to determine E^0 values for redox reactions at solid electrodes may be employed to determine standard potentials of transfer. Cyclic voltammetry is such a technique , and was the technique of choice here. It is often assumed in classical redox electrochemical experiments that $E_{1/2}$, the half wave potential is equal to the cell potential , E' , for the process giving rise to the voltammetric wave. In the case of ion transfer at the ITIES this is unlikely ever to be the case , as it implies identical difussion coefficients for one ion in two different solvents. There are two approaches to the determination of E' from $E_{1/2}$, the first being the application of Walden's rule [75].

$$D_1 \eta_1 \approx D_2 \eta_2$$

where D is the diffusion coefficient and η the viscosity of solvents 1 and 2. It is assumed here that this rule applies equally to the species under investigation and to the TMA^+ ion , used as an internal reference. The difference in half wave potentials for these two ions may then be used to determine the potential of transfer of the analyte ion.

The alternative approach lies in the determination of the diffusion coefficients of the ion in both solvents , simply by performing the voltammetric experiment twice , once with the analyte initially present in known concentration in each phase. This approach is not possible in all cases as will become clear.

Figure 3.2.2. Potential Distribution at the ITIES.
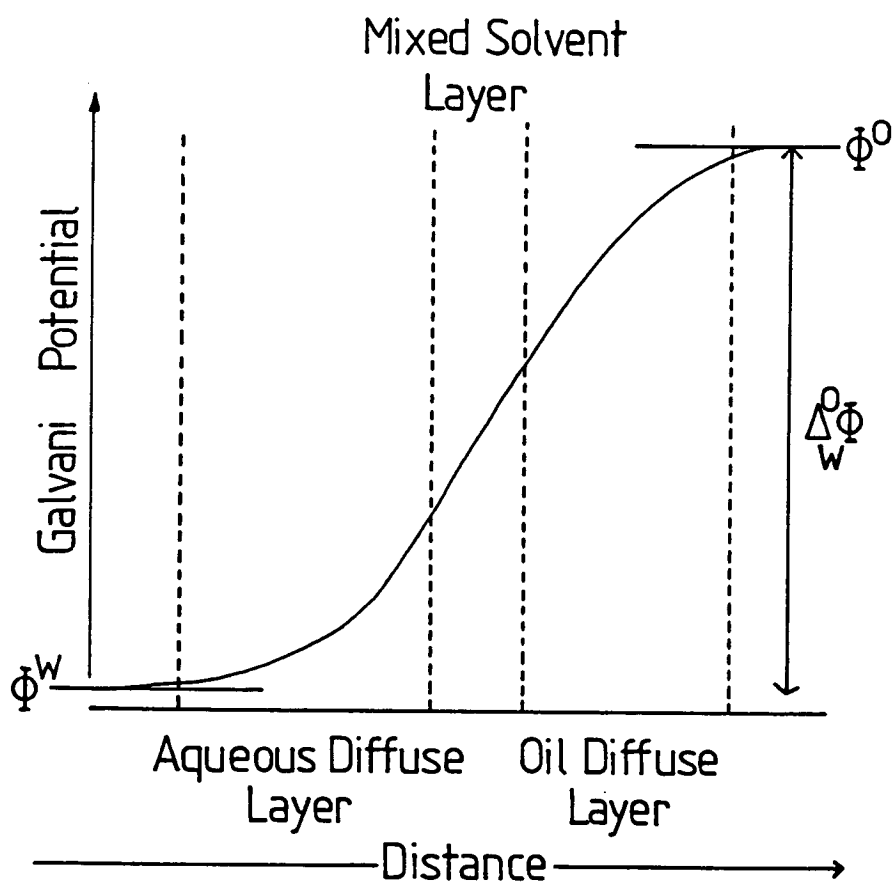
Section 3.2.2.   The Potential Distribution at the ITIES.

There have been several models proposed for the potential distribution across the ITIES , but a comprehensive review of these here would not be appropriate.

The Modified Verwey-Niessen model [77] describes a situation in which an ion free layer of oriented solvent molecules separating two diffuse space-charge regions. Girault and Schiffrin have proposed an alternative model in which the ITIES is described in terms of a mixed solvent layer (see figure 3.2.2) whose thickness is in the order of 100 pm , across which very little of the total potential drop across the ITIES takes place.

Whatever model of the potential distribution at the ITIES is used , for transfer of an ion from the bulk of one solvent to the other it is still true that the potential of transfer corresponds to the difference of the potentials of that ion in the bulk of each solvent:

$$\Delta_2^1\varphi = \varphi_2^0 - \varphi_1^0 = [\mu_1^0-\mu_2^0]/zF = -\Delta G_{tr,i}^{2\to1} /zF$$

Equation 3.2.2.

It can be seen then that allowing for variations in diffusion coefficient with phase transfer , cyclic voltammetry may be used to determine the potential of transfer of an ion from one phase to the other across the ITIES and from this , the free energy of transfer.

Section 3.3.   *In Situ* Electrogeneration Techniques.

A wide range of techniques have been developed to probe the properties of species electrogenerated through bulk electrolysis directly in the location in which the analysis is to take place. This technique obviates the

Figure 3.3.1. Cell for Preparative Electrolysis.
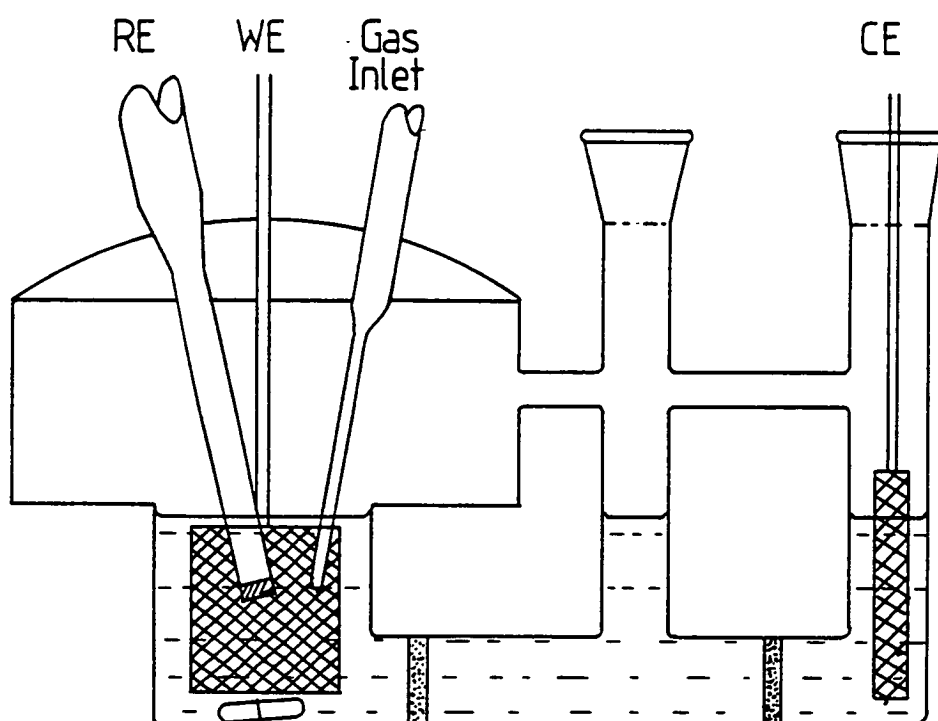
need for a separate isolation or transfer step which may give rise to experimental complications.

Section 3.3.1.   Electrogeneration by Bulk Electrolysis.

Electroanalytical techniques generally involve the passage of only small currents and the oxidation or reduction of only a small fraction of the electroactive species in solution. Bulk electrogeneration involves the use of a large electrode and the electrolysis under either controlled current or controlled potential conditions of all or a large fraction of the electroactive species present. Obviously , if a large current is passed at the working electrode , an equally large and opposite current must be passed at the counter electrode. In order to prevent diffusion of the products of electrolysis at the counter electrode , whose chemical identity is generally not clear , to the region of the working electrode , a salt bridge or fritted glass disks are generally employed. Preparative bulk electrolysis is carried out in a conventional "H" cell , as shown in figure 3.3.1. The products may then be probed electrochemically by means of a platinum minidisc electrode substituted for the basket electrode.

Section 3.4.   The ITIES as a Probe for Electrogenerated Species.

A new technique has been developed , which will be presented here , combining electrogeneration *via* a three electrode arrangement with conventional four electrode voltammetry as a probe to determine the potentials of transfer of the resulting ionic species from 1,2-DCE to water. The bulk electrolysis step is carried out in the organic phase , the adjacent aqueous phase then becoming in effect , a working electrode surface for phase transfer

electrochemistry.

Section 3.4.1.   Supporting Electrolytes.

The choice of organic phase supporting electrolyte was crucial in the development of this new technique , as the compound chosen was required to show the properties both of a redox and a phase transfer electrolyte. Phase transfer electrolytes for the organic phase are usually salts composed of hydrophobic ions , such as tetraaryl borates and tetraphenylarsonium or organic dyes such as crystal violet. Redox electrolytes meanwhile are generally composed of ions whose reduction and oxidation potentials lie at extreme potentials , examples being lithium perchlorate and tetraalkylammonium tetrafluoroborates. The ions chosen to constitute the electrolyte for this technique must then satisfy the requirements for both types of system. Consideration of these constraints led to the choice of bis(triphenylphosphoranylidene)ammonium tetrakis(pentafluorophenyl)borate (BTPPA TPFB) as the organic electrolyte. This compound was found to have no redox activity over the potential range -1.8 to +2.0V *versus* a silver/silver chloride reference electrode at a platinum minidisc electrode in $TBABF_4$ (0.5moldm^{-3}) in dichloromethane. There is however some evidence for reduction of the BTPPA$^+$ cation at extreme negative potentials in highly purified acetonitrile [78].   The preparation of BTPPATPFB is described in appendix 2.

Section 3.4.2.   Experimental Procedure.

The cell constructed for use in these experiments , of active area 2.54 cm^2, is shown in figure 3.4.1. The composition of the aqueous layer was initially LiCl (Fluka puris) 10 mmoldm^{-3} , and the results presented for the ferrocene / ferricenium system were obtained under those

Figure 3.4.1. Cell Constructed for Electrogeneration of Species at the ITIES.
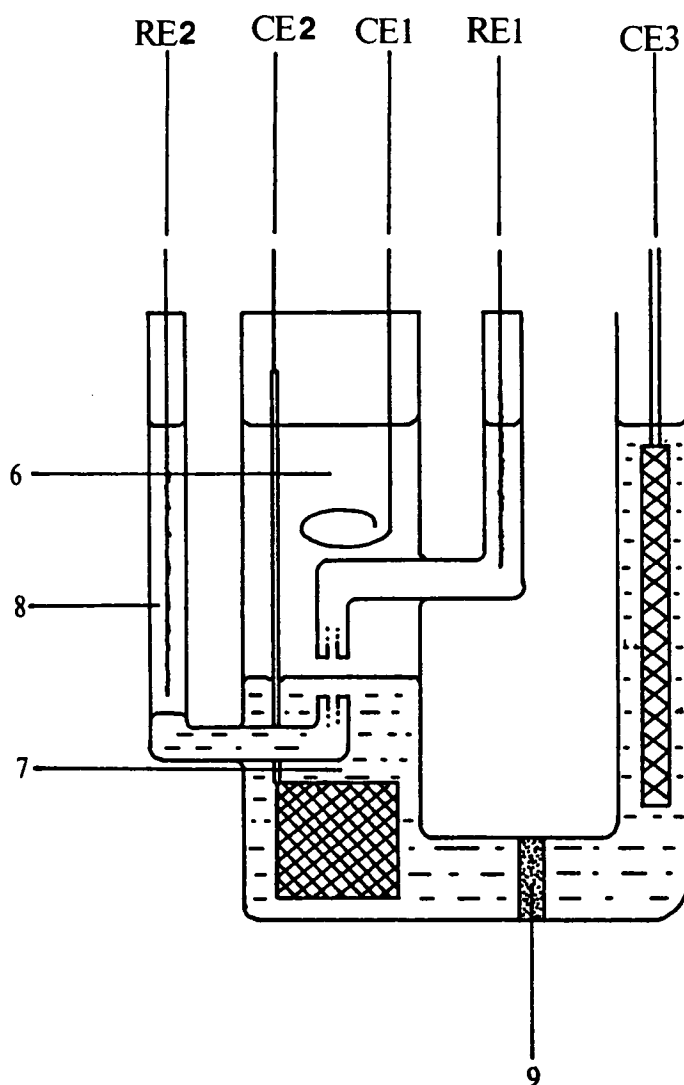
6. Aqueous electrolyte solution. 7. Organic electrolyte solution. 8. Aqueous solution for organic reference electrode. 9. Grade 2 sintered disc, diameter 1cm.

conditions. It was found necessary however to substitute lithium sulphate (*sic*) for the chloride for electrogeneration of systems with more extreme oxidation potentials. This also extends the limits of polarisation of the interface in four electrode mode [79]. Figure 3.3.2. shows the polarisation windows for both systems. The water was purified by reverse osmosis (Milli-RO 15 water purification system) followed by ion exchange (Milli-Q SP reagent water system). The organic layer was composed of BTPPATPFB in 1,2-DCE (BDH , used as received). Various concentrations were investigated before 10 mmoldm^{-3} was set for all experiments. This represented a compromise between the speed of electrogeneration , the limits of polarisability and the scarcity of the electrolyte.

With reference to figure 3.3.1. , the essence of the present approach may be distilled as follows. CE3 , RE2 and CE2 are used as the counter , reference and working electrodes respectively in a bulk electrolysis step separate from , and prior to , the use of CE1 , RE1 , CE2 and RE2 in a conventional four electrode investigation of the system. The electrogeneration step was carried out using a PAR model 170 potentiostat , four electrode experiments with the combined potentiostat / zerostat arrangement described in chapter 2.

The redox active compound to be studied was dissolved in the organic electrolyte in its air stable oxidation state , at a concentration of around 100 μmoldm^{-3}. The aqueous layer was then installed , and a potential some 200mV more extreme than the the couple under study applied to CE2. This , in conjunction with mild agitation of the solution by movement of the working electrode , ensured rapid and complete conversion of the starting material into the electrogenerated product. Once the current between CE2 and CE3 had decayed to a limiting value the cell was reconnected for four electrode operation and

cyclic voltammograms recorded. The temperature of the
system was recorded immediately after the last scan. All
solutions used were deaerated as described in chapter 2.
Ferrocene (Fluka purrum) , 1,1'-di-n-butylferrocene (TCI
99%) and 7,7,8,8-tetracyanoquinodimethane (Aldrich 99%)
were used without further purification. All other
materials were as described in chapter 1.

Section 3.4.3.   Results.

A typical four electrode cyclic voltammetric response
of the system prior to electrolysis is shown in figure
3.4.2. The limits to the window of polarisation are the
transfer of sulphate from aqueous to organic phase at the
positive end and transfer of lithium cations in the same
direction at the negative limit [79].

Figure 3.4.2. Cyclic Voltammograms Prior to
Electrolysis.
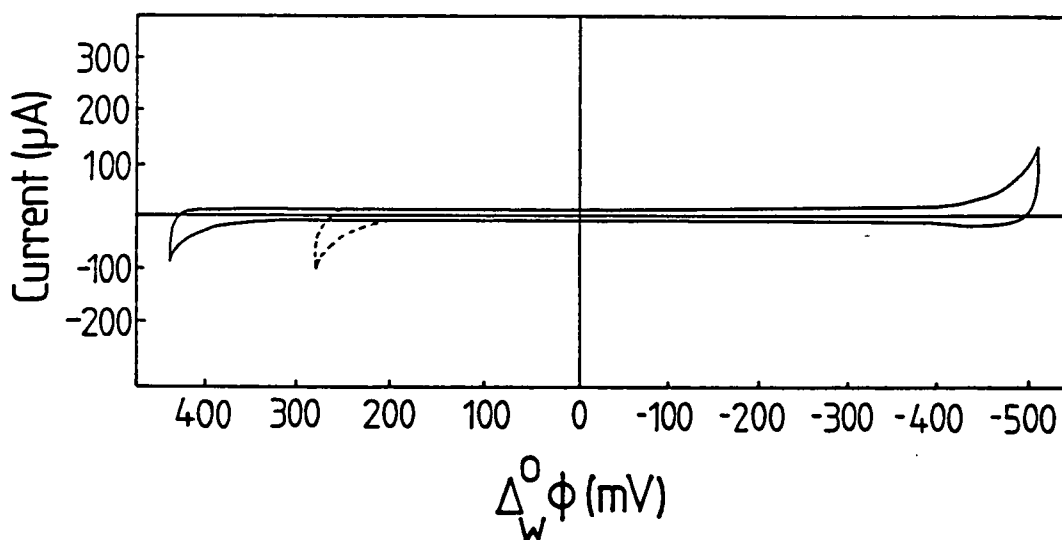
Table 3.4.1. summarises the data derived from the the
three compounds to which this technique was applied
successfuly. These were ferrocene , 1,1'-di-n-butyl-

ferrocene (DNBF) and 7,7,8,8-tetracyanoquinodimethane (TCNQ).

Table 3.4.1. Summary of Voltammetric Results.

Compound	E_{elec}(mV)[#]	Ion Produced	$\varphi_{w}^{o}1/2$ (mV)	$\Delta G_{tr,ion}^{o\rightarrow w}$ (kJmol^{-1})
Ferrocene	+927	Ferricenium	-40	-3.86
DNBF	+1130	DNBF^{+}	+255	+24.6
TCNQ	+570	TCNQ^{-}	-190*	<+18.3

[#] The electrolysis potentials are relative to a reference electrode ; Ag/AgCl/BTPPACl 1mM (aq)/.

* This value is not a half wave potential but an E_{p}^{f} value, the process of transfer being found to be irreversible.

Typical cyclic voltammograms for transfer of each of the ions in table 3.4.1. are shown in figures 3.4.3 to 3.4.5. All are recorded at a sweep rate of 100 mVs^{-1}. Figure 3.4.5. also shows a wave centred on -160 mV , corresponding to transfer of the TMA^{+} ion , added as an internal reference.

All attempts to investigate the transfer of the oxidised and reduced forms of [Ru(bpy)$_{3}$]$^{2+}$ failed. The species could be generated , witnessed by the development of their characteristic colours , but attempts at cyclic voltammetry were confounded by the loss of polarisability of the interface. The reason for this radical change in the voltammetric characteristics of the system was not clear , but may have been due to the incipient breakdown of the solvent at the extreme potentials employed. Because of this failure , and the importance of gaining some

Figure 3.4.3. Cyclic Voltammogram Showing Transfer of the Ferricenium Cation from 1,2-DCE to Water.
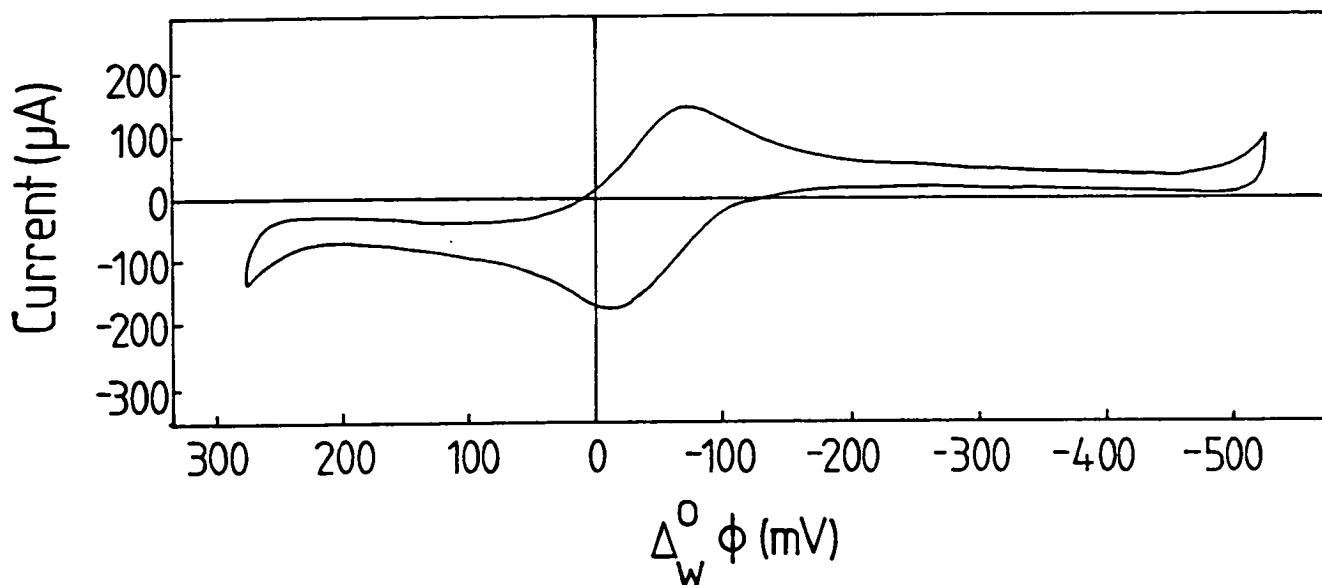
Figure 3.4.4. Cyclic Voltammogram Showing Transfer of the 1,1'-Di-n-butylferricenium Cation from 1,2-DCE to Water.
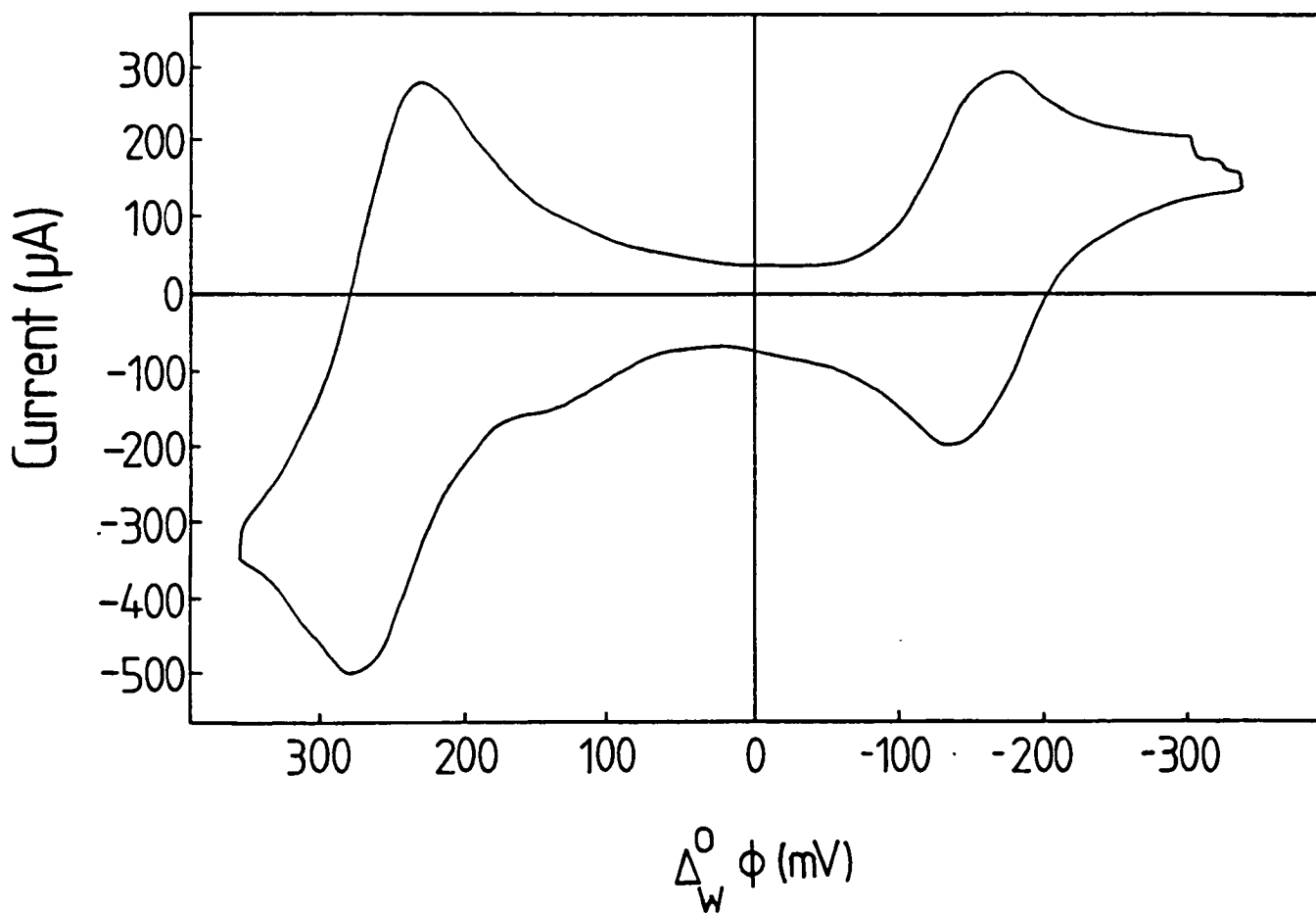
Figure 3.4.5. Cyclic Voltammogram Showing Transfer of the Radical Anion of 7,7,8,8-tetracyanoquinodimethane from 1,2-DCE to Water.
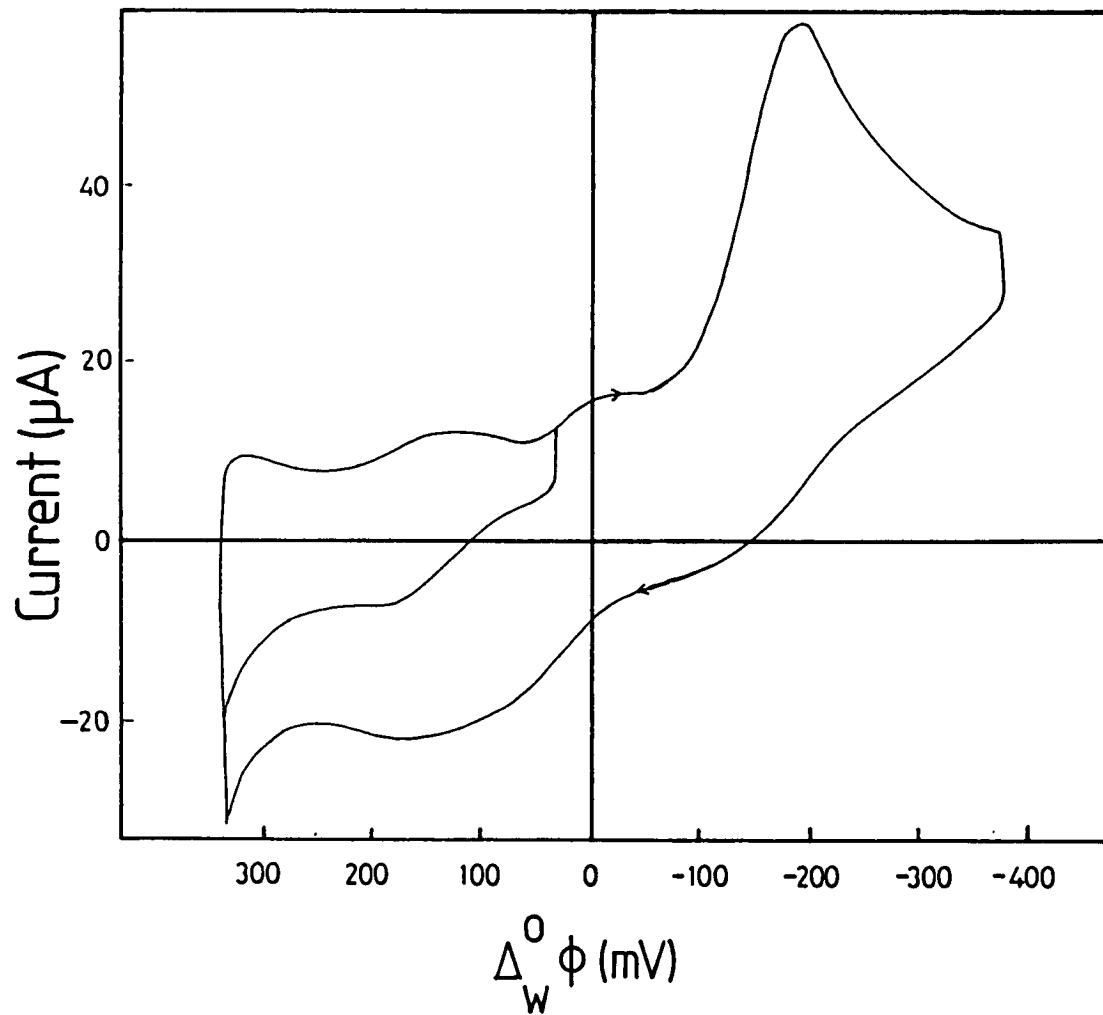
insight into this system , it was decided to adopt the approach of chemical synthesis and isolation.

[Ru(bpy)$_3$]$_2$[SO$_4$]$_3$ was synthesised as described in appendix 2. A four electrode cell was set up so;

Ag/AgCl/BTPPACl 1mM(aq)/BTPPA TPFB 10mM

/H$_2$SO$_4$ 10mM/AgCl/Ag'

Cell 3.1

The oxidised ruthenium complex is unstable in neutral or alkaline aqueous solution with respect to conversion to the Ru(II) species , hence the need for the the acidic aqueous phase. The concentration of the acid was chosen as a compromise between the voltammetric response of the system and the stability of the oxidised species. The resulting cyclic voltammogram is shown in figure 3.4.6. , together with the background voltammogram for this system.

Figure 3.4.6. Cyclic Voltammogram Showing Transfer of [Ru(bpy)$_3$]$^{3+}$ from Water to 1,2-DCE.

74
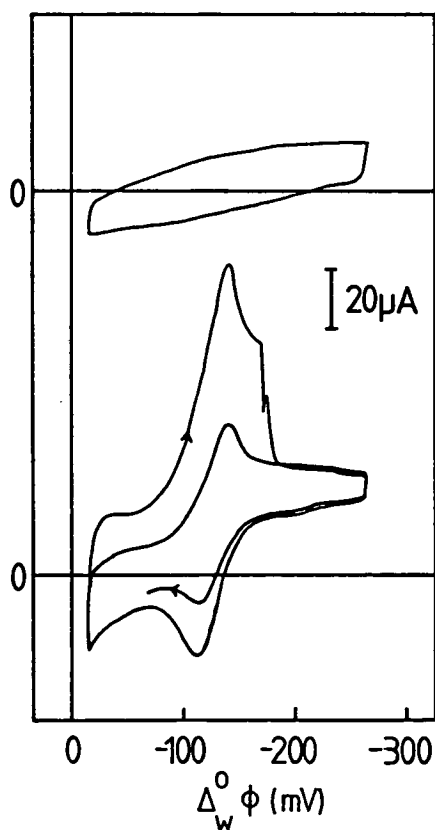
Figure 3.4.7. Cyclic Voltammogram for Cell 3.2.

$$\Delta_0^W \phi - \Delta_0^W \phi^0_{TMA^+} \text{ (mV)}$$
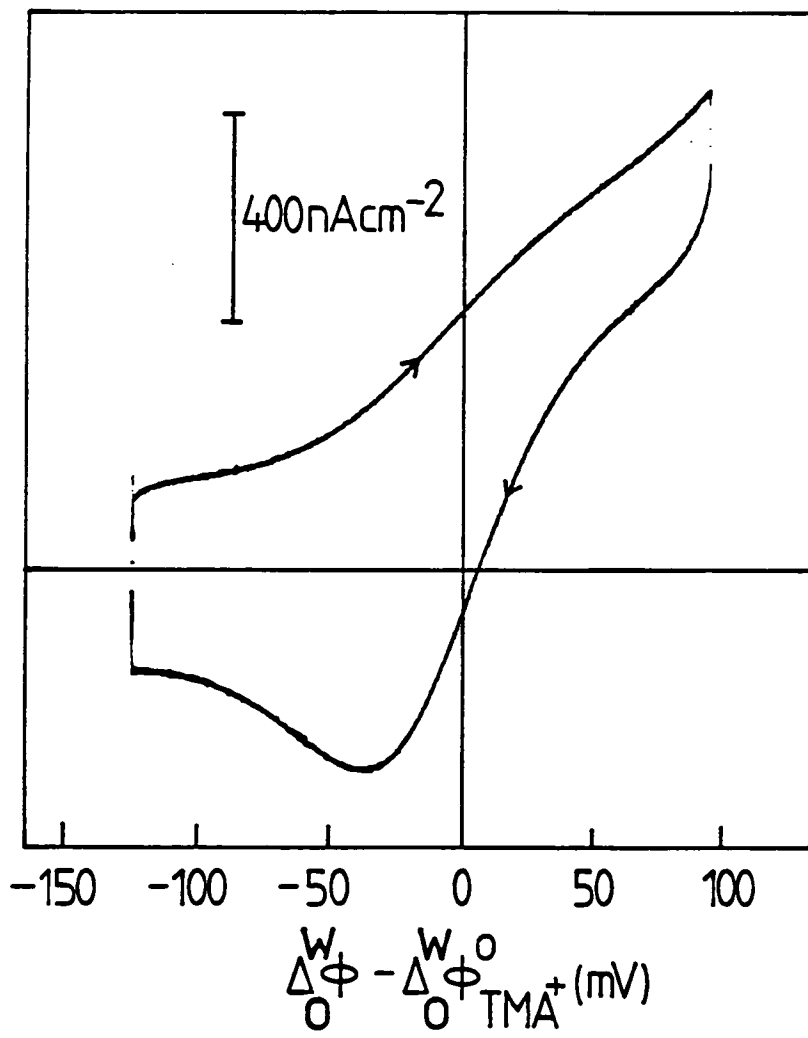
The free energy of transfer of ferrocene between water and 1,2-DCE was determined from solubility measurements. A saturated solution of ferrocene in 1,2-DCE at 293K was prepared and a sample of this filtered to remove excess solid and delivered to a 25ml standard flask. This solution was transfered to a preweighed Schlenk tube and the solvent removed under vacuum at room temperature. The tube was then reweighed. From these measurements a solubility of 0.524 $moldm^{-3}$ was determined. The reported value for the solubility of ferrocene in water [71] allows an approximate value of the free energy of transfer of ferrocene between the two solvents to be calculated from;

$$\Delta G_{tr,neut}^{w \rightarrow o} = -RT \ln(a^{o,sat}/a^{w,sat}) \approx -RT \ln(c^{o,sat}/c^{w,sat})$$

Equation 3.4.1.

substitution of the appropriate values leads to a value of $\Delta G_{tr,neut}^{w \rightarrow o}$ of -25.6 $kJmol^{-1}$.

The following cell was set up

$$\text{Ag/AgCl/}\quad\begin{array}{cc} & \text{ferrocene} \\ 10 \text{ mmoldm}^{-3} \text{ KCl} & 0.1 \text{ mmoldm}^{-3} \\ 10 \text{ mmoldm}^{-3} \text{ K}_4\text{FeCN}_6 /\!\!/ 10 \text{ mmoldm}^{-3} \\ 10 \text{ mmoldm}^{-3} \text{ K}_3\text{FeCN}_6 & \text{TBATPFB} \\ /10 \text{ mmoldm}^{-3} \text{ TBACl/AgCl/Ag'} \end{array}$$
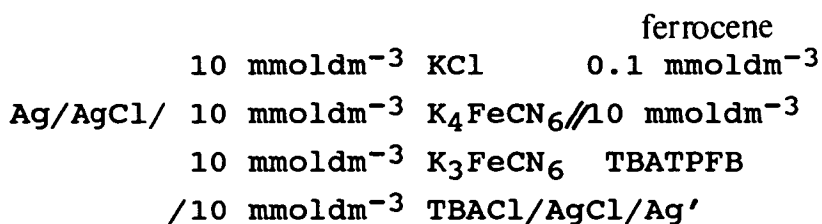
Cell 3.2

A cyclic voltammogram , at a sweep rate of 5 mVs^{-1} , for cell 3.2 is shown in figure 3.4.7. , showing the wave corresponding to the heterogeneous oxidation of ferrocene by hexacyanoferrate (III).

Section 3.5.   Discussion.

The results presented show that the technique of ion transfer of electrogenerated species , for which the author proposes the acronym EGSIT , at the ITIES is a valuable technique , allowing the direct determination of parameters whose determination by less direct means might prove irksome or even impossible.

Section 3.5.1.   Ferrocene

As a demonstration of the utility of such data in the analysis of electron transfer at the ITIES , we may consider the oxidation of ferrocene by hexacyanoferrate(III) at the water / 1,2-DCE interface. For this process a thermodynamic cycle may be constructed as shown in figure 3.5.1.

Figure 3.5.1.   _Thermodynamic Cycle for Oxidation of Ferrocene by Hexacyanoferrate(III) at the ITIES

$$
\begin{array}{ccc}
\text{[FeC](o)} + \text{[Fe(CN)}_6\text{]}^{3-}\text{(w)} \underset{\xrightarrow{\hspace{1cm}}}{\overset{\Delta G^0_{het}}{\rightleftharpoons}} & \text{[FeC]}^+\text{(o)} + \text{[Fe(CN)}_6\text{]}^{4-}\text{(w)} \\
\Big\downarrow \Delta G^{o\to w}_{tr,neut} & \Big\downarrow \Delta G^{o\to w}_{tr,ion} \\
\overset{\Delta G^0_{hom}}{} & \\
\text{[FeC](w)} + \text{[Fe(CN)}_6\text{]}^{3-}\text{(w)} \underset{\xrightarrow{\hspace{1cm}}}{\rightleftharpoons} & \text{[FeC]}^+\text{(w)} + \text{[Fe(CN)}_6\text{]}^{4-}\text{(w)}
\end{array}
$$
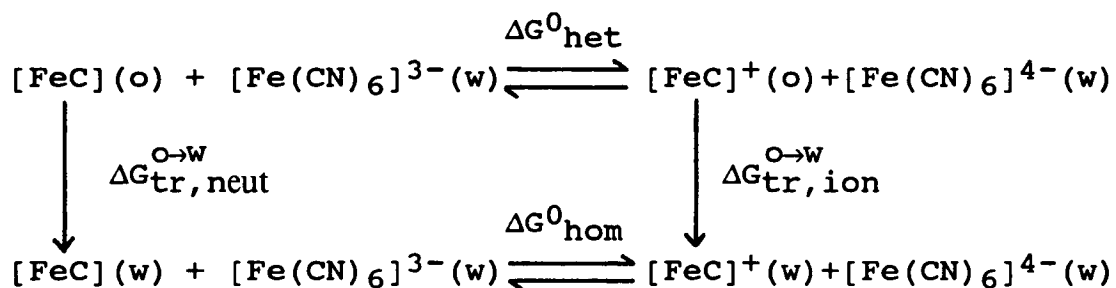
This figure shows the relationship between the free energy changes for homogeneous and heterogeneous electron transfer and the free energies of transfer of the neutral and oxidised forms of ferrocene. It can be seen then that;

$$\Delta G^0_{het} = \Delta G^0_{hom} - \Delta G^{0,O\to W}_{tr,ion}[FeC]^+ + \Delta G^{0,O\to W}_{tr,neut}[FeC] \quad \text{Eqn. 3.4.1.}$$

which is a specific case of the general relation for electron transfer at the ITIES [80];

$$\Delta^\beta_\alpha \varphi = E^{0,\alpha} - E^{0,\alpha} + (\Delta G^{\alpha\to\beta}_{tr,R2} - \Delta G^{\alpha\to\beta}_{tr,O2})/zF \quad \text{Eqn. 3.4.2.}$$

Figure 3.4.7. shows the wave corresponding to the heterogeneous oxidation of ferrocene by hexacyanoferrate (III) in cell 3.2. It is sure that the value of $E_{1/2}$ for this experiment is the same as the formal potential for this reaction because *pseudo* first-order conditions have been achieved [76]. That is to say that the aqueous redox couple is present in one hundredfold excess and both halves of this couple are present in equimolar amounts. The wave obtained is not well formed , but a half wave potential *relative to the transfer potential of TMA$^+$* of -0.005V could be determined.

Equation 3.4.2. may be rewritten for this affair;

$$\Delta^{DCE}_{H2O}\varphi^0 = E^{0,H2O}_{[Fe(CN)6]3-/4-} - E^{0,H2O}_{FeC/FeC+} + [\Delta G^{0,H2O\to DCE}_{tr,neut}/nF] + \Delta^{DCE}_{H2O}\varphi^0_{FeC+}$$

Equation 3.4.3.

Using then the value for the potential of transfer of the ferricenium ion, *again relative to that of TMA$^+$* , $\Delta^{DCE}_{H2O}\varphi_{FeC+}$, determined here to be -120 mV , then the oxidation potential of ferrocene in water may be calculated without recourse to any extrathermodynamic assumption. Using the known value for the standard potential of the hexacyanoferrate (II/III) couple in water of 0.413V *versus* the NHE [81], the oxidation potential of ferrocene in water is calculated to be 0.532V *versus* the NHE. This figure is not outrageously different to that reported for the oxidation of ferrocene on platinum in

water of 0.400V [81].

Equation 3.4.3. may be rewritten for any other pair of redox couples joined in a heterogeneous reaction;

$$\Delta_{H2O}^{DCE}\varphi^0 = E_{O1/R1}^{0,H2O} - E_{O2/R2}^{0,H2O} + [\Delta G_{tr,R2}^{0,H2O\to DCE}/nF] + \Delta_{H2O}^{DCE}\varphi_{O2}^0$$

Equation 3.4.4.

where the standard potential for the O1/R1 couple is taken relative to the NHE and that for the O2/R2 couple is reported relative to the ferrocene/ferricenium couple in solvent 2. This is in accordance with standard rules for the reporting of potentials in non-aqueous solvents [82]. The transfer potential for species O2 is then reported relative to that for the ferricenium cation , which seems a logical extension of the rules for redox potentials. A new scale is thus created allowing easy calculation of the potentials for heterogeneous electron transfer reactions

Section 3.5.2.   Transfer of DNBF$^+$.

Cyclic voltammograms for transfer of DNBF$^+$ across the water / 1,2-DCE interface, as shown in figure 3.4.4. , show a clear and reproducible prepeak , possibly corresponding to transfer of adsorbed DNBF$^+$. If this is so , then adsorbed product molecules formed in heterogeneous electron transfer may well lower the effective area of the interface and thus the observed current densities. Such an effect has indeed been observed using the hexacyanoferrate (II/III) couple in water [83].

Section 3.5.3.   Transfer of TCNQ$^-$.

The transfer of this ion across the water , 1,2-DCE interface is clearly irreversible. This almost certainly stems from the reaction of the radical ion with the

aqueous phase. The waves in figure 3.4.5. lying to higher potential than the large irreversible wave corresponding to TCNQ⁻ transfer may well then correspond to transfer of the products of decomposition of TCNQ⁻ in water.

Section 3.5.4.   Transfer of $[Ru(bpy)_3]^{3+}$.

The cyclic voltammogram obtained after addition of $Ru(bpy)_3^{3+}$ to the aqueous phase of cell 3.1 shows a wave with a peak to peak separation of 20mV , the value expected at 293K for a wave corresponding to reversible transfer of a tripositive species or heterogeneous transfer of three electrons. This wave was observed to diminish as the characteristic green colour of the Ru(III) complex was replaced by the yellow of the Ru(II) form.

It seems unlikely that in the absence of any electron donor in the organic phase the observed wave corresponds to an electron transfer process. Far more likely is the transfer of the Ru(III) complex across the interface. The position of the wave some 214mV more negative than that for transfer of the $[Ru(bpy)_3]^{2+}$ species allows calculation of the potential of transfer of -124 mV (see chapter 6.) , and thus a free energy of transfer , $\Delta G_{tr,ion}^{O \rightarrow W}$ = -35 kJmol⁻¹. This must be regarded as only an approximate value due to the instability of this species in water and the fact that this value is based on one experiment only. This value may be compared with that for the Ru(II) species of $\Delta G_{tr,ion}^{O \rightarrow W}$ = 17.3 kJmol⁻¹ (see Chapter 6.). Presumably the huge difference in the values for the two ions stems from the increased water/ion interactions for a tripositive species , as these two ions will have quite similar sizes , which will lead to similar values for the cavitation free energies in both solvents.

The value determined for the potential of transfer of the Ru(III) species shows conclusively that the experiments of Maracek [59] are carried out at a potential

at which this ion will spontaneously cross the interface ,
leading to an ion transfer current , complicating the
analysis beyond that which is presented.

References.

70. J. Hanzlik, J. Hovorka, Z. Samec, and S. Toma , Coll. Czeck. Chem. Com. 53(1988)903

71. J. Hanzlik , Z. Samec and J. Hovorka, J. Electroanal. Chem. 216(1987)303

72. G. Geblewicz and D.J. Schiffrin, J. Electroanal. Chem. 244(1988)27

73. V.J. Cunnane, D.J. Schiffrin, C. Beltram, G. Geblewicz and T. Solomon, J. Electroanal. Chem. 247(1988)203

74. S. Kihara , M. Suzuki, K. Maeda, K. Ogura, M. Matoui and Z. Yoshida, J. Electroanal. Chem. 271(1989)107

75. H. Matsuda and Y. Ayabe, Z. Electrochem., 59(1955)494

76. A.A. Stewart, J.A. Campbell, H.H. Girault and M. Eddowes, Ber. Bunsenges. Phys. Chem. 94(1990)83

77. C. Gavach, P. Seta and B.D'Epenoux, J. Electroanal. Chem., 83(1977)225

78. S.A. Macgregor, Personal Communication.

79. A.A. Stewart , Y. Shao, C.M. Pereira and H.H.Girault, J. Electroanal. Chem., in press

80. H.H.J. Girault and D.J. Schiffrin, J. Electroanal. Chem., 244(1988)15.

81. H.M. Koepp, H.Wendt and H. Strehblow, Z.Elektrochem., 64(1960)483.

82. G. Gritzner and J. Kuta, Recomendations on Reporting Electrode Potentials, Commission on Electrochemistry.

83. J.A. Campbell , PhD Thesis , University of Edinburgh (1991)

CHAPTER FOUR

Photosensitised Ion Transfer at the ITIES

I can make no boast of having contrived this ruse intentionally ; it is simply the remains of one of my many abortive building attempts, but finally it seemed to me advisable to leave this one hole without filling it in.

Franz Kafka "The Burrow"

Section 4.1.   Introduction.

In order to predict the potentials at which interfacial photoinitiated electron transfer should occur some information is required on the potential for interfacial transfer of the excited state sensitiser itself. In an attempt to observe the transfer of the $[Ru(bpy)_3]^{2+*}$ ion between water and 1,2-dichloroethane , the following cell was set up;

Ag/AgCl/

$[Ru(bpy)_3][Cl]_2(1 \text{ mmoldm}^{-3})(aq)/$

$[Ru(bpy)_3][TPBCl]_2(5 \text{ mmoldm}^{-3})(DCE)$

$//LiCl(10 \text{ mmoldm}^{-3})(aq)/AgCl/Ag'$
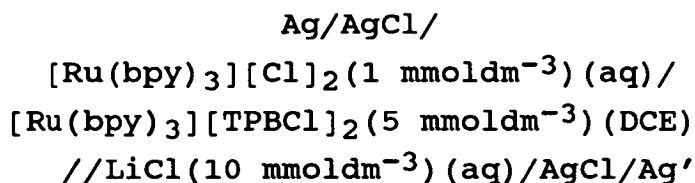
Cell 4.1

It was hoped that irradiation of the organic layer would lead to observation of a current corresponding to transfer of excited state ions from organic to aqueous phase. Hamnett *et al* [52] have observed the oxidation of this species at a titanium (IV) oxide semiconductor electrode , a phenomenon giving rise to currents in the nanoampere range , and it was hoped that a diffusion controlled ion transfer current of this magnitude could be

observed at the ITIES. The mean path length of an excited species is given approximately by $(2\tau D)^{1/2}$ where τ is the lifetime, D the diffusion coefficient of the excited species. Using a value of 600ns for τ and 2.8×10^{-6} $cm^2 s^{-1}$ for D (ie the value for the ground state ion determined in Chapter 6) leads to a value of 18nm for the path length. This value is quite large enough to allow transfer of the excited ion from the bulk of one solvent to the other.

What in fact transpired was that upon illumination of the interface a current much larger than , and in the opposite direction to , that expected was recorded. This fact was interpreted , for reasons to be discussed later in this chapter , on the basis of a new phenomenon of photosensitised ion transfer across the ITIES.

Photocurrents claimed to result from the reaction of tetraarylborates with excited dyes have been previously reported. Meyer *et al* [84] described a system in which methyl viologen was used as a sensitiser in the photo-oxidation of the tetraphenylborate anion , present as counter ion in acetonitrile solution. A photocurrent was generated at a platinum mesh electrode from reoxidation of the reduced viologen species generated in the photoreaction.

Kuzmin and Kotov [85] have described the use both of protoporphyrin IX to generate the radical anions of quinones and quinones themselves to photo-oxidize TPB⁻ at the liquid / liquid interface. Both these systems were reported to give rise to photocurrents corresponding to transfer of negative charge from the organic to the aqueous phase. The species carrying the negative charge was , in the case of the photoreduction of quinones by protoporphyrin IX , identified as the quinone radical anion.

Section 4.1.1.   Experimental.

84

The experimental procedures , materials and equipment used are the same as those detailed in Chapter 2 , with the following additions. NMR spectra were recorded on the Bruker WP 200 SY instrument. $[Ru(bpy)_3][TPBCl]_2$ and $[Ru(bpy)_3][TPFB]_2$ were prepared as described in appendix 2. Fresh solutions were used for each experiment , and an interfacial potential of -200 mV was used for all measurements unless otherwise stated.

Section 4.2.   Results.

Illumination of cell 4.1 from above resulted in a photocurrent , the typical development with time of which is shown in figure 4.2.1.

Figure 4.2.1.   Typical Photocurrent-Time Transient for Cell 4.1.
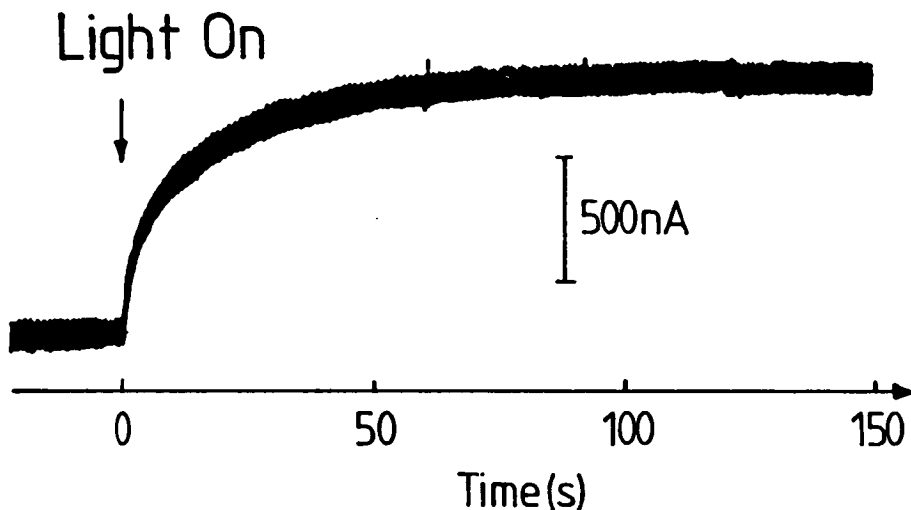
The scheme used in the analysis of the photocurrent -time transients is the same as that used in chapter 2. The signal was found to be independent of the concentration and nature of the supporting electrolyte in the aqueous phase. The use of HCl instead of LiCl also had no effect on the photocurrent recorded. Saturation of the solutions with argon prior to use , however , resulted in

a tenfold increase of the signal compared to a cell
assembled with air saturated solutions.

A cyclic voltammogram showing the typical limits of
polarisability of cell 4.1 is shown in figure 4.2.2. The
response of the photocurrent to variation in the intensity
and wavelength of the incident radiation is shown in
figures 4.2.3. and 4.2.4. The response to alterations of
the concentrations of the ruthenium complex and of TPBCl$^-$
are shown in figures 4.2.5. and 4.2.6. The effect of the
applied interfacial potential difference on i_{lim} is shown
in figure 4.2.7.

The data in figure 4.2.5. were obtained by adding
[Ru(bpy)$_3$]$^{2+}$ as its TPFB$^-$ salt to a stock solution of
TBATBPCl (21.1 mmoldm^{-3}) in 1,2-DCE. The TPFB$^-$ salt , if
used in place of the TPBCl$^-$ salt in cell 4.1 gives rise
only to very small photocurrents (see Chapter 5.) which
may only be detected by the use of chopped light and a
lock-in analyser. Data for figure 4.2.6. were obtained by
addition of TBATPBCl to a stock solution of [Ru(bpy)$_3$]
[TPFB]$_2$ (1.8 mmoldm^{-3}) in 1,2-DCE.·

Carbon-13 NMR spectra are shown in figure 4.2.8. for
[Ru(bpy)$_3$][TPFB]$_2$ in an argon saturated mixture of 1,2-DCE
and CD$_2$Cl$_2$ before and after irradiation of the tube for 24
hours with light of wavelength 450 nm. Fluorine-19 NMR
spectra for [Ru(bpy)$_3$][TPFB]$_2$ subjected to the same
treatment were identical before and after illumination.
Figure 4.2.9. shows the UV-Vis. spectrum of a solution of
[Ru(bpy)$_3$][TPBCl]$_2$ (0.1 mmoldm^{-3}) in argon saturated
1,2-DCE before (A) and after (B) irradiation for twelve
hours with light of wavelength 450 nm. Figure 4.2.10.
shows the UV-Vis spectrum of TBATPBCl in 1,2-DCE and
iodoethane. The responses of TBATPBCl and TBATPB to cyclic
voltammetry at a platinum minidisc electrode are shown in
figures 4.2.11. and 4.2.12.

Section 4.3.   Discussion.

Figure 4.2.2. Cyclic Voltammogram for Cell 4.1.

$$\Delta_W^O \phi \text{ (mV)}$$
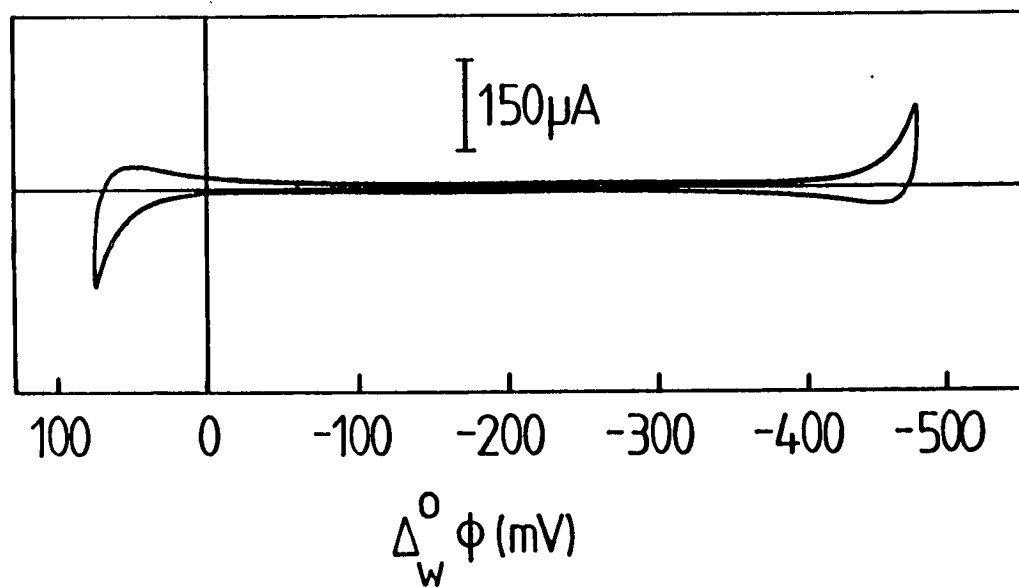
Figure 4.2.3.   Variation of limiting photocurrent for Cell 4.1 with incident   light intensity.
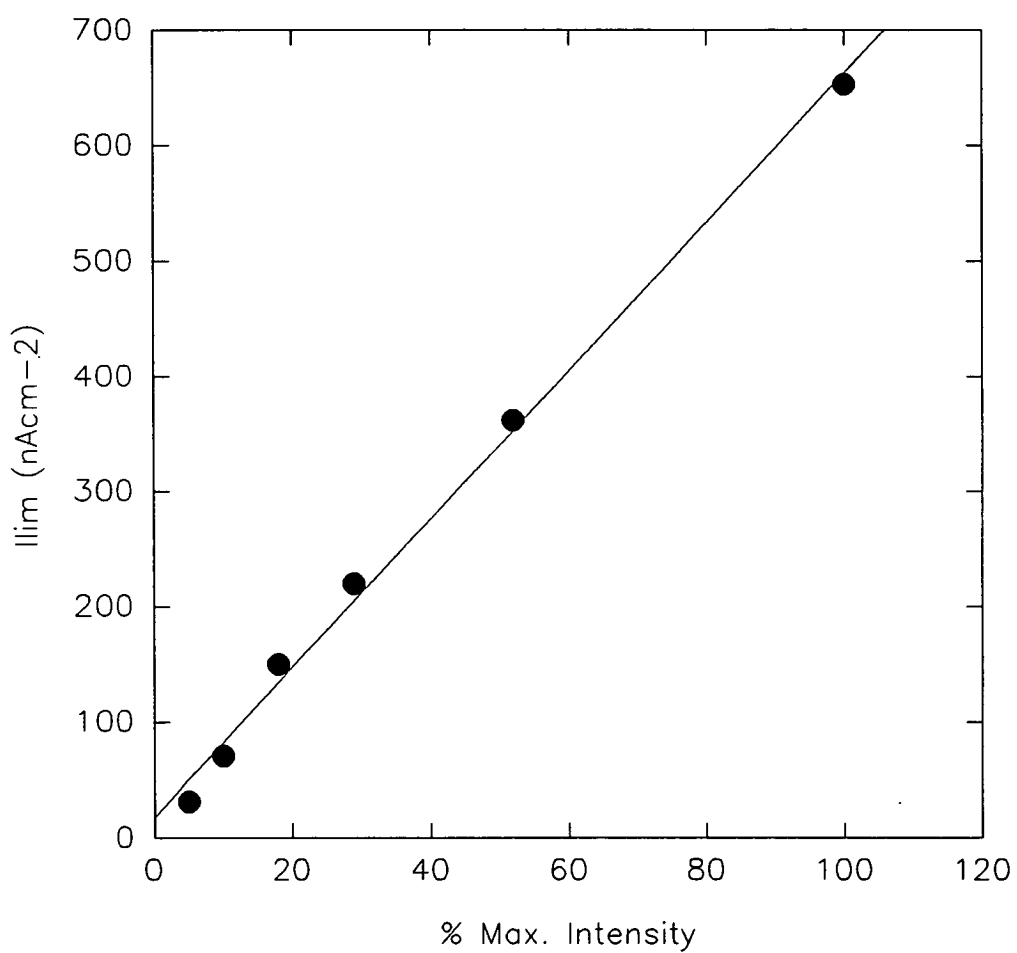
Figure 4.2.4. Action Spectrum , Corrected for Lamp Emission , for the Signal for Cell 4.1.
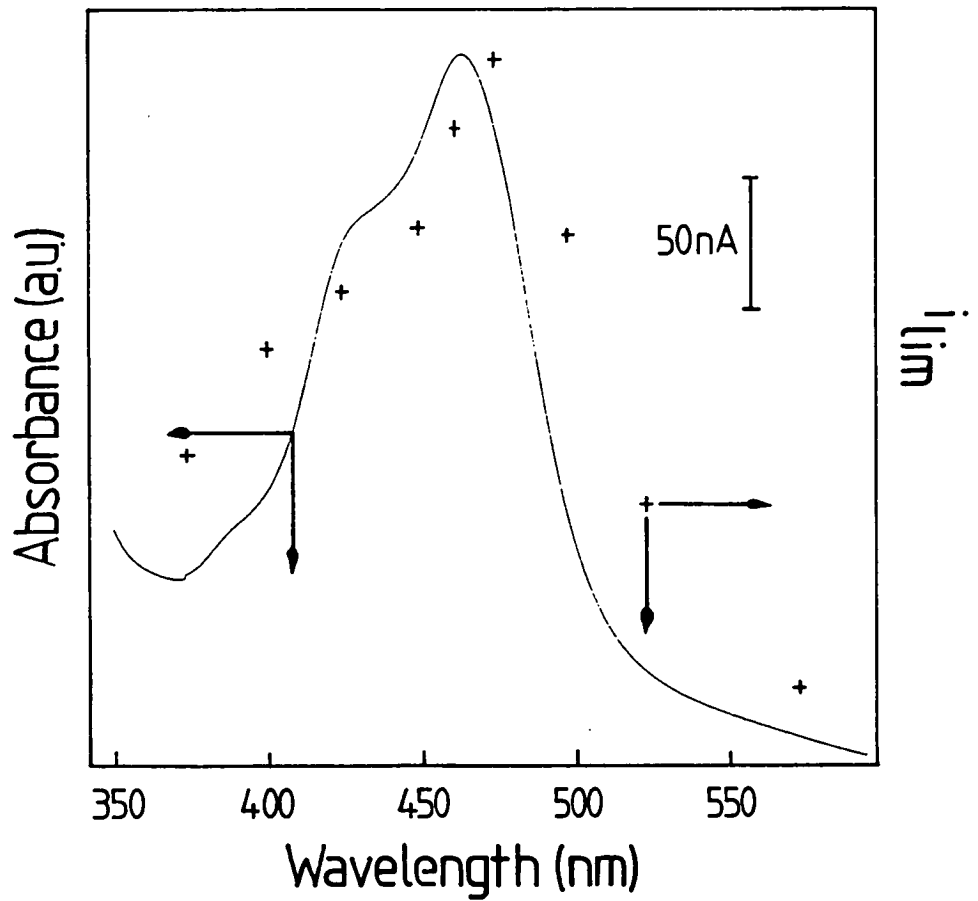
Figure 4.2.5.   Variation of the limiting photocurrent for cell 4.1 with concentration of the sensitiser.
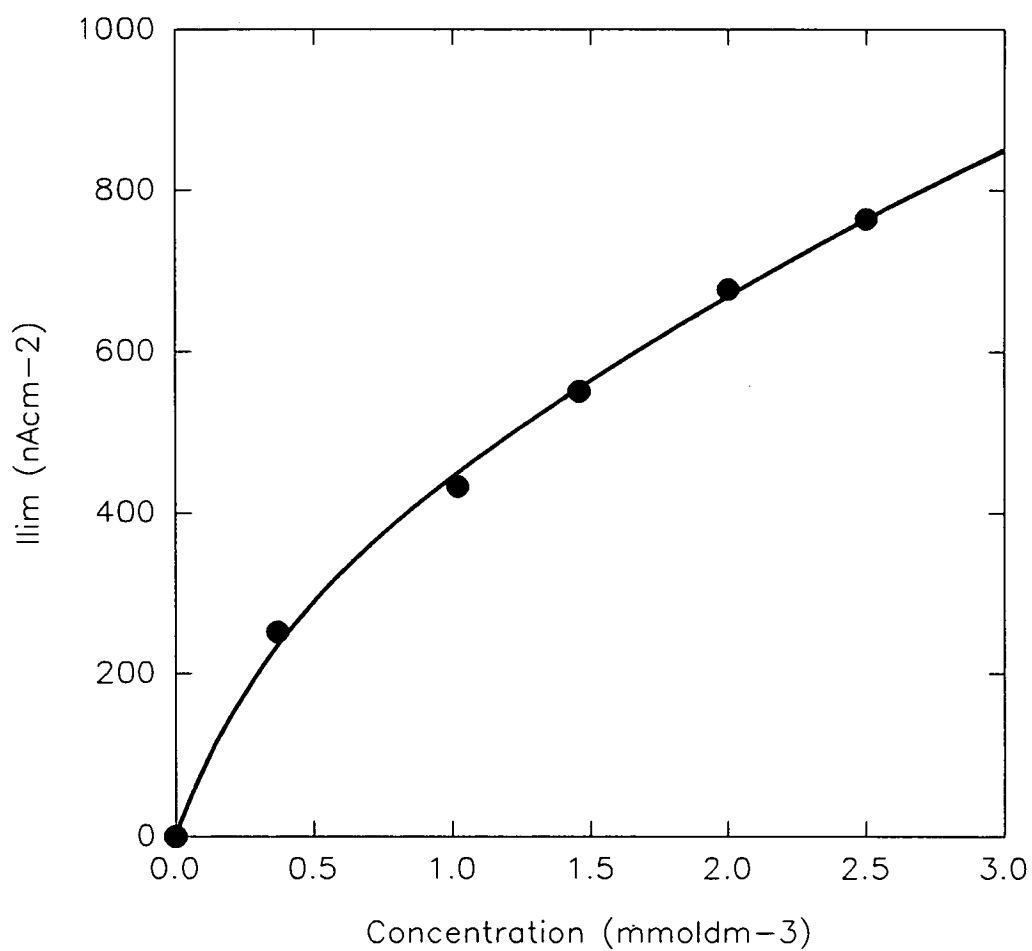
Figure 4.2.6. Variation of the Limiting Photocurrent for
Cell 4.1 with Concentration of TBATPBCl.
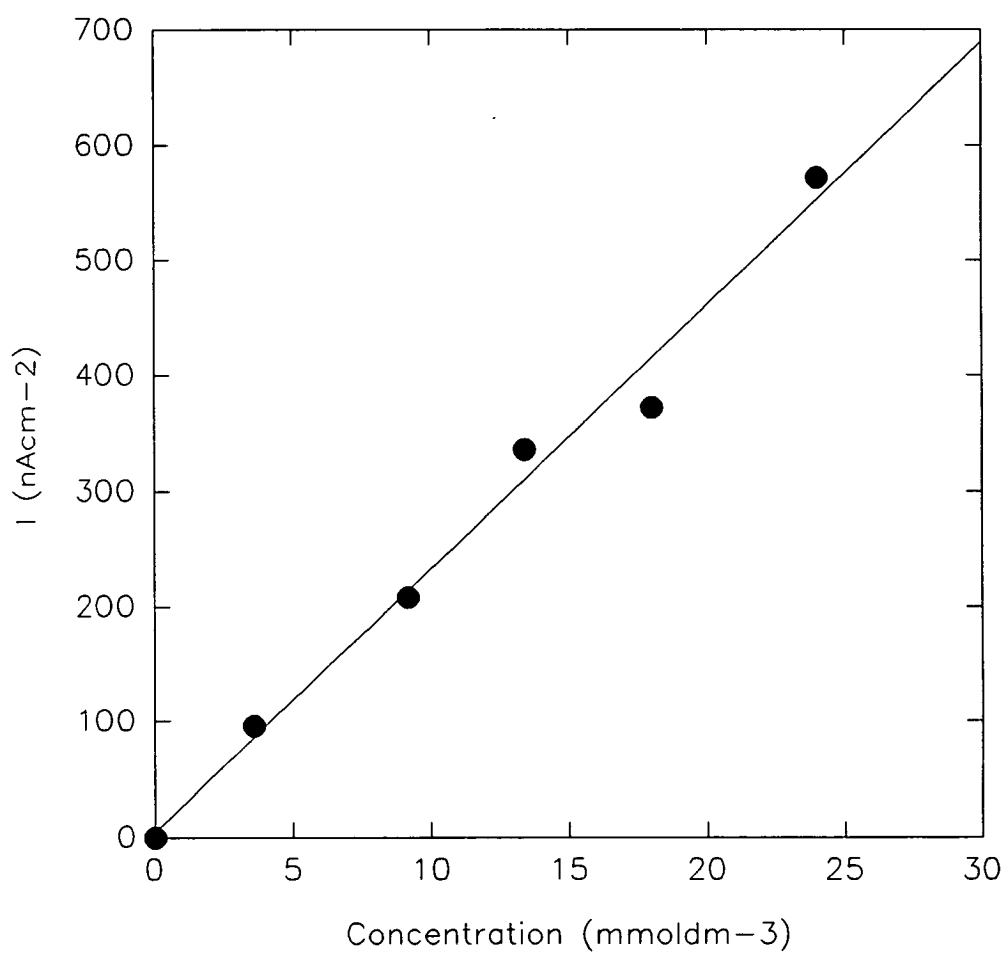
Figure 4.2.7. Variation of the limiting photocurrent for cell 4.1 with interfacial potential difference..
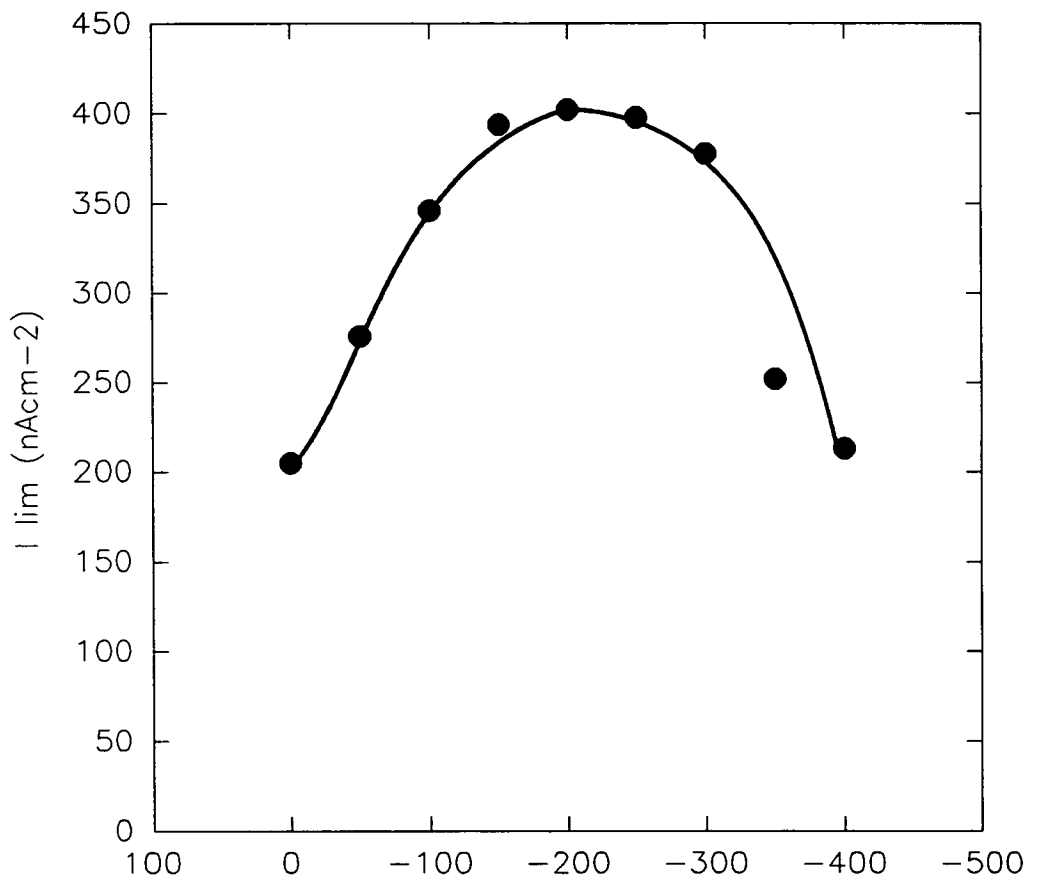
Figure 4.2.8. ^{13}C-NMR Spectra for $[Ru(bpy)_3]^{2+}[TPBCl]_2^-$ Before and After Irradiation.

CHEMICAL SHIFT
(ppm)
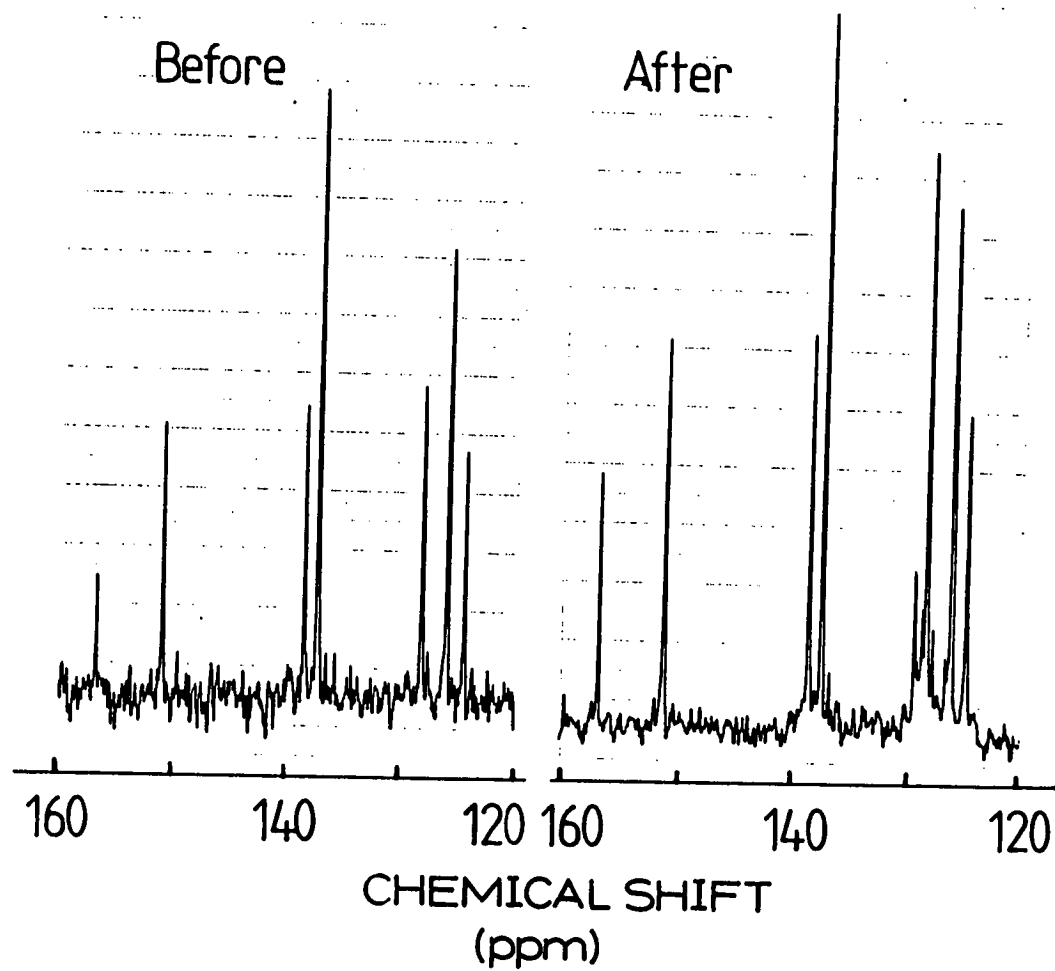
Figure 4.2.9. UV-Vis. Spectrum of $[Ru(bpy)_3]^{2+}[TPBCl]_2^-$ (0.1 mmoldm^{-3}) in 1,2-DCE , Before and After Irradiation.
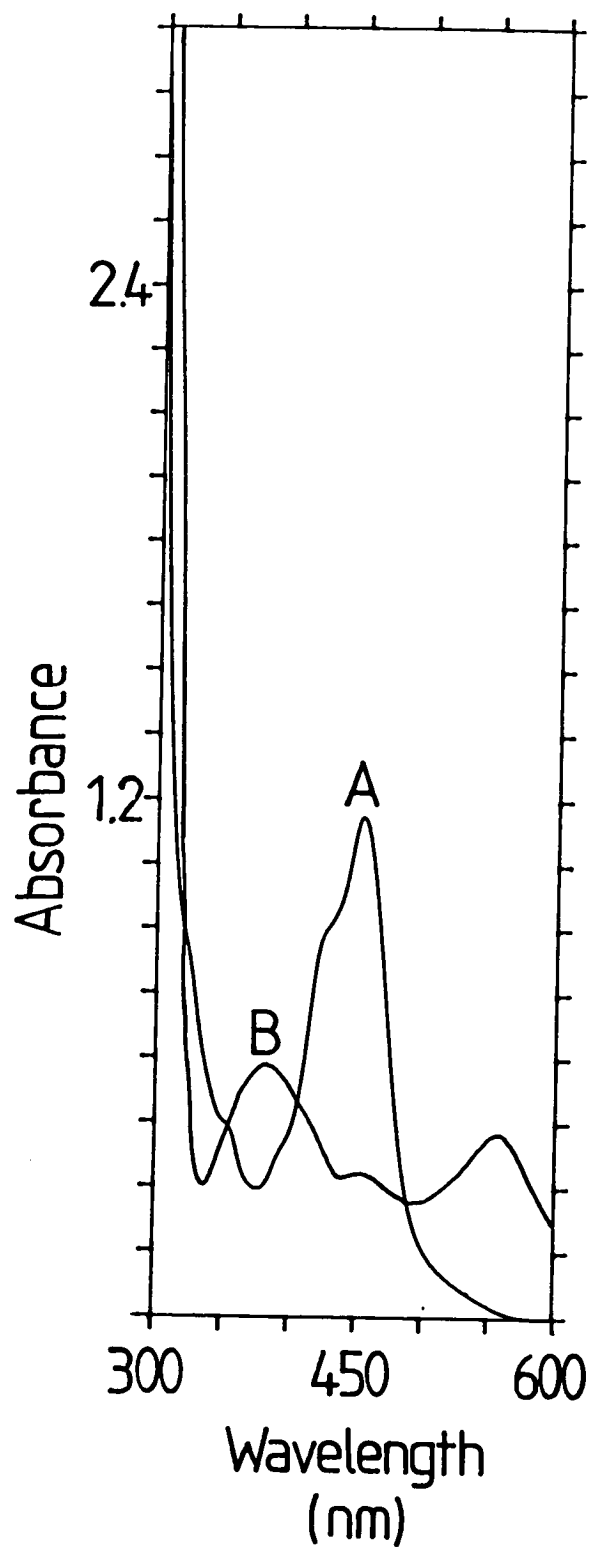
Figure 4.2.10. UV-Vis. Spectra for A. TBATBPCl in Iodoethane B. Pure Iodoethane and C. TBATPBCl in 1,2-DCE.
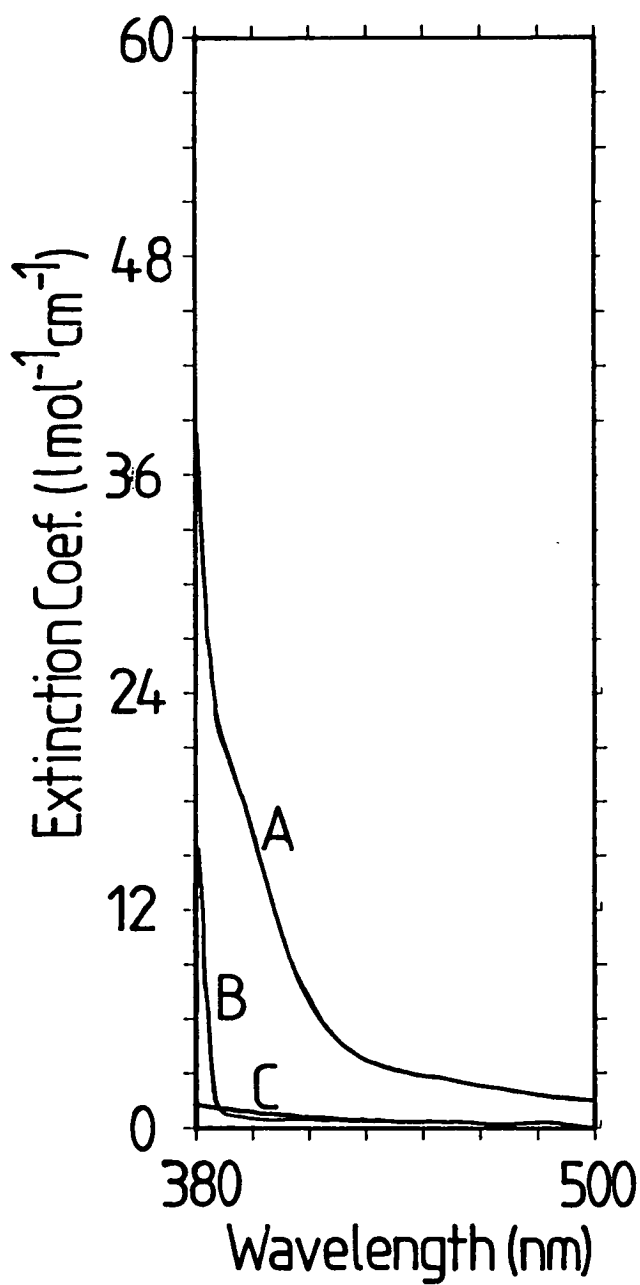
Figure 4.2.11. Cyclic Voltammogram for TBATPBCl in TBABF$_4$ (0.5 moldm^{-3}) in Dichloromethane.

Potentials are quoted *versus* Ag/AgCl/TBACl(0.05moldm^{-3}) + TBABF$_4$(0.45moldm^{-3})/.
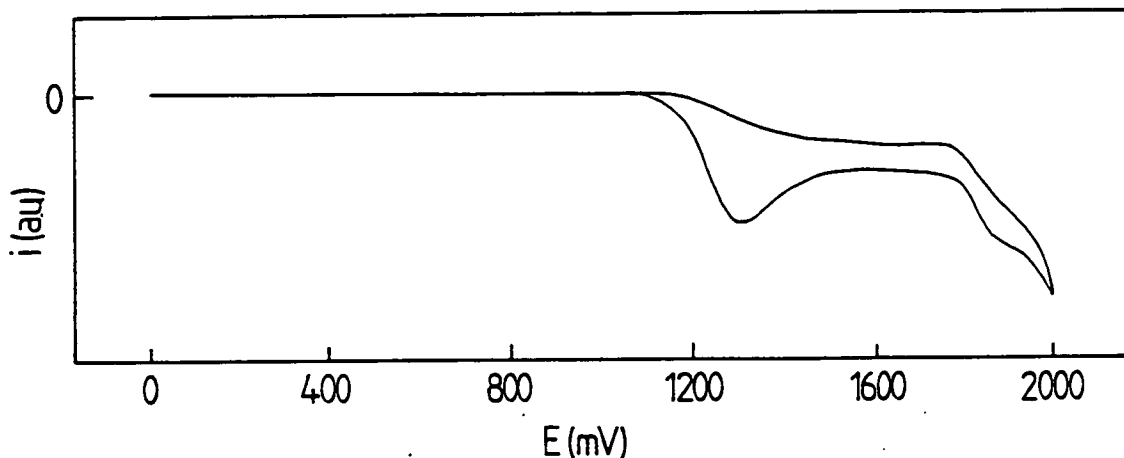
Figure 4.2.12. Cyclic Voltammogram for TBATPB in TBABF$_4$ (0.5 moldm^{-3}) in Dichloromethane.

Potentials are quoted *versus* Ag/AgCl/TBACl(0.05moldm^{-3}) + TBABF$_4$(0.45moldm^{-3})/.
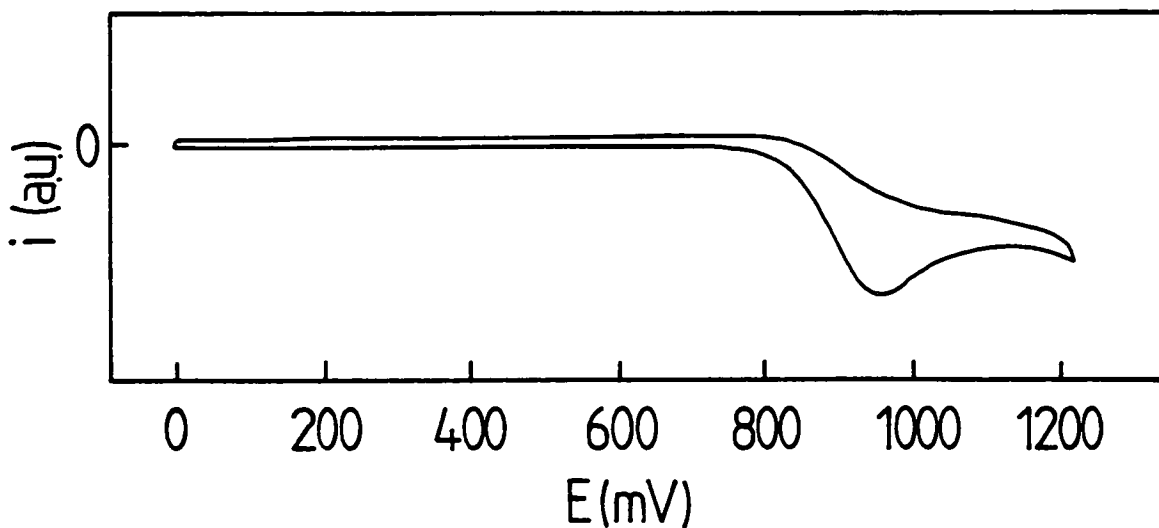
It is apparent from figure 4.2.3. that the process resulting in charge transfer is uniphotonic. Figure 4.2.4. indicates that the generation of the photocurrent is closely allied to the production of an excited state of the $[Ru(bpy)_3]^{2+}$ ion. Figures 4.2.5. and 4.2.6. show that the signal increases with the concentration both of the ruthenium complex and the borate anion. That the signal is unaffected by the composition of the aqueous phase suggests that any photochemistry takes place exclusively in the organic phase. These considerations led to the conclusion that the photocurrent measured resulted from the transfer of some species resulting from the reaction of the $[Ru(bpy)_3]^{2+*}$ ion with $TPBCl^-$. As noted in chapter 1 , there are three mechanisms generally recognized for the quenching of this excited state , namely reductive , oxidative and energy transfer quenching.

In order for energy transfer quenching to play a significant role , the energy of the lowest triplet state of the quenching species must be equal to or lower than that of $[Ru(bpy)_3]^{2+*}$. Figure 4.2.10. shows the absorption spectrum of TBATPBCl (4 $mmoldm^{-3}$) in iodoethane , clearly showing a shoulder not present in the spectrum of pure iodoethane or of TBATPBCl in 1,2-DCE. This band may then be assigned as a spin forbidden triplet ← singlet transition , intensified through the external heavy atom effect [86]. Although the full band is obscured by the solvent front , it appears to be centred at around 420nm ie an energy of around 23800 cm^{-1}. This transition is then higher in energy even than the first MLCT transition of $[Ru(bpy)_3]^{2+}$ [87]. An energy transfer quenching mechanism is therefore unlikely in this case.

Electron transfer quenching is left as a possible means of reaction , and figure 4.2.11. shows the $TPBCl^-$ anion to have a reasonably facile oxidation at a platinum electrode. This oxidation was found to be irreversible

under all conditions used , sweep rates up to 500mVs^{-1} and temperatures down to 233K. No reduction process was observed over the potential range available , +2.0 → -1.8V *versus* Ag/AgCl. Because the oxidation is irreversible , no cell potential for the process may be quoted , although it is unlikely to lie more positive than E_p^f , found to be +1.28V *versus* Ag/AgCl at a sweep rate of 100mVs^{-1}. Using

the value for the $[Ru(bpy)_3]^{3+/2+*}$ couple in water [47] of
−0.81V *versus* the NHE and an approximate oxidation
potential for TPBCl⁻ of +1.5V *versus* the NHE , the
reductive quenching process would seem unfeasible.
However, oxidative quenching has been reported using
nitrobenzene, a situation for which the energetics are
almost as unfavourable [42]. The irreversible nature of
the oxidation of TPBCl⁻ will also aid the generation of a
net reaction. The ^{13}C NMR spectra in figure 4.2.8. show
the development of a set of peaks between 125 and 130 ppm
subsequent to irradiation of the tube and its contents ,
indicating that permanent chemical change has taken place.
Figure 4.2.9. shows the collapse of the band due to the
lowest energy MLCT transition of $[Ru(bpy)_3]^{2+}$ upon
irradiation of the quartz cell contents. Concomitant with
this collapse is the appearance of two new bands , centred
at 557 and 383nm *ie* energies of 17900 and $26100cm^{-1}$. These
two new bands do not correlate very well with those of the
$[Ru(bpy)_3]^{+}$ ion expected to be produced in a reductive
quenching step. They do however tie in fairly well with
two bands in the UV-Vis spectrum of $[Ru(bpy)_2Cl_2]$ at 27000
and $17900cm^{-1}$ [87]. This species might arise directly
through chloride abstraction from a TPBCl⁻ ion or it may
result from a reaction of the Ru(I) species formed in a
reductive quenching step with the oxidised borate. It is
not possible to choose between these two mechanisms on the
evidence presented here. The fact that a similar photo-
electrochemical phenomenon may be demonstrated using TPB⁻
rather than TPBCl⁻ suggests that chloride abstraction is
not crucial to the production of a photocurrent.

The reductive nature of the quenching process then
seems likely , being in accord with most of the
experimental evidence presented here , with one exception.
The photocurrent was recorded without the deliberate
addition of any quenching species to the aqueous phase ,
and did not depend on the presence of chloride or the pH

of the solution used. It may be concluded then with reasonable certainty that the charge transfer process stimulated by light is that of ion transfer across the ITIES. This raises the one objection to the proposition that the quenching process is reductive , as the initial product of a one electron oxidation of TPBCl$^-$ would be neutral , and thus unable to give rise to an ion transfer current. In order to account for this apparent contradiction one further step in the quenching process must be postulated , as shown in figure 4.3.1.

Section 4.3.2. Analysis of the Photocurrent for Cell 4.1.

On the basis of these results the scheme in figure 4.3.1. is proposed to explain the photocurrent recorded.

Figure 4.3.1. Scheme Proposed to Explain the Photocurrent for Cell 4.1.

$$S^{2+} \underset{k_f}{\overset{h\nu}{\rightleftharpoons}} S^{2+*}$$

$$S^{2+*} + Q^- \underset{k_{-1}}{\overset{k_1}{\rightleftharpoons}} [S^{2+*},Q^-]$$

$$[S^{2+*},Q^-] \underset{k_{-2}}{\overset{k_2}{\rightleftharpoons}} [S^+,Q] \underset{k_{-3}}{\overset{k_3}{\rightleftharpoons}} [S^+,Z] \underset{k_{-4}}{\overset{k_4}{\rightleftharpoons}} [S^{2+},Z^-] \underset{k_{-5}}{\overset{k_5}{\rightleftharpoons}} S^{2+} + Z^-$$

$$\downarrow k_6$$

$$[S^+,X]$$

$$Z^- \xrightarrow{k'} \text{Charge Transfer}$$

$$k_9 \downarrow \qquad \overset{k_8}{\searrow}$$

$$Y \qquad \qquad \text{Diffusion to Bulk}$$
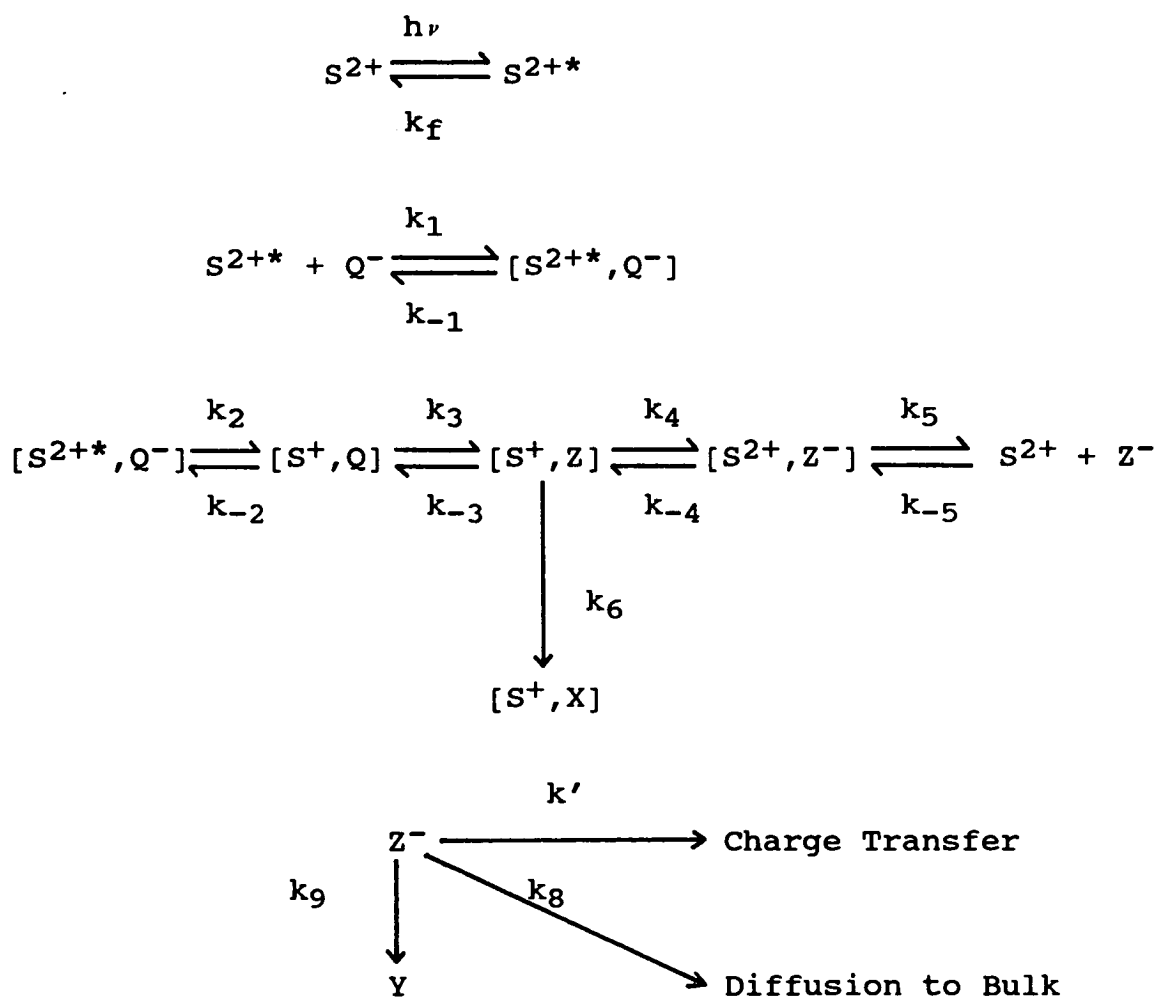
where S^{2+} is $[Ru(bpy)_3]^{2+}$
Q^- is $TPBCl^-$
Z^- is the species responsible for charge transfer
Y and X are inactive species.

In order to avoid the complexities of evaluating the kinetics of formation of the donor-acceptor encounter complex $[S^{2+*}, Q^-]$ the simplifying assumption of Meyer *et al* [84] may be used. These workers assumed that paraquat and tetraphenylborate are almost completely ion paired in acetonitrile in the millimolar concentration range. If this assumption is valid for solutions in acetonitrile , then it should also be true for 1,2-DCE , a solvent whose dielectric constant is only one third that of acetonitrile [88]. This assumption of the pre-existence of a potential donor-acceptor complex considerably simplifies the scheme for kinetic analysis. This simplification is shown in figure 4.3.2.

Figure 4.3.2. A Scheme of Reduced Complexity for Analysis of the Photocurrent for Cell 4.1.

$$[S^{2+}, Q_2^-] \underset{k_f}{\overset{h\nu}{\rightleftharpoons}} [S^{2+*}, Q_2^-]$$

$$[S^{2+*}, Q_2^-] \underset{k_{-1}}{\overset{k_1}{\rightleftharpoons}} [S^+, Q'Q^-] \underset{k_{-2}}{\overset{k_2}{\rightleftharpoons}} [S^+, X, Q^-] \underset{k_{-3}}{\overset{k_3}{\rightleftharpoons}} [S^{2+}, X^-, Q^-] \underset{k_{-4}}{\overset{k_4}{\rightleftharpoons}} [S^{2+}, Q^-] + X^-$$

$$\downarrow k_5$$

$$[S^+, Z, Q^-]$$

$$Y \overset{k_6}{\longleftarrow} X^- \overset{k'}{\longrightarrow} \text{Transfer}$$

$$\downarrow$$

$$\text{Diffusion}$$

The value of k_f is known to be typically around $1.5 \times 10^6 s^{-1}$ in deaerated solution [42] and so the fact that any reaction takes place at all implies that k_1 is reasonably large. This scheme is still consistent with the data shown in figure 4.2.6., as increasing concentration of TPBCl$^-$ will enhance the release of X$^-$ from the ion [S^{2+}Q$^-$X$^-$] ion triple through dynamic exchange.

Due to these considerations it was hoped that it would be possible to analyse the data on the basis of the equations outlined in chapter 2 for the diffusion to the interface of a species produced in a fast photochemical reaction. This would have been possible using a number of further simplifying assumptions. Separation rate constants could have been estimated on the basis of the Eigen equation [89];

$$k_{sep} = [3(D_A + D_B)/ a^2].[-b/ (1 - e^b)] \quad \text{Equation 4.3.2.}$$

where D_A and D_B are the diffusion coefficients of the separating particles , a the distance between their centres and b a term to cover the coulombic work of separating two ions. The diffusion coefficients required by this equation could have been estimated from the Stokes-Einstein equation in conjunction with estimates of the size of the particles based on analogy to species of known size.

It was however decided , despite the fact that Equation 2.5.4. may be fitted very well to the data obtained, that the number of assumptions involved would have made any figure obtained from this process meaningless.

Section 4.3.3.   The Nature of the Interfacial Charge Transfer Reaction.

It can be said with reasonable certainty that the charge transfer reaction observed is an ion transfer reaction. Because the quenching reaction has been demonstrated to be reductive in nature the final photoproduct would be expected to be neutral , as in the case for oxidation of TPB⁻ at a platinum electrode , where triphenylboron and biphenyl are formed [84]. For this reason it seems likely that the process responsible for the ion transfer reaction results from back electron transfer from the Ru(I) species initially formed to the partially decomposed borate. This process must also be in competition with irreversible decomposition of the TPBCl⁻ ion , which results in the net formation of the Ru(I) complex.

There has been one structural study on the results of photooxidation of TPB⁻ , [66] , using diphenylacetylene as a sensitiser. In an interesting parallel to the work reported here , a back reaction with the reduced sensitiser was postulated by these workers to explain the eventual photo-oxidation products in air saturated acetonitrile. These were found to be diphenylborinate and biphenyl. No direct comparison can be drawn because the intermediate postulated in this paper is formed through addition of an organoboron radical across the triple bond of the diphenylacetylene radical anion. Perhaps the most that can be said is that the detection of an ion transfer current here lends credence to the previous postulation of back reaction in the photo-oxidation of tetraarylborates.

Section 4.4.   Conclusion.

The ability of the ITIES to detect the presence of ionic intermediates in photochemical reactions has again been demonstrated. A kinetic analysis of the phenomenon has however proved too complex for the time being. There are though , certain conclusions that can be made , and

chief amongst these is that the TPB$^-$ and TPBCl$^-$ ions should not be present in systems intended to demonstrate any effect other than photosensitised ion transfer.

References.

84. B.P.Sullivan, W.J. Dressick and T.J.Meyer, J. Phys. Chem., 86(1982)1473.

85. N.A. Kotov and M.G. Kuzmin, J. Electroanal. Chem., 285(1990)223.

86. M.Kasha, J. Chem. Phys., 20(1952)71.

87. A.J. Mackenzie, PhD Thesis, University of Edinburgh (1987)

88. A. Weissberger (Ed.) Technique of Organic Chemistry, Volume VII, Interscience (1955).

89. M. Eigen, Z.Phys.Chem. 1(1954)176.

CHAPTER FIVE

Some Interfacial Photoelectrochemical Effects at the ITIES Constructed with the Sensitiser Present in the Organic Solvent.

Section 5.1.   Introduction.

It was shown in Chapter 3 that the work of Marecek and De Armond [56] fails to take into account ion transfer reactions following electron transfer. Chapter 4 suggests that the use of TPAsCBB as supporting electrolyte may also have caused complications due to homogeneous quenching reactions in the organic phase. Given these factors , it would seem that there has been no report of the proper characterisation of an interfacial photocurrent at the ITIES arising through a heterogeneous process using the $[Ru(bpy)_3]^{2+}$ cation in the organic phase.

Clearly it is necessary for any investigator in this field first to understand and minimise the background processes in the chosen system. Once this has been achieved a given effect may be demonstrated with a greater degree of certainty. This chapter reports the design and characterisation of such an arrangement and the demonstration of truly heterogeneous photoelectrochemical processes.

Section 5.1.1.   System Design.

In order to demonstrate simple photoinitiated electron transfer using the $[Ru(bpy)_3]^{2+}$ ion in the organic phase , following ion transfer reactions must be avoided. It follows then that the intended electron transfer reaction should produce a hydrophobic species in

the organic phase and a hydrophilic species in the aqueous layer. It was shown in Chapter 3 that the $[Ru(bpy)_3]^{3+}$ ion is much more hydrophilic than the $[Ru(bpy)_3]^{2+}$ ion. No data could be obtained for transfer of the $[Ru(bpy)_3]^{+}$ ion but it seems likely that this species is less hydrophilic than the $[Ru(bpy)_3]^{2+}$ ion. The implication for the design of systems intended to demonstrate photoinitiated electron transfer at the ITIES using the $[Ru(bpy)_3]^{2+}$ cation as a sensitiser in the organic phase is clear. The intended electron transfer reaction should be reductive in nature if the applied interfacial potential difference $\Delta_W^O\varphi$ is greater than the transfer potential of $[Ru(bpy)_3]^{3+}$ and oxidative if the potential difference is less than that value. In addition , the quenching reaction in the aqueous phase should give rise only to stable , hydrophilic species.

Supplementary to these criteria it would seem to be important that the two species intended to react should both be brought towards the interface at the potential employed. At potentials at which the $[Ru(bpy)_3]^{2+}$ ion is brought towards the interface from the organic phase , anions are brought towards the interface from the aqueous side. It seems then that the type of system most likely to show photoinitiated electron transfer reactions are those in which the aqueous phase contains an anion with a facile one electron oxidation giving rise to another anion.

Section 5.2. Experimental Details.

Figure 5.2.1. shows the equipment used , in block form. The experimental procedure was as described in chapter 2 , with the following exceptions. Current measurements were performed by connecting a two phase lock-in analyser (EG&G , model 5206) to the output of the battery operated potentiostat previously described. This lock-in analyser was used in the 0° (resistive) mode and
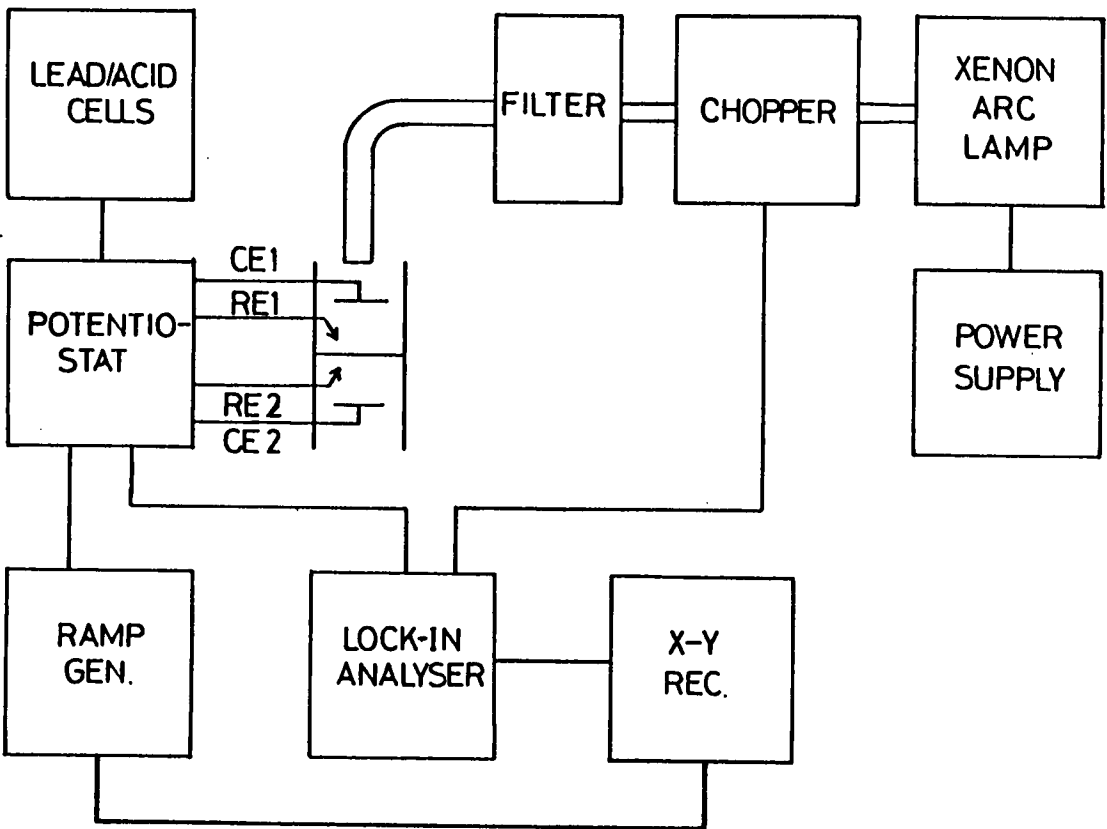
Figure 5.2.1.   Block Diagram of the Apparatus Used.

the real component of the in-phase signal displayed on the chart recorder. The integration period was set to 30s. The light source was modulated by means of a two bladed variable frequency optical chopper (Bentham , model 218) and the reference output of this unit connected to the reference input of the lock-in analyser. The chopping frequency was 10 Hz for all experiments.

The light was directed onto the cell from above , passing through a glass filter to select the visible and low energy UV radiation from the spectrum of the xenon arc lamp.

Chemicals Used.

Potassium hexacyanoferrate(II) (BDH, Analar) potassium hexacyanoferrate(III) (Fisons, SLR) and lithium bromide (BDH) were used as received. Hydrochloric acid and sulphuric acid (BDH, Analar) were used as received after suitable dilution. Cerium (IV) sulphate (Aldrich) (0.01 $moldm^{-3}$) in 0.2 $moldm^{-3}$ H_2SO_4 (M&B) was obtained by tenfold dilution of a stock solution previously standardised and generously provided by Mr. D. Robertson of the Inorganic Teaching Laboratory. All other chemicals were as previously described.

Section 5.3. Results for those Systems Containing Only Supporting Electrolyte in the Aqueous Phase.

The first systems to be investigated were those in which only [Ru(bpy)$_3$][TPFB]$_2$ was present in the organic phase and the aqueous phase contained only supporting electrolyte. This supporting electrolyte was either LiCl, HCl, LiBr, Li_2SO_4 or H_2SO_4

Figure 5.3.1. Cyclic Voltammograms for Cell 5.1.

MX equal to A) LiCl , B) HCl , C) LiBr , D) Li_2SO_4 , E) H_2SO_4 , all recored at a sweep rate of $100mVs^{-1}$.
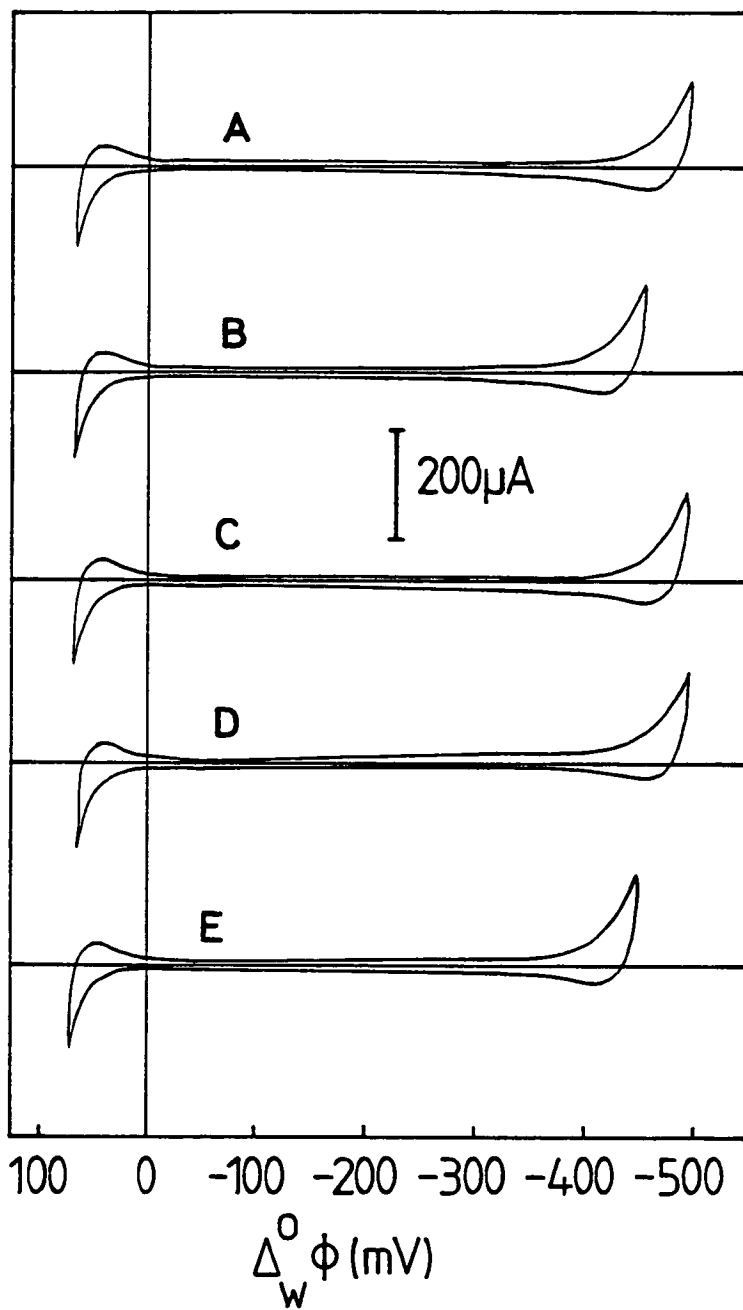
Figure 5.3.2.   Photocurrent-Time Transient Recorded for
Cell 5.1 , MX Equal to LiCl.
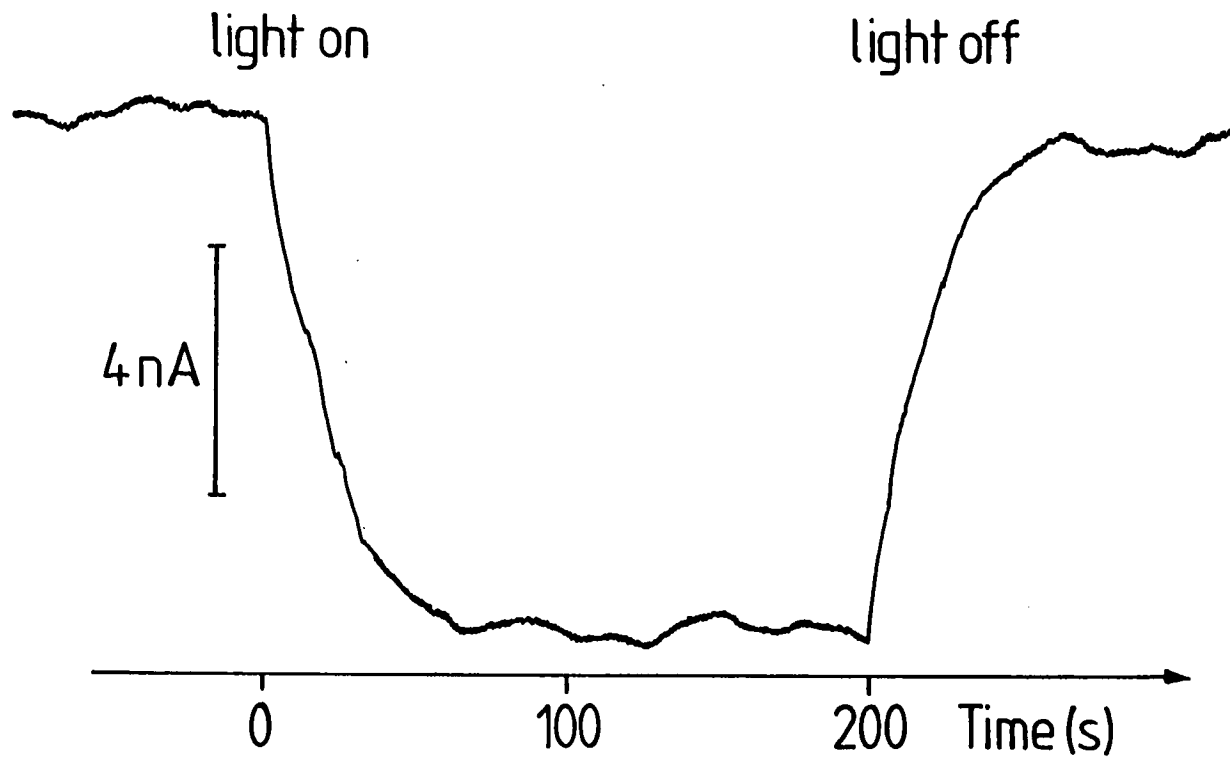
Section 5.3.1.   Cyclic Voltammetry

The limits of polarisability of these five systems were all determined by cyclic voltammetry of cell 5.1 with the appropriate aqueous supporting electrolyte in place.

$$Ag/AgCl/[Ru(bpy)_3][Cl]_2 (1\ mmoldm^{-3}) (aq)/$$
$$[Ru(bpy)_3][TPFB]_2\ (5\ mmoldm^{-3}) (1,2-DCE)//$$
$$MX\ (10\ mmoldm^{-3}) (aq)/AgX\ or\ Ag_2X/Ag'$$
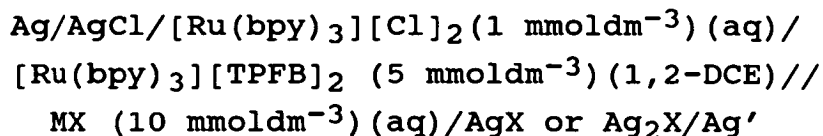
Cell 5.1
where MX is the aqueous supporting electrolyte

The resulting cyclic voltammograms are shown in figure 5.3.1.

Section 5.3.2.   Photocurrents Produced by Irradiation of Cell 5.1 and Related Cells.

It was found that upon irradiation of cell 5.1 with MX equal to LiCl , no photocurrent could be detected without the use of the lock-in analyser. Using phase sensitive detection however it was possible to measure a photocurrent , whose direction corresponded to the transfer of negative charge from aqueous phase to organic or of positive charge in the opposite direction. The typical form of the photocurrent-time transient is shown in figure 5.3.2. The rise-time of the signal may be seen to be roughly the same as the integration period , indicating that the process giving rise to the signal is fast. This photocurrent was found to reduce sharply in magnitude when the experiments were repeated using air saturated solutions. The interposition of neutral density filters in the light path allowed the effect of varying the incident light intensity to be measured and these results are shown in figure 5.3.3. Table 5.3.1. shows the

effect of varying the concentration of LiCl in the aqueous phase on the observed photocurrent.

Table 5.3.1. Effect of the Variation of the Concentration of LiCl in Cell 5.1. on the Photocurrent Recorded.

Concentration of LiCl	Average Photocurrent (Over Three Runs)(nA)
10	11.8±1
50	11.9±1
100	9.7±1

Illumination of a cell constructed as cell 5.1 with LiCl (10 mmoldm^{-3}) as the aqueous phase but with TBATPFB and TBACl substituted for [Ru(bpy)$_3$][TPFB]$_2$ and [Ru(bpy)$_3$][Cl]$_2$ resulted in no measureable photocurrent. Substitution of HCl or LiBr (10 mmoldm^{-3}) for LiCl in cell 5.1 resulted in no change in the magnitude of the photocurrent obtained. Substitution of Li$_2$SO$_4$ or H$_2$SO$_4$ (10 mmoldm^{-3}) for LiCl does not lead to a measureable photocurrent.

The variation of the photocurrent obtained for illumination of cell 5.1 (LiCl 10mmoldm^{-3}) with variation of the applied interfacial potential difference is shown in figure 5.3.4. The trace labelled (a) in this figure is a plot of the output of the lock-in analyser against potential , which was swept at a rate of 0.2 mVs$^{-1\cdot}$ The trace labelled (b) was recorded in the same manner but with the interface under illumination. The dark current (a) increases with potential due to the onset of ion transfer at the end of the potential window.

Figure 5.3.3. Variation of the photocurrent for cell 5.1
, MX = LiCl with filter transmittance.
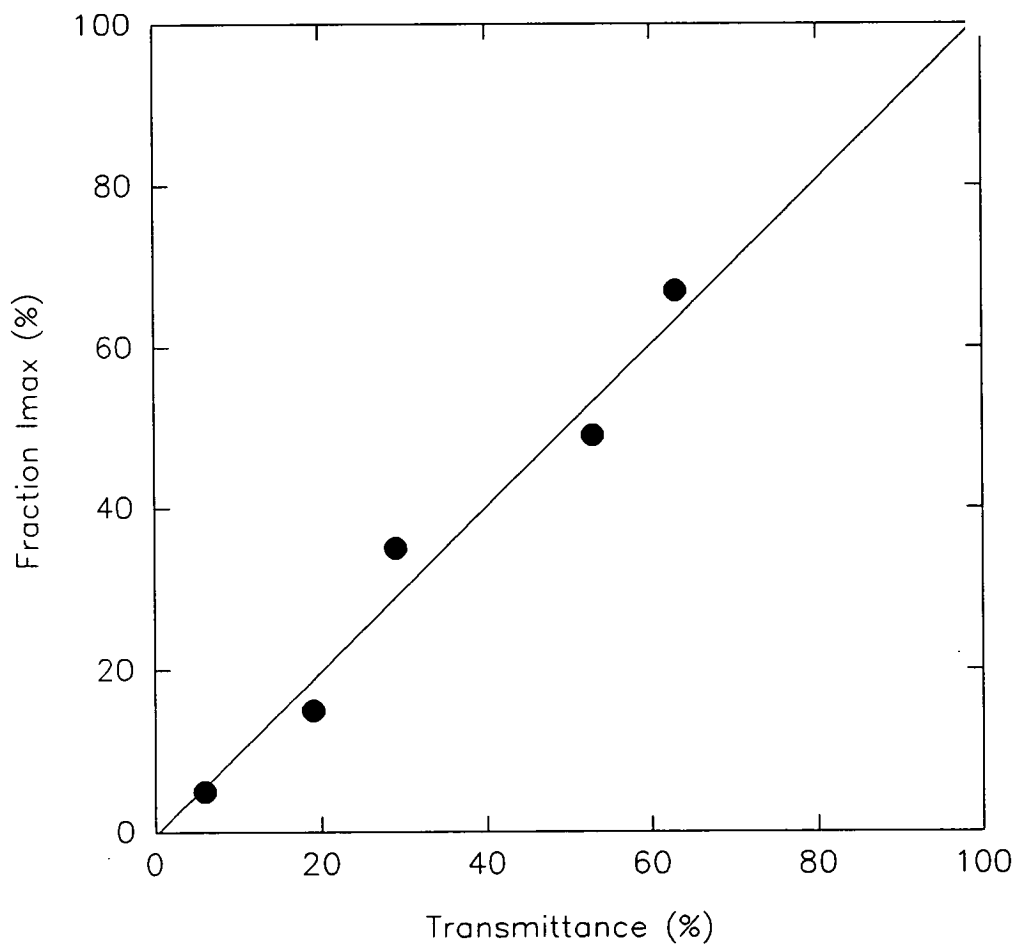
Figure 5.3.4. Variation of a) the Dark Current b) the Photocurrent with Applied Interfacial Potential for Cell 5.1 , MX equal to LiCl.
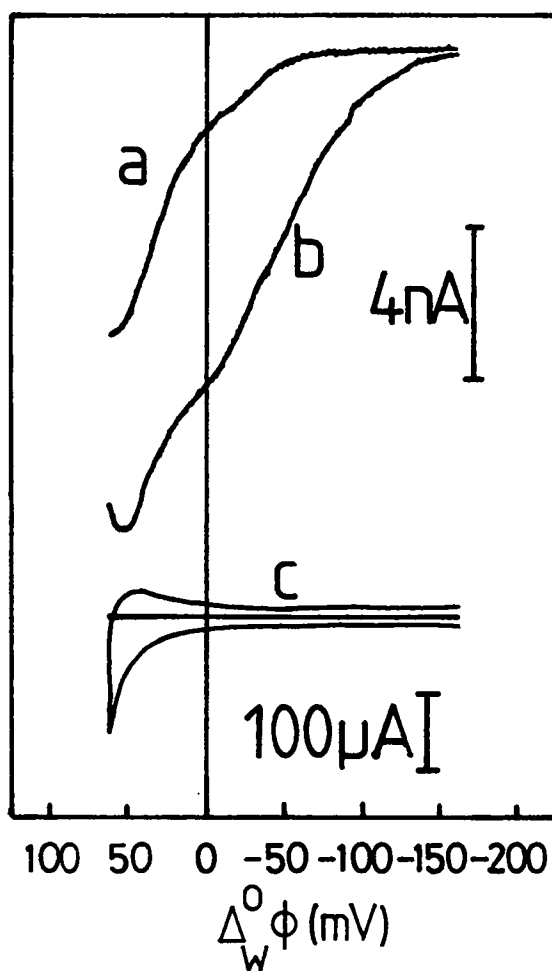
A portion of the cyclic voltammogram for this system is shown in c) on the same potential scale , sweep rate of 100mVs^{-1}.

Section 5.4. Systems Containing Quencher Species in the Aqueous Phase.

Results are presented here for those systems studied here containing $[Ru(bpy)_3][TPFB]_2$ in the organic phase and some species intended to be an electron transfer quencher in the aqueous phase.

Section 5.4.1. Results for Systems Containing Electron Transfer Quenchers in the Aqueous Phase.

The following cells were set up;

$$Ag/AgCl/BTPPACl(1 \ mmoldm^{-3}(aq))/$$
$$BTPPATPFB(3 \ mmoldm^{-3})+[Ru(bpy)_3][TPFB]_2(2 \ mmoldm^{-3})$$
$$(1,2-DCE)$$
$$//Li_2SO_4(10 \ mmoldm^{-3}) + MX(10 \ mmoldm^{-3})/$$
$$Ag_2SO_4/Ag'$$
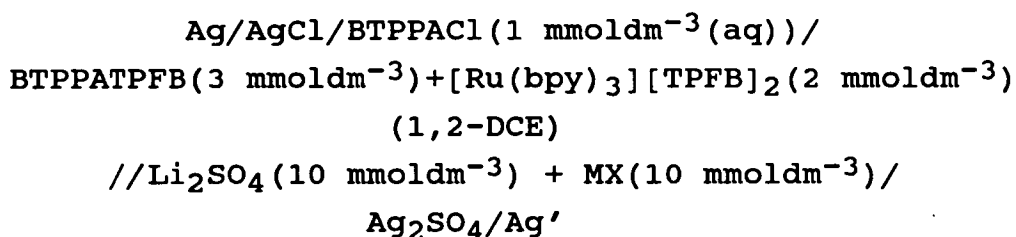
Cell 5.2

where MX was $K_4[Fe(CN)_6]$, $K_3[Fe(CN)_6]$ or $Fe[SO_4]$.

Even at the interfacial potentials most likely to give rise to electron transfer reactions and under the most rigourously anoxic conditions attainable no photocurrent could be measured for any of these systems.
The following cells were set up;

$$Ag/AgCl/BTPPACl(1 \ mmoldm^{-3})(aq)/$$
$$BTPPATPFB(3 \ mmoldm^{-3}) + [Ru(bpy)_3][TPFB]_2 \ (2 \ mmoldm^{-3})$$
$$(1,2-DCE)$$
$$//Ce[SO_4]_2 \ (10 \ mmoldm^{-3}) + H_2SO_4 \ (0.2 \ moldm^{-3})/$$
$$Ag_2SO_4/Ag'$$

Cell 5.3

Ag/AgCl/BTPPACl(1 mmoldm^{-3}(aq))/

BTPPATPFB(3 mmoldm^{-3})(1,2-DCE)//

Ce[SO$_4$]$_2$ (10 mmoldm^{-3}) + H$_2$SO$_4$ (0.2 moldm^{-3})/

Ag$_2$SO$_4$/Ag'
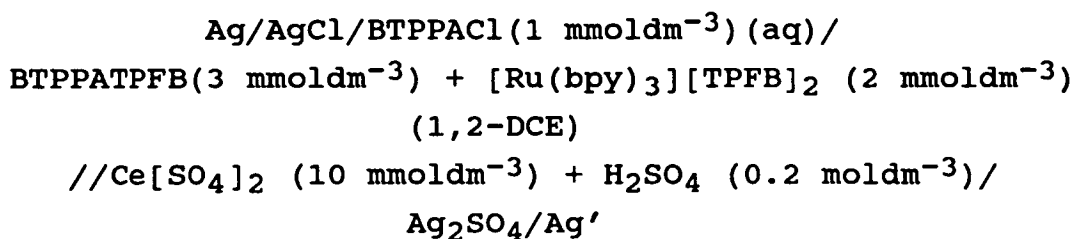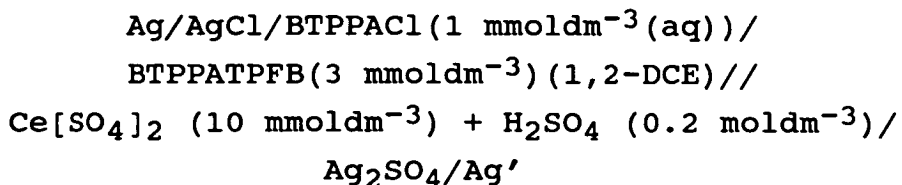
Cell 5.4

These cells were investigated by means of cyclic voltammetry , the voltammograms obtained being shown in figures 5.4.1 to 5.4.3.

Illumination of cell 5.3. with the light from the xenon lamp resulted in the detection of a photocurrent , the variation of which with the applied interfacial potential difference is shown in figure 5.4.4. This figure shows a portion of a cyclic voltammogram recorded on the same potential scale at a sweep rate of 100 mVs^{-1}, labelled A , the wave in which corresponds to transfer of the [Ru(bpy)$_3$]$^{3+}$ ion (see Section 5.5.2.). This voltammogram is superimposed on two curves labled B and C. These are plots of the lock-in analyser output against the applied potential , which was swept at a rate of 0.2 mVs^{-1} , B recorded in the dark , C under illumination. Illumination of cell 5.4 did not lead to any measureable photocurrent.

Section 5.5.1. Discussion of Results for Systems Containing Only Supporting Electrolyte In the Aqueous Phase.

The results presented in section 5.3 show that a photocurrent may be demonstrated at the ITIES using cell 5.1 only in the presence of halide ions in the aqueous phase. This signal does not appear to be sensitive to the pH of the aqueous phase , and is enhanced by the saturation of the solutions employed with argon. The

Figure 5.4.1. Cyclic Voltammogram for Cell 5.4 , ν = 100mVs^{-1}.

$\Delta_W^O \phi \, (mV)$
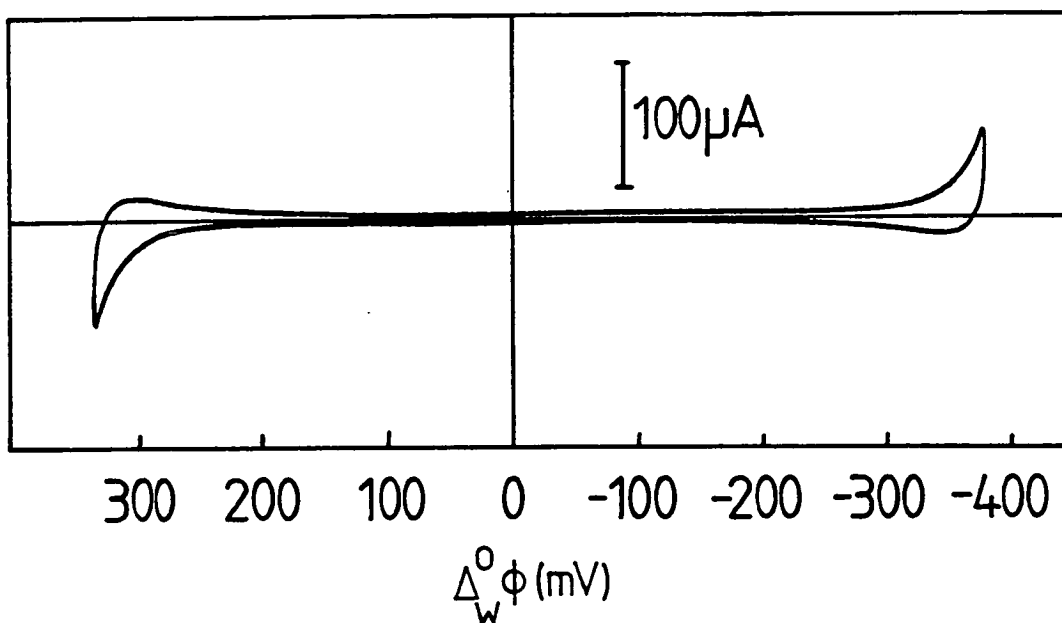
Figure 5.4.2. Cyclic Voltammograms , ν = 100mVs^{-1}, for Cell 5.3 Showing the Transfer of the $[Ru(bpy)_3]^{2+}$ Ion from Organic to Aqueous Phase.

$\Delta_W^O \phi \, (mV)$
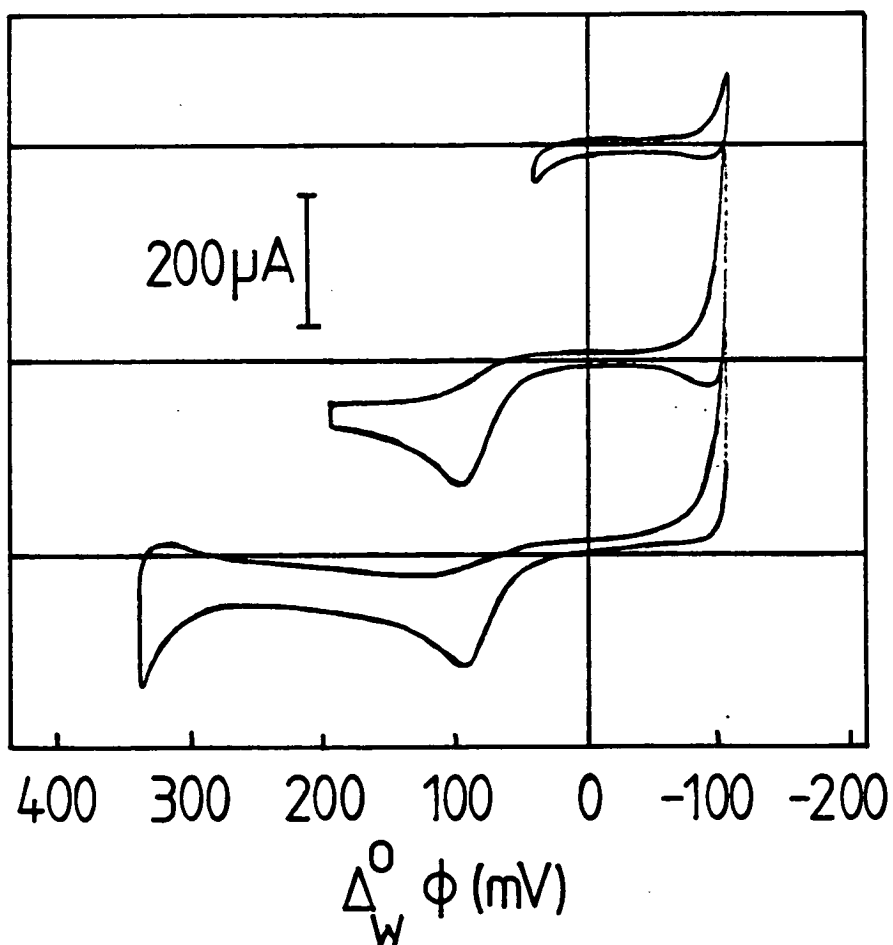
Figure 5.4.3. Cyclic Voltammogram for Cell 5.3. , ν = 20mVs^{-1} , Showing Transfer of the [Ru(bpy)$_3$]$^{3+}$ Ion.
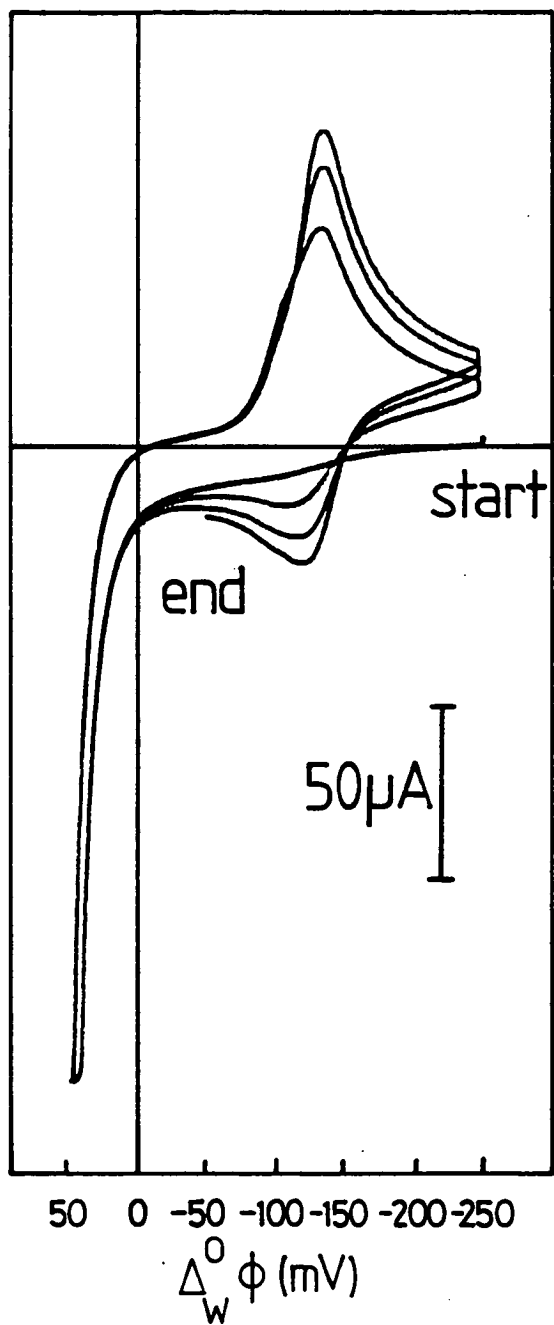
Figure 5.4.4. Cyclic Voltammogram for Cell 5.3 , ν = 100mVs^{-1} ,A , Superimposed on B the Dark Current and C the Photocurrent on the Same Potential Scale.
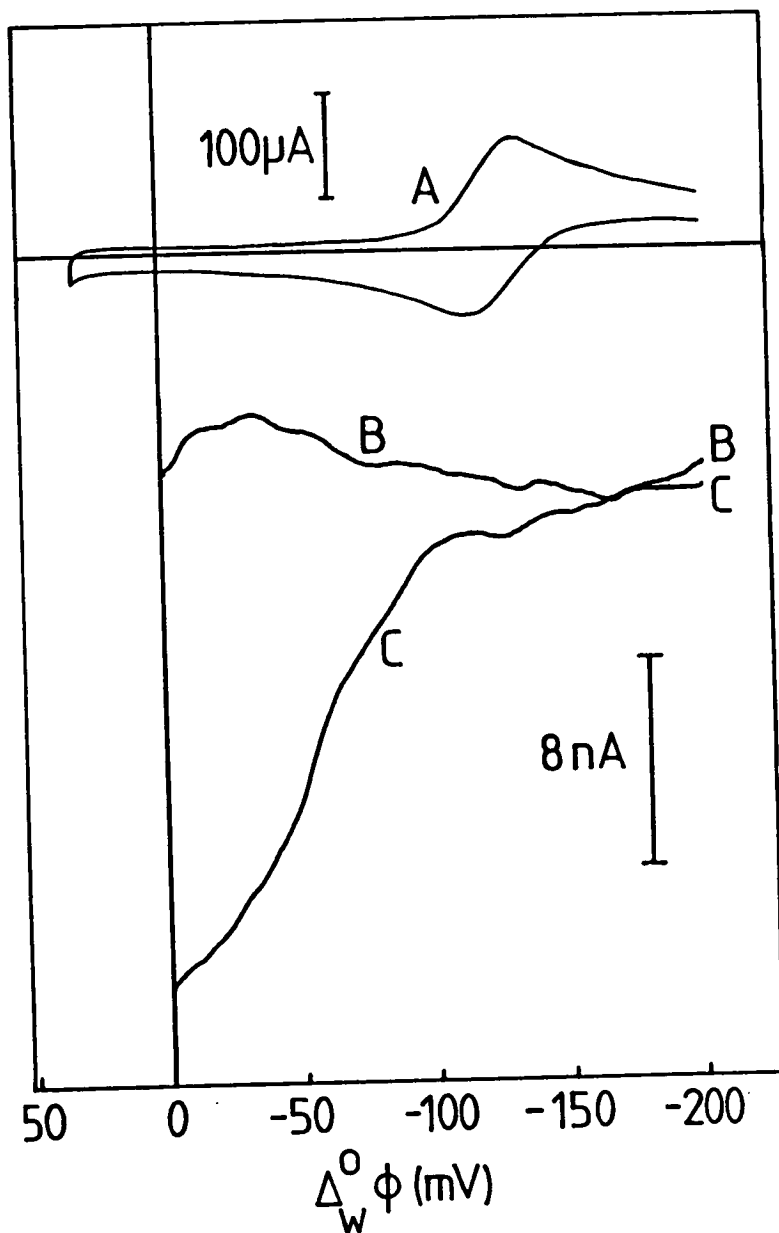
photocurrent cannot be demonstrated in the absence of the [Ru(bpy)$_3$]$^{2+}$ ion and is proportional to the incident light intensity.

That the observation of a photocurrent depends on the presence of both the sensitizer in the organic phase and halide ion in the aqueous phase shows that the signal is generated through an interfacial process. This assignment is backed up by the data in figure 5.3.4. which show that the signal is maximised at those potentials at which the [Ru(bpy)$_3$]$^{2+}$ ion is brought into the closest association with any anionic species in the aqueous phase. Two possible processes which would account for the transfer of charge in the direction found by means of an interfacial reaction are proposed and these are shown schematically in figure 5.5.1.

Figure 5.5.1. Two Schemes to Account for the Photocurrent Obtained for Cell 5.1.

Scheme One.

Aqueous

$$X^- \qquad X\cdot$$

Organic e^-

$$[Ru(bpy)_3]^{2+} \xrightarrow{\ h\nu\ } [Ru(bpy)_3]^{2+*} \qquad [Ru(bpy)_3]^{+}$$

Scheme Two.

Aqueous

$$X^-$$

Organic

$$[Ru(bpy)_3]^{2+} \xrightarrow{\ h\nu\ } [Ru(bpy)_3]^{2+*} \qquad [Ru(bpy)_2(py-py)(X)]^{+}$$
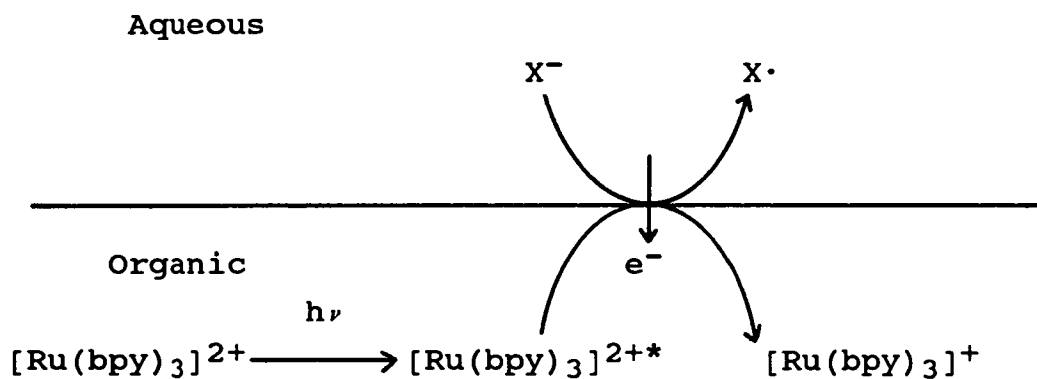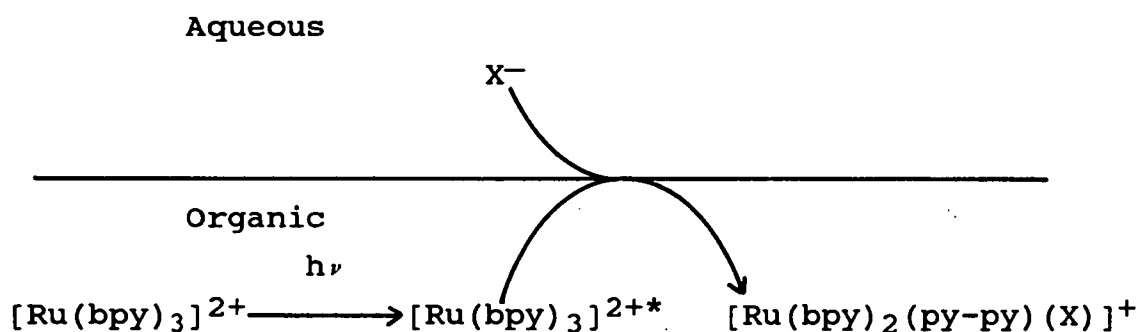
where X is either chloride or bromide and (py-py) indicates a monodentate bipyridyl ligand.

Neither of these two schemes account for the data in table 5.3.1. , but this may well result from the fact that no concentration of LiCl less than 10 mmoldm^{-3} was investigated. Whatever process leads to the photocurrent may well not be limited by the availability of the halide in the concentration range studied. In any case , the halide is certainly necessary to produce a signal. Scheme

123

One in figure 5.5.1. seems fairly unlikely as the excited state ion $[Ru(bpy)_3]^{2+*}$ is thermodynamically incapable of oxidizing chloride through a homogeneous reaction in water. Also it was found , as stated in section 5.4.2. , that no photoinitiated electron transfer could be demonstrated for a system containing hexacyanoferrate (II). The thermodynamics for oxidation of this ion at the ITIES are more favourable , the E^0 value for oxidation of this ion being almost exactly one volt easier than for chloride in water [90]. It could be argued that the chemically irreversible nature of the oxidation of chloride enhances the net rate of electron transfer relative to the highly reversible hexacyanoferrate (II/III) couple. The irreversibility of this couple however seems likely to stem from following dimerisation of chlorine atoms to form Cl_2. The currents recorded here are so small that it seems unlikely that any great concentration of chlorine atoms would be present at the interface and this bimolecular reaction would be slow. An electron transfer process then makes a poor explanation for the results obtained.

It has been reported [92] that the $[Ru(bpy)_3]^{2+}$ ion is photo-substitutionally inert in 0.1 moldm^{-3} HCl at 25°C , although some reaction may be observed at 95°C under the same conditions. In contrast to this finding the same ion has been found to be highly susceptible to photo-substitution in dimethylformamide [93] and to photoanation in dichloromethane and 1,2-DCE [94,95]. These photochemical properties have been rationalised [94] on the basis of a five co-ordinate intermediate as shown in figure 1.4.3.2. The inertia of the $[Ru(bpy)_3]^{2+}$ ion towards photoanation in aqueous solution is ascribed to the greater relative rate in this solvent of self chelation to that of anation of this five co-ordinate complex. This in turn is explained on the basis of the large negative free energies of hydration of the halide

ions , which must be overcome in order for anation to take place. This is exactly the case that occurs at the ITIES under the conditions employed here. The photocurrent is at a maximum at those potentials where chloride ions are being brought into the mixed solvent layer [13]. The free energy of solvation of chloride in water has been determined to be 30.5 $kJmol^{-1}$ greater than in 1,2-DCE [96]. After a partial or complete transfer into 1,2-DCE then , these ions are more available to the $[Ru(bpy)_3]^{2+*}$ species , which is potentially reactive to halides in all solvents but only actually so in those of low dielectric constant. The absence of a photocurrent in cell 5.1 using Li_2SO_4 as supporting electrolyte is then explained on the basis of the poor co-ordinating properties of the anion in this salt. Scheme Two seems a more satisfactory explanation than Scheme One for the signals obtained.

Section 5.5.2.   Discussion of the Results for Systems with Quenchers in the Aqueous Phase.

No photoinitiated processes could be detected for any of the three variations of cell 5.2 at any one of the available range of interfacial potentials. This is despite the fact that photoinitiated electron transfer may apparently be demonstrated using a sensitizer in the aqueous phase (see Chapter 6). It is not possible at this point to make an informed speculation on the reason for this failure , although the use of an extremely easily reducible compound as a quencher in the latter case may have proved decisive.

At first sight it would seem that cell 5.3 should be unstable with respect to oxidation of the ruthenium complex by the Ce^{4+} ion.   On the basis of the known oxidation potentials of the Ce^{3+} and $[Ru(bpy)_3]^{2+}$ ions [90,42] this reaction , which is known to be fast in aqueous solution [91], may be calculated to be exothermic

in this same solvent by around 19 $kJmol^{-1}$. For the heterogeneous reaction;

$$[Ru(bpy)_3]^{2+}(aq) + Ce^{4+}(aq) \qquad [Ru(bpy)_3]^{3+}(aq) + Ce^{3+}(aq)$$

at equilibrium , the system has only one degree of freedom. This is because there are four components of the system linked by three relationships.

$$c_{(O1)} + c_{(R1)} = c_1 \qquad \text{Equation 5.5.1.}$$
$$c_{(O2)} + c_{(R2)} = c_2 \qquad \text{Equation 5.5.2.}$$
$$\Delta G^0_{reactn.} = -RT \ln(a_{(O2)}a_{(R1)}/a_{(O1)}a_{(R2)})$$
$$\text{Equation 5.5.3.}$$

where O1 is Ce^{4+} , R1 is Ce^{3+} , O2 is $[Ru(bpy)_3]^{3+}$ and R2 is $[Ru(bpy)_3]^{2+}$

The physical state of the system is then determined by the choice of the concentration of only one of the reactants. For the heterogeneous reaction;

$$[Ru(bpy)_3]^{2+}(DCE) + Ce^{4+}(aq) \longrightarrow [Ru(bpy)_3]^{2+}(DCE) + Ce^{3+}(aq)$$

at a liquid/liquid interface amenable to electron transfer but not to partition of any of the ionic species , the variance is equal to two. The conditions expressed in equations 5.5.1. and 5.5.2. remain the same , but equation 5.5.3. must be modified to take the interfacial potential difference into account.

$$\Delta G^0_{reactn.} + RT \ln(a_{(O2)}a_{(R1)}/a_{(O1)}a_{(R2)}) + zF\Delta^1_2\varphi = 0$$

$$\text{Equation 5.5.4.}$$

where 1 is water and 2 is 1,2-DCE

There are now five adjustable parameters , four as

before and the Galvani potential difference in addition , hence a variance of two. This implies that it is possible to vary independently two physical parameters , for instance the concentrations of two of the reactants. Thus when two solutions are placed in contact , one strongly reducing , one oxidizing , a Galvani potential difference , determined according to equation 5.5.4. , is set up between the two phases. If the value of this Galvani potential is positive then the two solutions will be stable in contact.

Figure 5.4.1. shows the cyclic voltammogram for cell 5.4. The potential window will be limited to the positive end by transfer of sulphate to the organic phase and at the negative end by transfer of H^+ or Ce^{4+} , probably the former. Figure 5.4.2. shows a cyclic voltammogram for cell 5.3 , demonstrating transfer of the $[Ru(bpy)_3]^{2+}$ ion from organic to aqueous phase , which process may be seen to be grossly irreversible. Figure 5.4.3. shows a multi-scan cyclic voltammogram for the same system. The switching potential is set such that transfer of the $[Ru(bpy)_3]^{2+}$ ion to the aqueous phase is incipient , and the growth of a wave corresponding to a reasonably reversible process centred at −125mV can be seen. The peak to peak separation for this wave was found to be 20mV as expected for a process for which $z = 3$.

These results may be rationalised on the basis of a scheme shown in figure 5.5.2.

Figure 5.5.2. Scheme to Explain the Response of Cell 5.3 to Cyclic Voltammetry.

Aqueous

$$Ce^{4+} \quad Ce^{3+}$$

$$[Ru(bpy)_3]^{2+} \qquad [Ru(bpy)_3]^{3+}$$

Organic
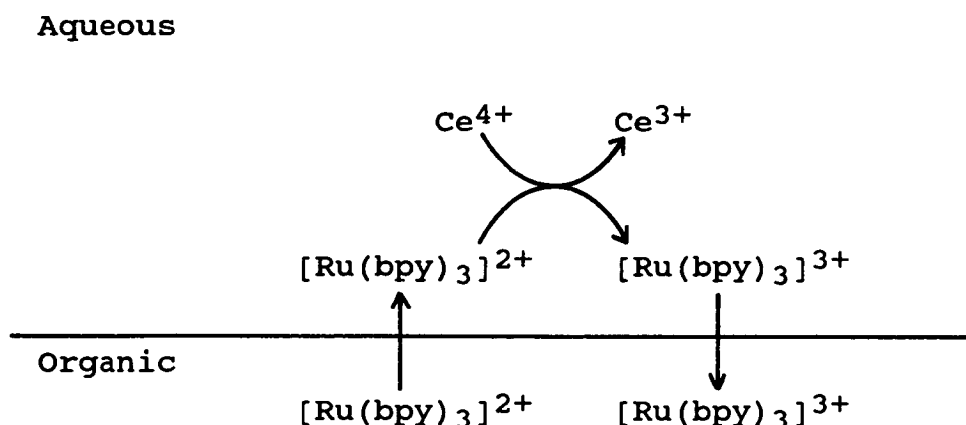
$$[Ru(bpy)_3]^{2+} \qquad [Ru(bpy)_3]^{3+}$$

The cyclic voltammograms shown in figures 5.4.1. to 5.4.3. are now explained on the basis of the transfer of the $[Ru(bpy)_3]^{2+}$ ion to the aqueous phase as the potential is swept positive towards the formal potential for transfer of this ion. Once in the aqueous phase , the situation is univariant as described before and the ruthenium (II) complex is oxidized by the cerium (IV) ion to the ruthenium (III) species. This oxidised form of the complex is then available to be transfered across the interface as the potential is swept negative. This accounts for the wave found in figure 5.4.3. , the position of which agrees reasonably well with that found in section 3.4.3. for transfer of the $[Ru(bpy)_3]^{3+}$ species across the $H_2SO_4 (10 \quad mmoldm^{-3}) (aq) //$ BTPPATPFB (10 $mmoldm^{-3}) (1,2-DCE)$ interface. The only other species to which it would be possible to ascribe this wave is the Ce^{3+} ion , but this is likely to be highly hydrophilic.

This now provides a firm foundation on which to assign the process giving rise to the photocurrent recorded. This was found to correspond to transfer of positive charge from the organic phase to the aqueous. It can be seen from figure 5.4.4. that the photocurrent

128

occurs only at potentials more positive than that found for transfer of the $[Ru(bpy)_3]^{3+}$ species , and increases as the potential for transfer of the $[Ru(bpy)_3]^{2+}$ ion is approached. Two schemes may be proposed , shown in figure 5.5.3. , to explain this photocurrent.

Scheme One in figure 5.5.3. is certainly feasible , as it is known from the voltammetric results that the transfer of the ground state $[Ru(bpy)_3]^{2+}$ ion is irreversible. The transfer of the excited state ion would then certainly be irreversible , due to the fact that this ion is approximately 2.1V [42] easier to oxidize in water than the ground state. Transfer of the excited state ion may well take place at more negative potentials than for the ground state , due to its likely higher dipole moment and thus hydrophilicity. Scheme Two involves the transfer of a $[Ru(bpy)_3]^{3+}$ ion generated subsequent to a genuinely heterogeneous electron transfer.

Scheme Two should lead to a photocurrent at potentials more negative than that for transfer of the ruthenium (III) complex , but in the opposite direction , resulting from straightforward electron transfer without a following ion transfer reaction. Scheme One may or may not imply a photocurrent at these potentials , depending on whether or not the excited ion can cross the interface and gain access to a Ce^{4+} ion. No photocurrent could be obtained in this region of the potential window , although time did not allow for a thorough investigation.

In any case if the interface is considered as a mixed solvent layer , then Schemes One and Two become one as the thickness of the mixed layer increases. This may be illustrated schematically by increasing the width of the line used to denote the interface in figure 5.5.3. , the question of which solvent the electron transfer takes place in having less meaning as the mixed solvent layer becomes thicker.

Figure 5.5.3. Two Schemes to Account for the Photocurrents Obtained for Cell 5.3.

Scheme One.
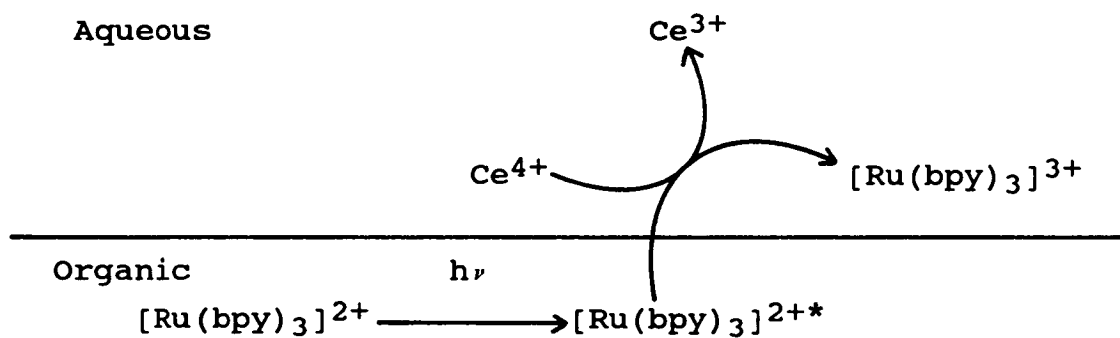
Scheme Two.
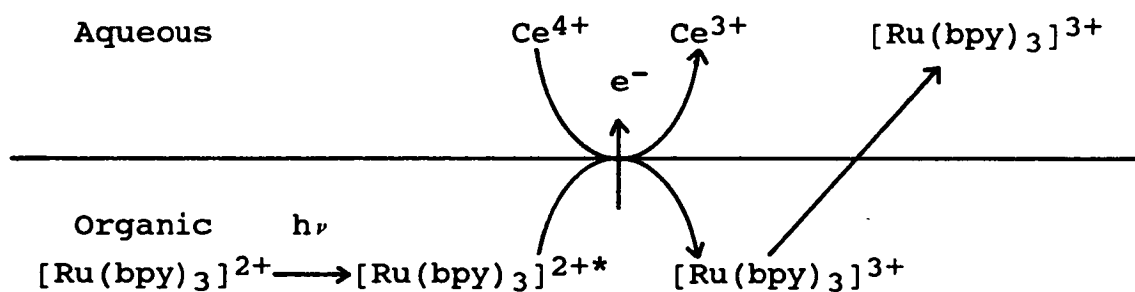
Section 5.6.   Conclusion.

The phenomenon of interfacial photoanation has not been demonstrated conclusively. Only a long-term photolysis followed by the isolation of the appropriate complex from the 1,2-DCE solution would prove that this process has taken place. It seems highly unlikely though , due to the unfavourable thermodynamics that the currents measured stem from an electron transfer reaction.

The experiments carried out using the cerium (IV) ion have a good parallel in the work of Hamnet [52] who observed the oxidation of the luminescent state of the $[Ru(bpy)_3]^{2+}$ ion at a semiconductor electrode. The results are valuable not only because they may lead to information on the potential of transfer for the excited ion , but because they demonstrate a genuine interfacial reaction of this species. This may lead to the design of systems capable of showing simple photoinitiated electron transfer reactions at the ITIES. The compound $[Ru(bpy)_3][TPFB]_2$ has been shown to be a good sensitiser for these systems , free of the photosensitised ion transfer reactions characteristic of tetraarylborate salts of this ion at the ITIES.

References.

90.   Handbook of Chemistry and Physics, 53rd Edn., CRC Press, 1972.

91.   P. George and D.H. Irvine, J. Chem. Soc. (1954)587.

92.   J. Van Houten and R.J. Watts, Inorg. Chem., 17(1978)3381

93.   P.E. Hoggard and G.B. Porter, J. Amer. Chem. Soc. 100(1978)1457.

94.   M. Gleria, F. Minto, G. Beggatio, P. Bortulus, J. Chem. Soc. Chem. Commun., (1978)285.

95.   B. Durham, J.V. Caspar, J.K. Nagle and T.J. Meyer, J. Amer. Chem. Soc., 104(1982)4803.

96.   M.H. Abraham and A.E. Danil de Namor, J. Chem. Soc. Faraday Trans. 1., 72(1976)955

CHAPTER SIX

Photoinitiated Electron Transfer Across the
Interface Between Two Immiscible Electrolyte Solutions.

Section 6.1.   Introduction.

The work whose report this thesis comprises ,
disparate and diverse though it may appear , was carried
out with one purpose. This was the demonstration, through
amperometric techniques, of photoinitiated electron
transfer at the ITIES, a goal which has to date eluded
those who have sought it. Though this chapter may not
demonstrate the effect unambiguously, the burden of proof
is placed firmly on the shoulders of the critic , whereas
before the onus was upon those who claimed such a
phenomenon could be demonstrated.

Such claimants have not been numerous , and the only
relevant paper left which has not been dealt the *coup de
grâce* by the work reported here is that of Girault *et al*
[4]. This article contains certain inherent flaws that
render the authors modest claims suspect. These workers
used a two electrode arrangement to investigate a toluene
/ water interface. This interface was non-polarisable due
to the similar free energies of transfer of the sensitiser
and quencher ions, the $[Ru(bpy)_3]^{2+}$ and heptylviologen
dications. One implication of this situation is that even
small shifts in potential will induce the passage of
current across the interface. For the apparatus reported
there are a number of sources for small potential shifts
upon illumination , the main problem being that both
platinum electrodes were situated in the light path. Small
photoinduced potentials at metallic electrodes have been

reported [97] as have photoinduced potentials at the ITIES [59]. Given that these platinum electrodes served both as counter and reference electrodes it can be seen that shifts in potential may have taken place which may in turn have led to photocurrents.

Another unacknowledged complication is that of the existence of reactive excited states of viologens , capable of oxidizing the tetraphenylborate anion [84], which was unfortunately present here as the counter ion for the viologen. The luminescent state of the $[Ru(bpy)_3]^{2+}$ ion is also capable of oxidizing this borate , which can lead to ion transfer currents at the ITIES (see Chapter 4). This system is then not suitable for the demonstration of a simple photoinitiated electron transfer (PET) at the ITIES.

The shortcomings of this system were always borne in mind in designing the system whose characterisation is reported here. One factor generally agreed upon in this field is that the quencher should be an easily reduced or oxidized species. Because of the problems of finding such species which are stable in water , it was decided that the quencher should be located in the organic phase. If the sensitiser ion , $[Ru(bpy)_3]^{2+}$, is then to be placed in the aqueous phase , the quenching reaction must be oxidative in order to generate the more hydrophilic $[Ru(bpy)_3]^{3+}$ species. As the experiment must be carried out at an interfacial potential more positive than that for transfer of the $[Ru(bpy)_3]^{2+}$ ion , by implication this potential will be more positive than that for transfer of the $[Ru(bpy)_3]^{3+}$ ion , which will then remain in the aqueous phase subsequent to its nascence.

The quencher chosen must consequently have a facile reductive couple which should furthermore be reversible in water saturated 1,2-DCE. This condition is necessary in order that no small ionic species are generated following reduction , which might then give rise to an ion transfer

signal. Initially it was hoped to use the TPFB⁻ salts of dodecyl and heptadecylviologen as quenchers , but these were found to be of only moderate solubility in 1,2-DCE. Their synthesis is described in appendix 2. Attention then turned to the classical organic electron acceptor 7,7,8,8-tetracyanoquinodimethane (TCNQ). This compound is very easily reduced and , as reported in chapter 3 , the transfer potential of the corresponding radical anion lies negative to that for transfer of the $[Ru(bpy)_3]^{2+}$ cation. Thus , in a system using this sensitiser in the aqueous phase , the TCNQ⁻ anion will remain firmly in the organic phase, should it arise. Because TCNQ is neutral , a supporting electrolyte for the organic phase was required. This electrolyte must not only be redox inactive but must be highly hydrophobic. This is necessary to gain a window of polarisation in a system in which the fairly hydrophobic $[Ru(bpy)_3]^{2+}$ cation is located in the aqueous phase. In short, the cation of the supporting electrolyte must transfer at more positive potentials than the $[Ru(bpy)_3]^{2+}$ cation. The salt BTPPATPFB fulfils all the necessary criteria and was chosen for the organic phase in conjunction with Li_2SO_4 in the aqueous phase. The useful window of polarisation then available is limited by the difference in potentials of transfer of the $[Ru(bpy)_3]^{2+}$ cation and the sulphate anion. The presence of the lithium cation and the TPFB⁻ anion also allows voltammetric measurements to be made well beyond the transfer potential for the ruthenium complex. The sensitiser was used as its sulphate salt in order to avoid complications due to both transfer of chloride and photoanation reactions.

Furthermore it was decided to operate the cell in four electrode mode in order to gain the advantages of having the interfacial potential controlled through a potentiostat. This precaution obviates recourse to argument concerning photoinduced potentials , provided that the reference electrodes are shielded from the light

source.

The cell chosen after consideration of the constraints enumerated above as being most likely to demonstrate PET was cell 6.1.

$$Ag/Ag_2SO_4/$$

$[Ru(bpy)_3][SO_4]$ (x mmoldm^{-3}) + Li_2SO_4 (10 mmoldm^{-3})(aq)//
BTPPATPFB (10 mmoldm^{-3}) + TCNQ (y mmoldm^{-3})(1,2-DCE)/
BTPPACl (1 mmoldm^{-3}) + LiCl (10 mmoldm^{-3})(aq)/
AgCl/Ag'
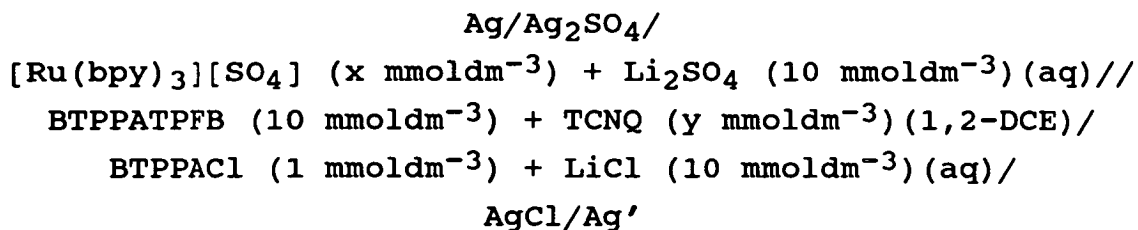
Cell 6.1

Section 6.2.   Experimental Details.

The equipment , procedures and materials employed were those described in Chapter 5 with the following exceptions. $[Ru(bpy)_3][SO_4].6H_2O$ was prepared as described in appendix 2. L-α phosphatidylcholine type IV-S (Sigma, 40%) was used, to block the interface as an adsorbed monolayer, without further purification.

All cyclic voltammograms were recorded in the dark. The cell used was of active area 1.00 cm^{-2} , the bottom surface being polished to allow the unhindered passage of light to the interface from below. Addition of substances to the aqueous phase was accomplished by means of direct injection by micropipette , folowed by gentle agitation of the aqueous phase. Phosphatidylcholine was added to the organic layer as a 1,2-DCE stock solution (2mmoldm^{-3}) as required to give the desired final concentration in the organic layer which was of known volume. In order to maintain the height of the interface from the bottom of the cell constant , an identical volume of the organic layer was removed after addition of a given volume of stock solution. The cell was allowed to equilibrate for twenty minutes after each addition before any measurements

were made.

The equipment for measurements on tin(IV)oxide semiconductor was essentially similar to that used for four electrode studies. The four electrode cell though was replaced with another , the bottom of the inside of which was covered with tin(IV)oxide. This semiconductor layer was used as the working electrode , a platinum wire as the counter electrode and a silver / silver chloride electrode as the reference electrode. These were connected to a home-built three electrode potentiostat , the output of which was connected to the lock-in analyser. The cell was filled with [Ru(bpy)$_3$][SO$_4$] (20 mmoldm^{-3}) in sulphuric acid (0.1 moldm^{-3}) and illuminated from below , an optical glass cuvette of path length 4.00cm being placed between the end of the light guide and the bottom of the cell. This cuvette was filled with the solution under test.

Section 6.3.   Results.

Results are presented here detailing the voltammetric an photoelectrochemical characteristics of cell 6.1.

Section 6.3.1.   Voltammetric Behaviour of Cell 6.1.

Cyclic voltammetry, carried out at ambient temperature of 293±3K, was used to determine the limits of polarisability of cell 6.1 with x = 2 , and the resulting voltammogram is shown in figure 6.3.1. The presence of TCNQ in any quantity in the organic phase was found not to distort this voltammogram.

On scanning the potential beyond the limits of polarisability for cell 6.1 with x = 0.1 and y = 0 , a wave corresponding to transfer of the [Ru(bpy)$_3$]$^{2+}$ ion was observed. This wave , shown in figure 6.3.2. , was found to correspond to the reversible transfer of an ion with z = 2 , with a half-wave potential of 90 mV. The diffusion

137

Figure 6.3.1. Cyclic Voltammogram for Cell 6.1, x = 2.

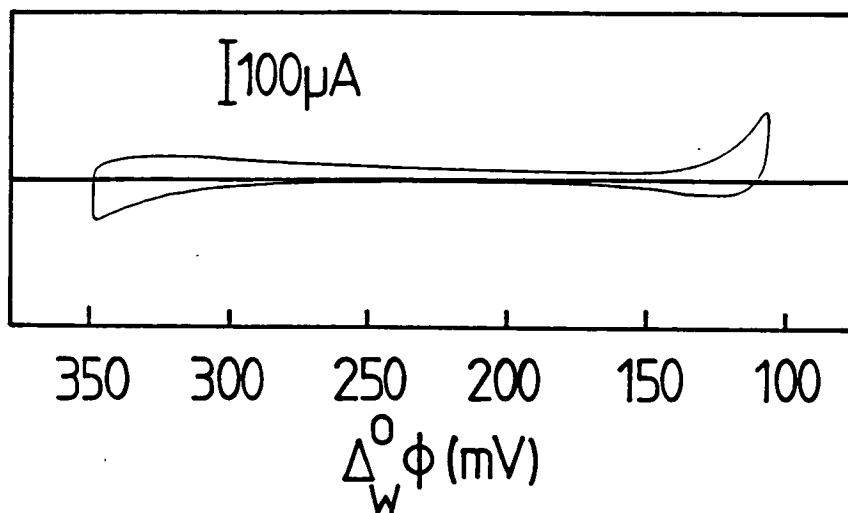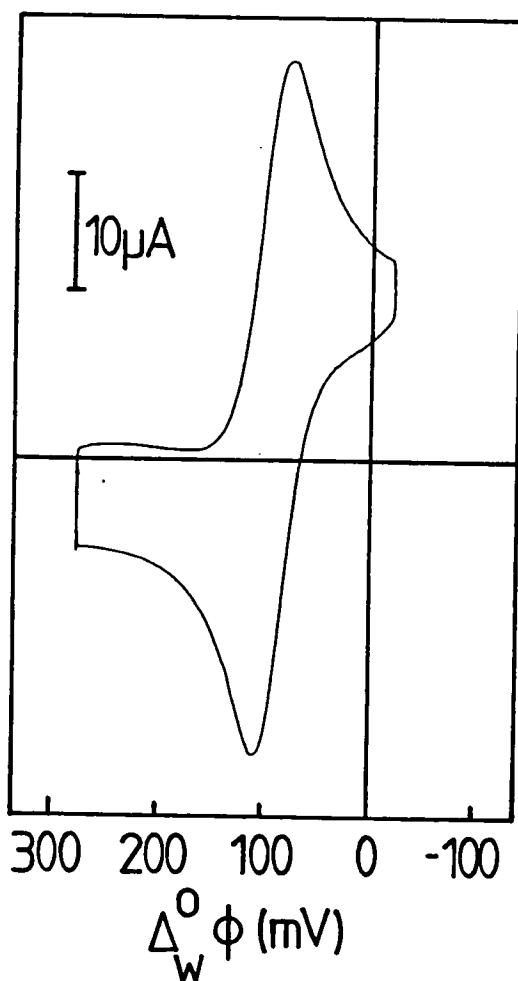**Figure 6.3.2.** Cyclic Voltammogram for Cell 6.1, x = 0.1.

Figure 6.3.3.   Variation of the peak current for cell 6.1 with
square root of scan rate, x=0.1 , y=0.
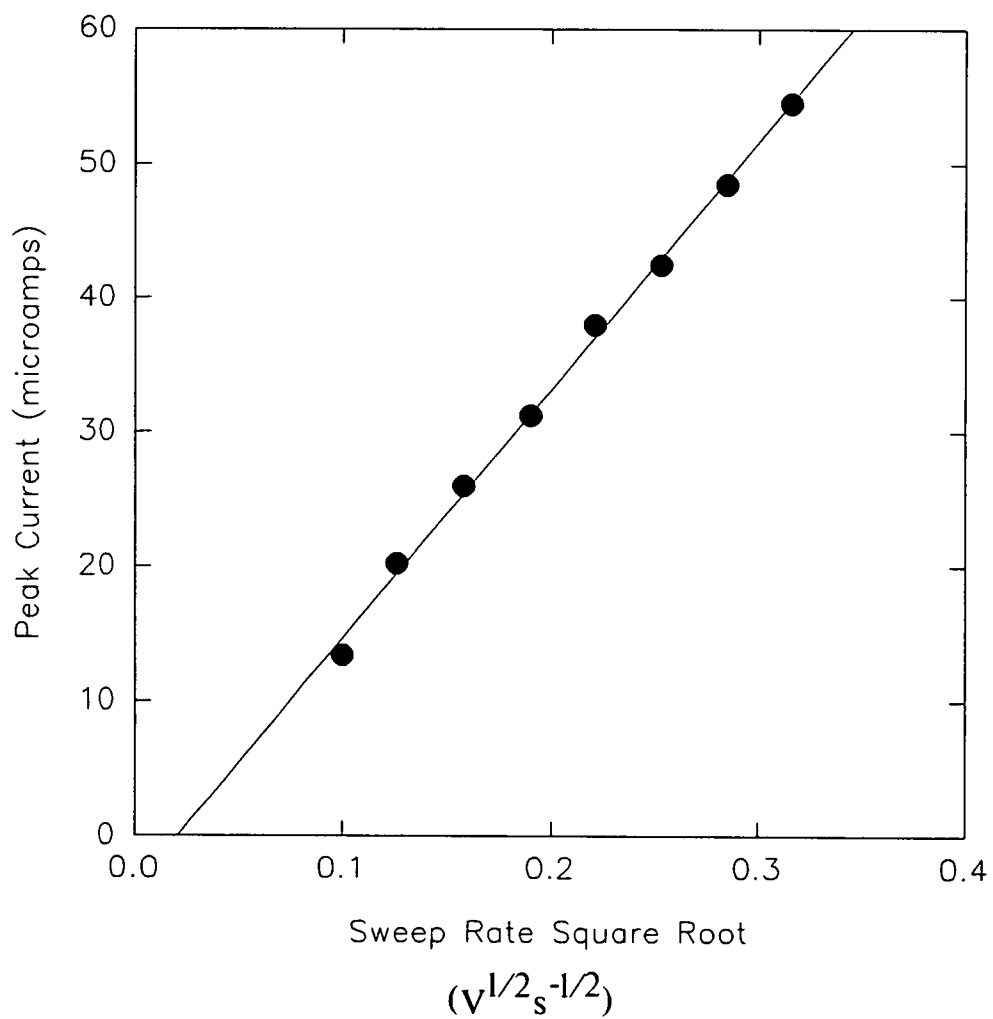
Figure 6.3.4. Cyclic Voltammogram for Cell 6.1,
x = 0.1 , y = 6.25.
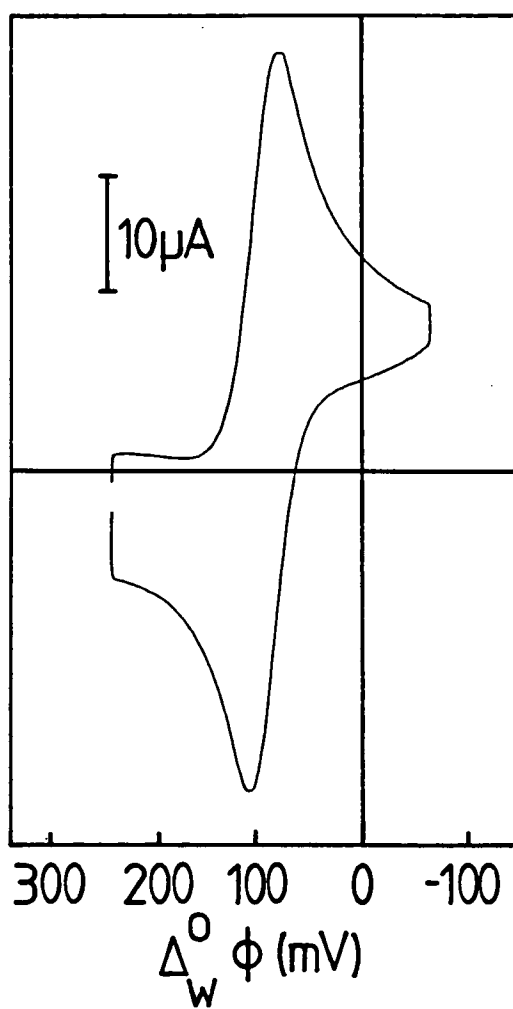
Figure 6.3.5. Variation of peak current with square root of the scan rate for cell 6.1 , x=0.1 , y=6.25.
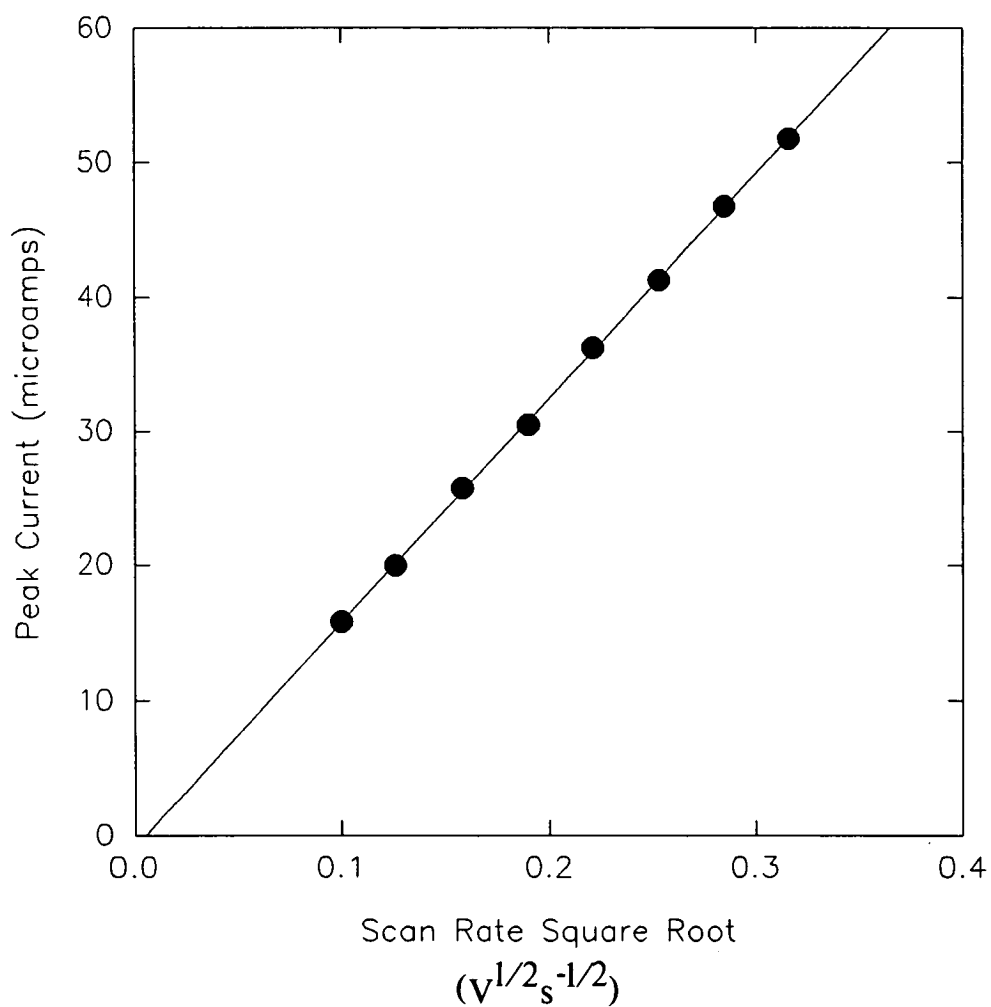
Figure 6.3.6. Extended Cyclic Voltammogram for Cell 6.1, x = 0.1 , y = 6.25.
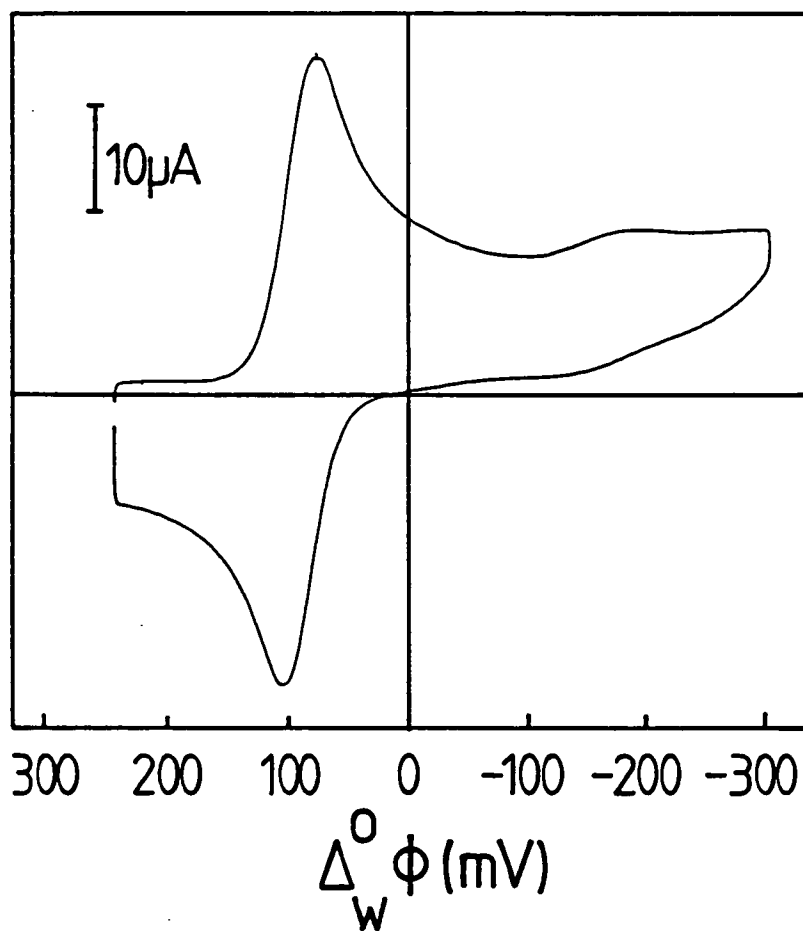
coefficient for the transferring species , calculated from the Randles-Sevcik equation was found to be 3.61 x 10^{-6} cm^2s^{-1}. The data from which this value is calculated are shown in figure 6.3.3. Data were collected at lower scan rates than those shown , but these values were found to be irreproducible , probably for instrumental reasons. No other waves could be observed for this system.

The voltammetric characteristics of cell 6.1 constructed with x = 0.1 and y = 6.25 were found to be broadly similar to those above. A wave , half wave potential 90 mV , corresponding to reversible transfer of an ion with z = 2 was found , shown in figure 6.3.4. The diffusion coefficient for this species was found to be 3.26 x 10^{-6} cm^2s^{-1} , the relevant data being shown in figure 6.3.5. In addition to this , a second wave was observed at lower potential corresponding to an irreversible process. The forward peak potential for this wave , shown in figure 6.3.6. , was found to be -195 mV at a sweep rate of 100 mVs^{-1}.

Cell 6.2 , was set up;

Ag/Ag_2SO_4/Li_2SO_4 (10 mmoldm^{-3})(aq)
//BTPPATPFB (10 mmoldm^{-3})
+ [Ru(bpy)$_3$][TPFB]$_2$ (0.145 mmoldm^{-3})(1,2-DCE)
/BTPPACl (1 mmoldm^{-3}) + LiCl (10 mmoldm^{-3})(aq)
/AgCl/Ag'
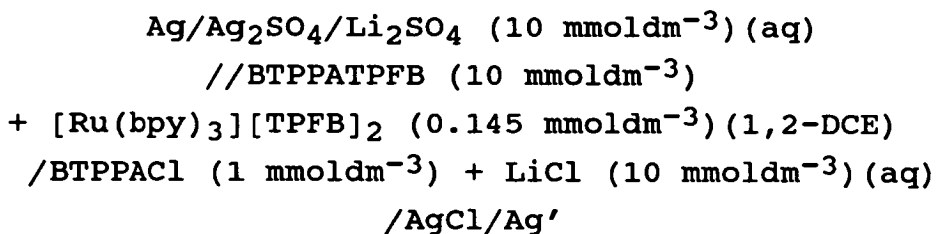
Cell 6.2.

The wave corresponding to transfer of the [Ru(bpy)$_3$]$^{2+}$ ion , shown in figure 6.3.7. was found to correspond to reversible transfer of a species , z = 2 , with a diffusion coefficient of 2.76 x 10^{-6} cm^2s^{-1}. The relevant data are shown in figure 6.3.8.

143

Figure 6.3.7. Cyclic Voltammograms for Cell 6.2.
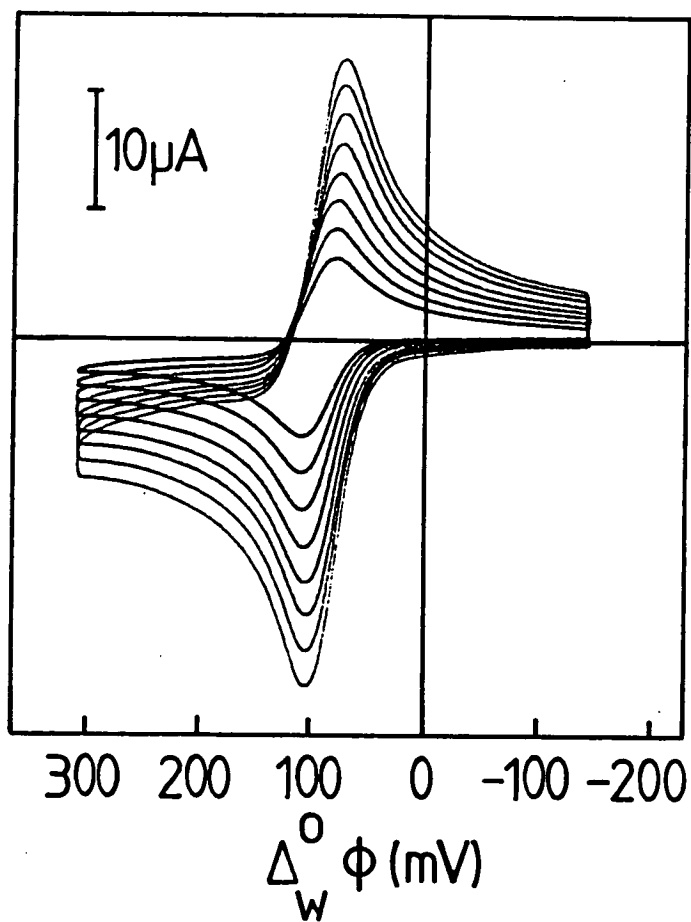
Sweep Rates 100, 81, 64, 49, 36, 25, 16, and 9 mVs^{-1}

Figure 6.3.8.   Variation of peak current with scan rate square root for cell 6.2.
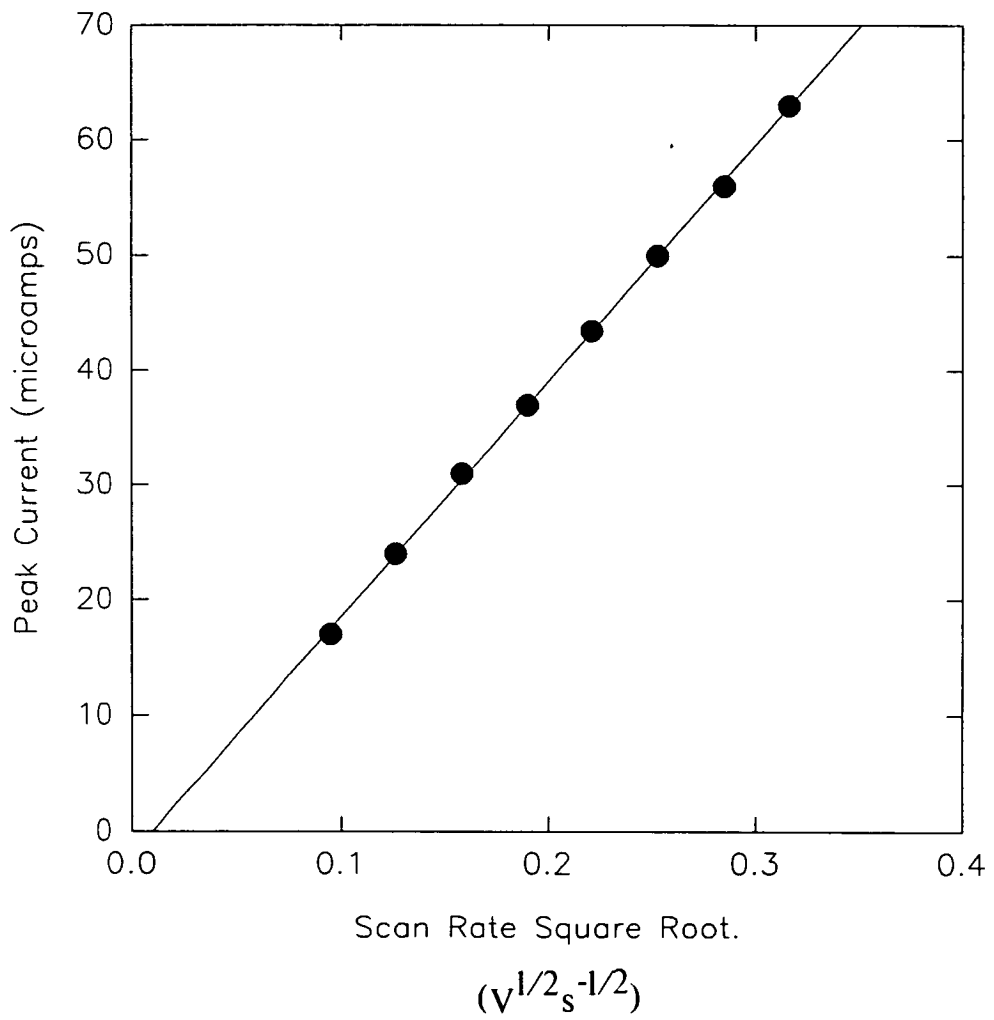
Section 6.3.2.   Photoelectrochemical Behaviour of Cell 6.1.

Irradiation of the interface of cell 6.1 constructed with $x = 2$, $y > 1$, with light from the xenon arc lamp led to the detection of a photocurrent corresponding to transfer of negative charge from the aqueous phase to the organic or of positive charge in the opposite direction. The typical development of this signal with time is shown in figure 6.3.9. All photocurrent measurements were made at an interfacial potential of 225mV unless otherwise indicated. The magnitude of this photocurrent was found to be highly reproducible, and did not depend on the time elapsed since the interface was assembled. Illumination of the interface for cell 6.1 with $x = 2$ and $y = 6.25$ constructed with air saturated solutions did not lead to a measureable photocurrent. Illumination of cell 6.1 assembled with $x = 0$ did not lead to any measureable signal with any concentration of TCNQ. A small signal, in the same direction as that found before was found upon irradiation of cell 6.1 with $x = 2$ and $y = 0$. All results presented here are corrected for this effect unless otherwise stated, the magnitude of this correction being determined from illumination of a suitable cell containing no TCNQ.

The response of the photocurrent to variation in the intensity of the incident radiation, controlled by means of neutral density filters, is shown in figure 6.3.10. The variation of the photocurrent for cell 6.1 with x, $y = 6.25$ is shown in figure 6.3.11. The change in the photoinduced signal with concentration of TCNQ is shown in figure 6.3.12. Derivation of the data for this figure was not as simple as for figure 6.3.11.

Because irradiation took place from below, light incident on the interface had passed through a solution of TCNQ. This compound is greenish-yellow in 1,2-DCE solution

Figure 6.3.9.   Typical Photocurrent for Cell 6.1.

Figure 6.3.10. Variation of the photocurrent for cell 6.1 with the transmittance of filter used.
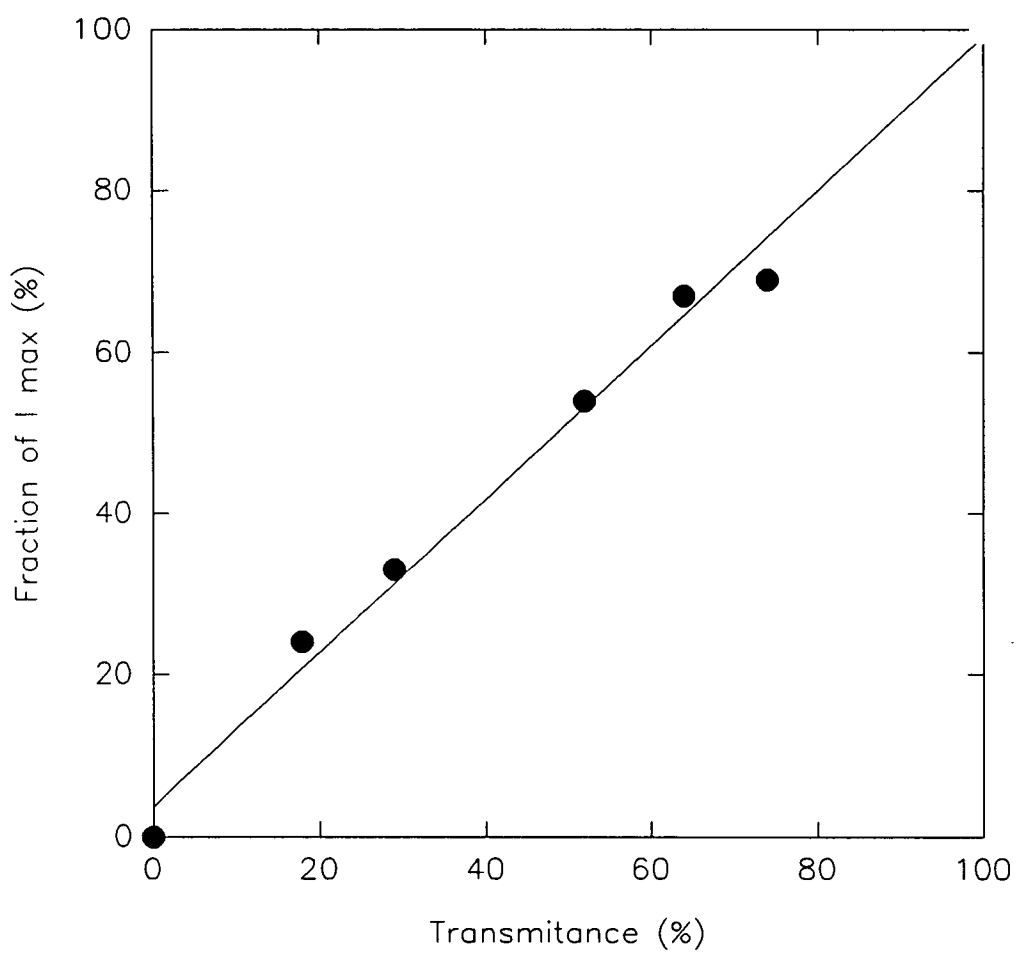
Figure 6.3.11. Variation of the photocurrent for cell 6.1 , y = 6.25 with x.
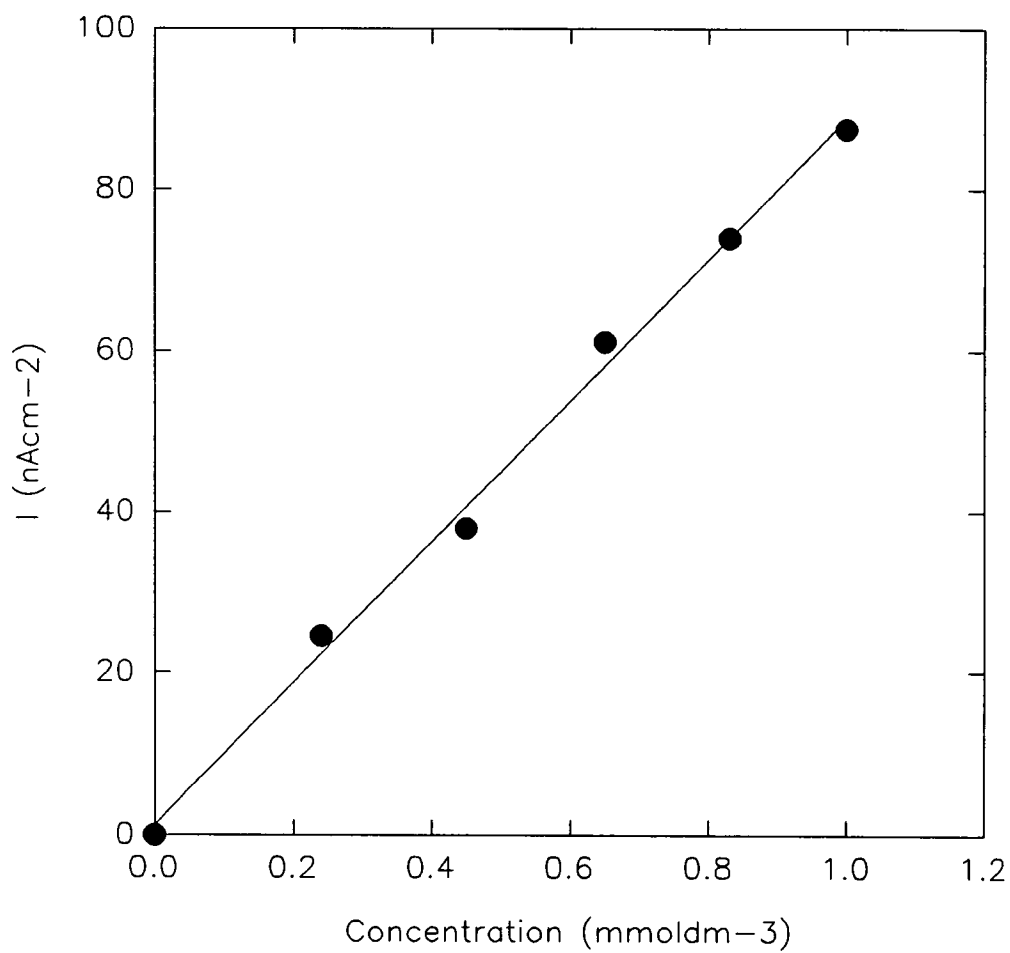
Figure 6.3.12.   Variation of the corrected photocurrent for cell 6.1 , x = 1 with y.
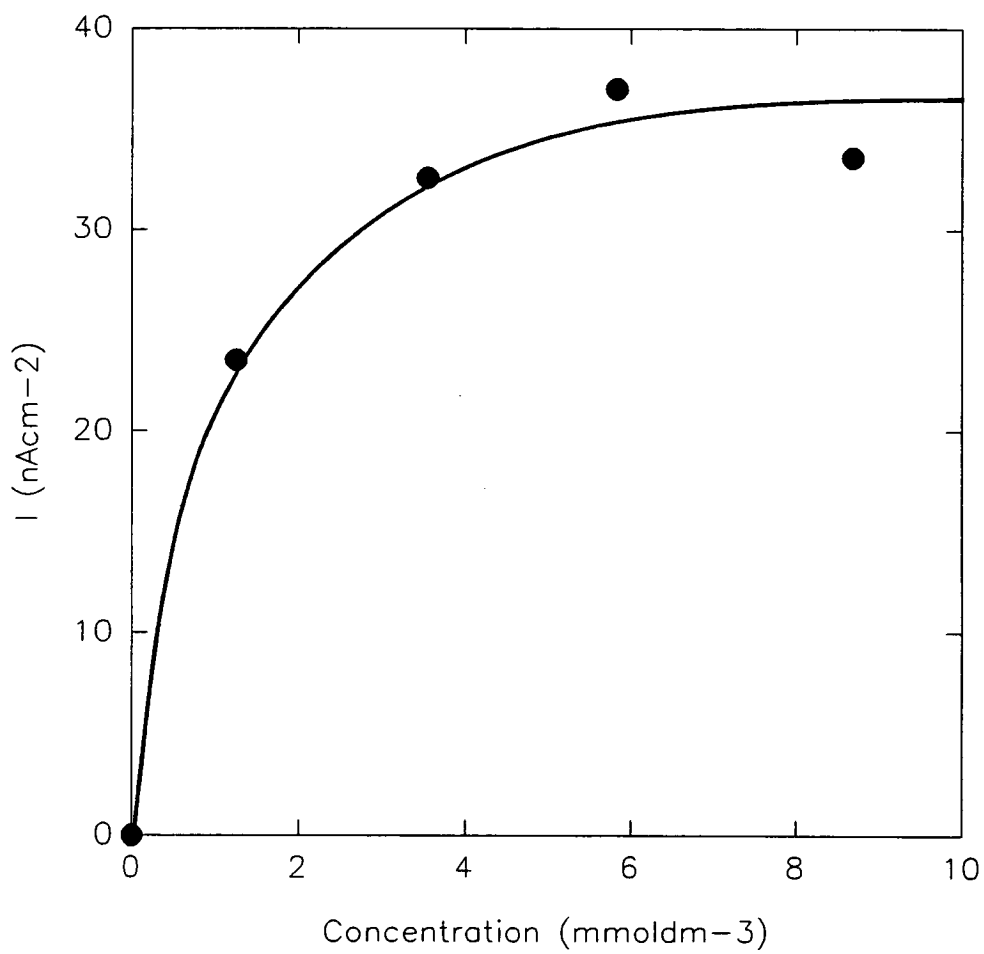
, and considerable overlap was found in the absorption spectra of TCNQ and the $[Ru(bpy)_3]^{2+}$ ion. This overlap is shown in figure 6.3.13. Because of this , changing the concentration of TCNQ in the organic phase also changes the light intensity at the interface and thus the concentration of excited $[Ru(bpy)_3]^{2+*}$ ions in the aqueous phase. This phenomenon is complex , involving as it does the overlap of the emission spectrum of the xenon lamp with the absorption spectra of two substances. It would not therefore be sufficient to use the extinction coefficient of TCNQ at one particular wavelength to calculate a correction factor for the light intensity. Instead , a new factor must be defined which relates specifically to the ability of TCNQ in 1,2-DCE solution to hinder the production of $[Ru(bpy)_3]^{2+*}$ ions in aqueous solution by light from this particular lamp having passed through that TCNQ solution.

The action spectrum for sensitisation of semiconductor electrodes by $[Ru(bpy)_3][SO_4]$ is known [52] to follow closely the absorption spectrum of the ruthenium complex. The value of the photocurrent is also known to depend in linear fashion on the incident light intensity. It was decided then to define an action coefficient , Ξ , to describe the extent to which solutions of TCNQ placed between the light source and the semiconductor could attenuate the photocurrent obtained. This action coefficient is analagous to the extinction coefficient in the Beer-Lambert law and is defined by;

$$\Xi = \log[S_0/S]/cL \quad \text{Equation 6.3.1.}$$

where S_0 is the photocurrent obtained with pure solvent in the cuvette , S that with TCNQ to a concentration c present in the same cuvette , of path length L. Figure 6.3.14. shows a plot of $\log[S_0/S]$ with TCNQ concentration. From the gradient of this line of

Figure 6.3.13. UV-Vis. Spectra for A. [Ru(bpy)$_3$][BF$_4$]$_2$ and B. TCNQ in 1,2-DCE.
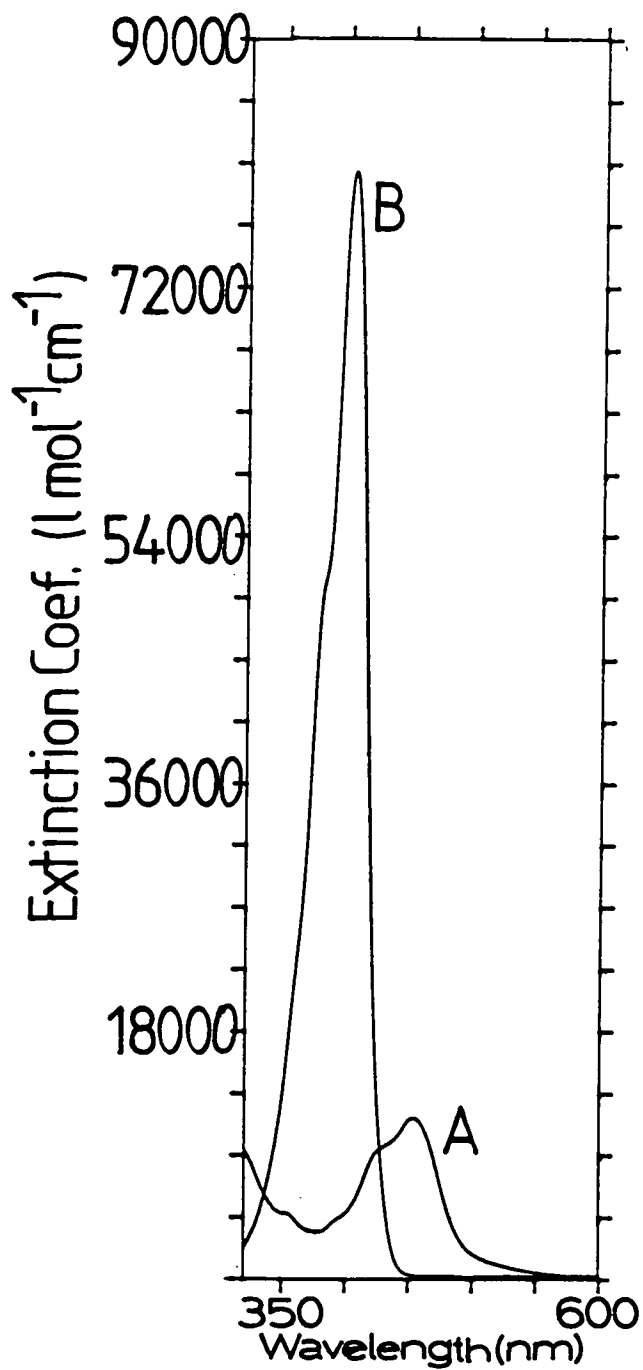
Figure 6.3.14.   Variation of log[So/S] with concentration of TCNQ
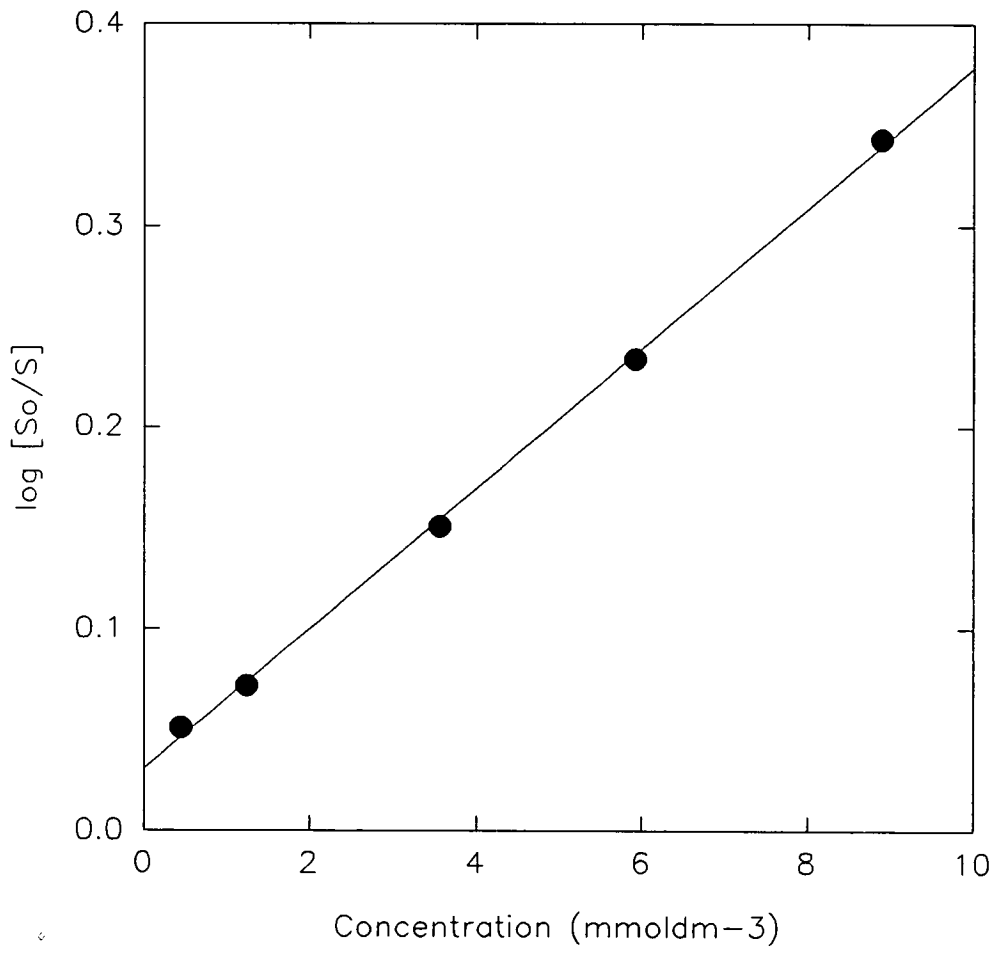
34.81 dm^3mol^{-1} ., and the value of L equal to 4cm , Ξ may be calculated to be 8.70 $dm^{-3}mol^{-1}cm^{-1}$.

The distance from the bottom of the four electrode cell to the interface was found to be 1.5cm so , assuming that the action spectrum for cell 6.1 is the same as that for the situation described above , the signal obtained from cell 6.1 with a given value of y may be corrected for absorption effects from;

$$S_o = S.10^{13.05y} \qquad \text{Equation 6.3.2.}$$

where S is the uncorrected signal , S_0 the corrected value , y the concentration of TCNQ in the organic phase. Table 3.6.1. details the treatment of the original data required to generate figure 6.3.12. This shows the variation of the photocurrent obtained for cell 6.1, x = 1 with the concentration of TCNQ , corrected for background signal and absorption effects.

Table 6.3.1. Data for Figure 6.3.12.

y (mmoldm^{-3})	S (nAcm^{-2})	S_0 (nAcm^{-2})	Background Signal(nAcm^{-2})	Corrected Signal(nAcm^{-2})
0.00	11.6	11.6	11.6	0.0
1.25	33.8	35.1	11.6	23.5
3.55	39.7	44.2	11.6	32.6
5.84	40.8	48.6	11.6	37.0
8.68	34.8	45.2	11.6	33.6

The variation of the signal from cell 6.1 , x = 1 , y = 6 , with interfacial potential difference is shown in figure 6.3.15. The curve labelled B corresponds to the dark current , that labelled C to the photocurrent. The potential was swept at a rate of 0.2 mVs^{-1} for these two curves. A is a cyclic voltammogram for this cell on the same potential scale. Figure 6.3.16. shows the variation
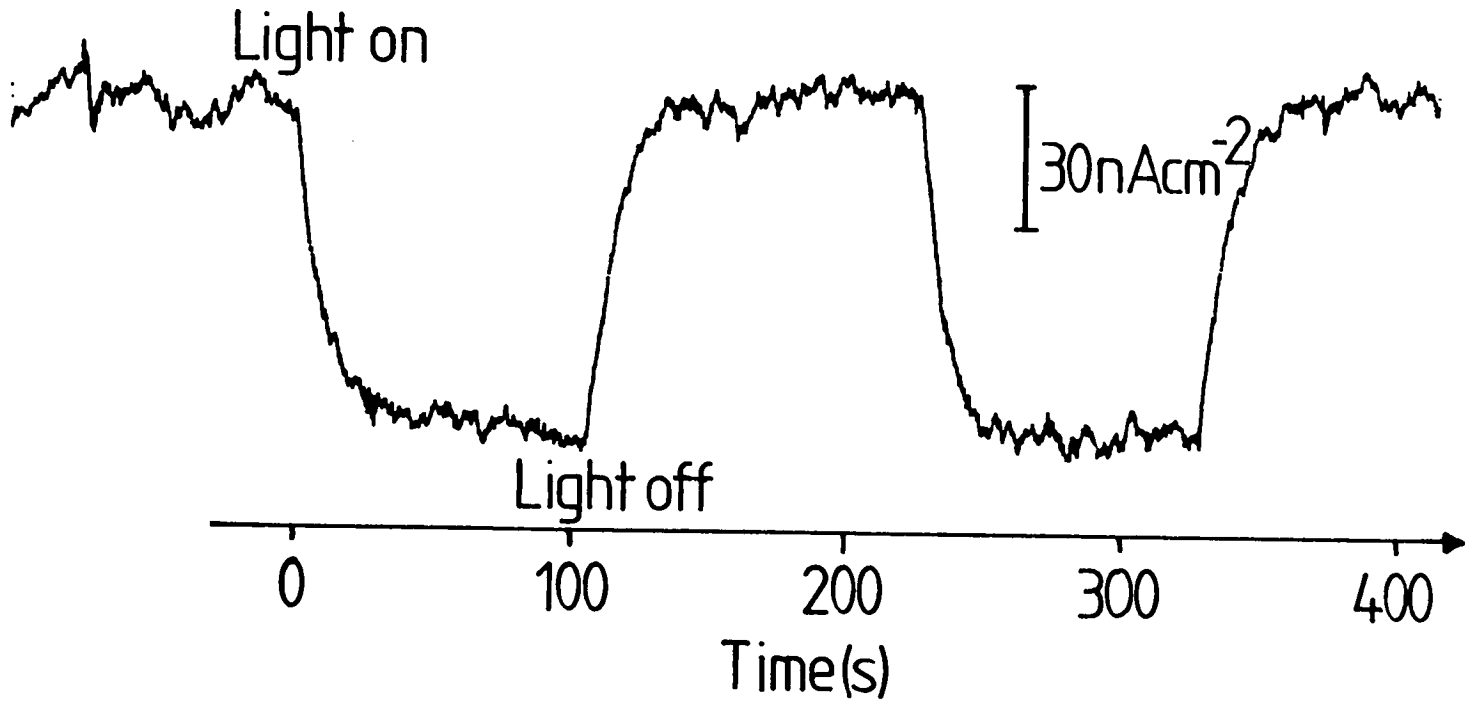
Figure 6.3.15. Variation of the Photocurrent for Cell 6.1 with Interfacial Potential.
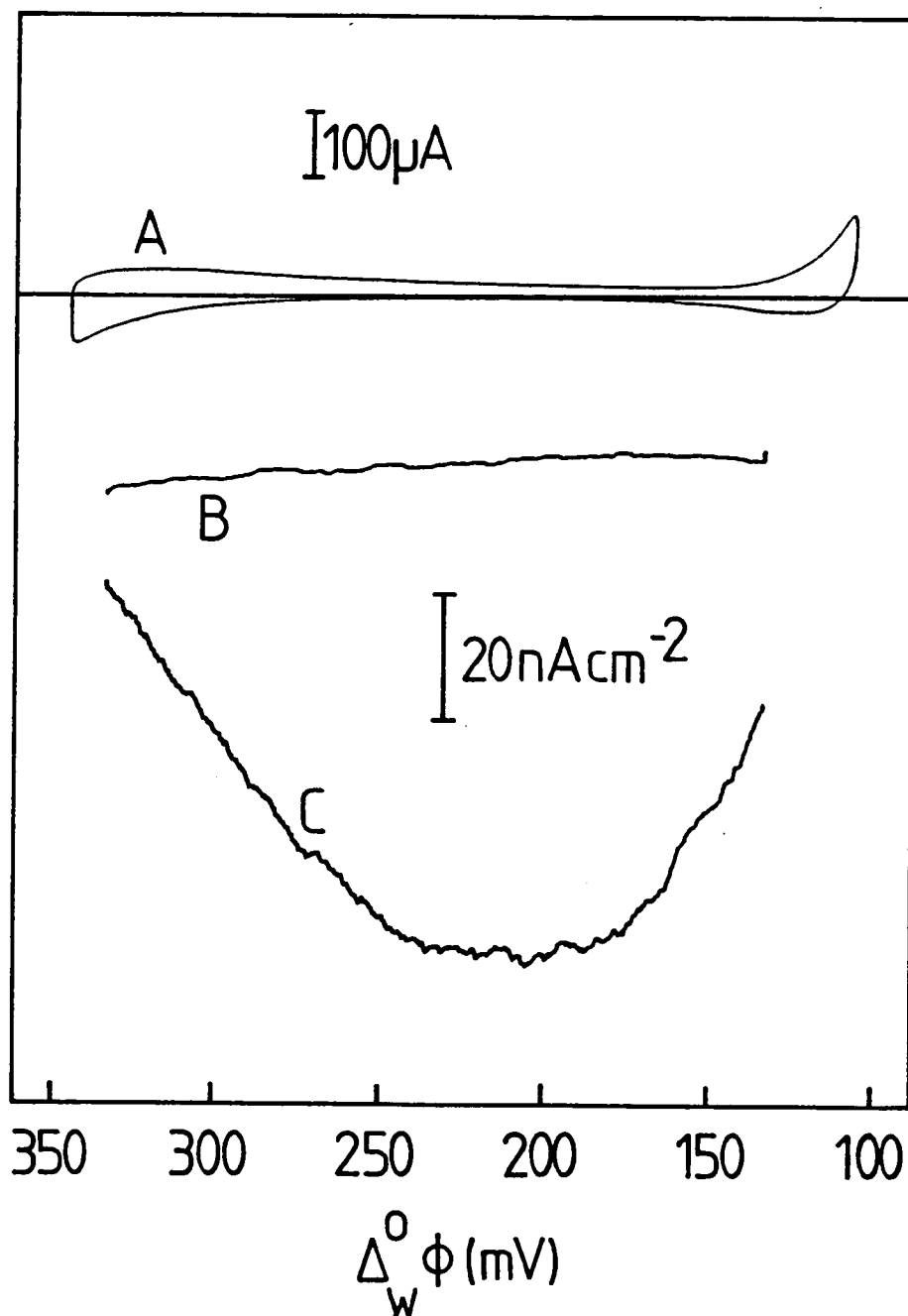
Figure 6.3.16   Variation of the photocurrent for cell 6.1 with concentration of phosphatidylcholine.
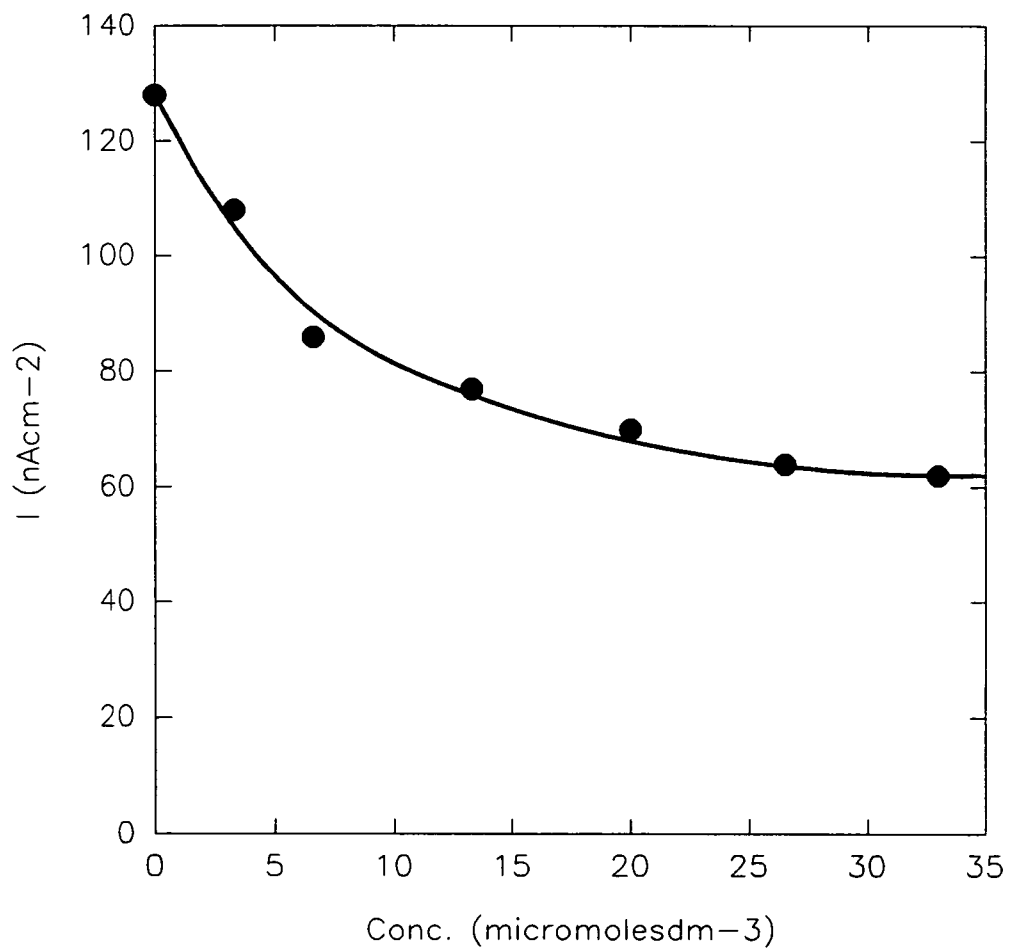
of the photocurrent from cell 6.1 , x = 2 , y = 6.25 with variation of the concentration of phosphatidylcholine in the organic phase.

The first reduction of TCNQ at a platinum minidisc electrode , $E_{1/2}$ = -190mV *versus* FeC^+/FeC , in $TBABF_4$ (250 mmoldm^{-3}) in water saturated 1,2-DCE was found to be reversible at sweep rates between 100 and 10 mVs^{-1}.

The potential for the first oxidation of $[Ru(bpy)_3]^{2+}[BF_4]$ in $TBABF_4$ (500 mmoldm^{-3}) in 1,2-DCE was found to be 930 mV *versus* FeC^+/FeC at the same electrode.

Section 6.4.1.   Discussion of the Voltammetric Results.

The values of the diffusion coefficients determined for the $[Ru(bpy)_3]^{2+}$ ion in water and DCE , using cells 6.2 and 6.1 , x = 0.1 , y = 0 allow calculation of the formal cell potential for transfer of this species from equation 6.4.1.

$$\Delta\varphi_W^{O\,0\prime} = \Delta\varphi_W^O{}_{1/2} - RT/zF.\ln[D^W/D^O] \quad \text{Eqn. 6.4.1.}$$

Using the relevant experimental values leads to a formal cell potential for transfer of the $[Ru(bpy)_3]^{2+}$ ion of 93mV at 293K at the water 1,2-DCE interface , and thus a free energy of transfer from 1,2-DCE to water of 17.9 kJmol^{-1}. The values of D^O and D^W are in good accord with Walden's rule, D^W/D^O being 1.18 against an expected value of 1.2 [67].

Intuitively it would be expected that the value of D^O calculated for cell 6.1 would be independent of y , the concentration of TCNQ in the organic phase. This indeed was found to be the case , within the limits of experimental error, which were rather larger than they might have been. Figure 6.3.6. also shows a wave , corresponding to an irreversible process , with a forward peak potential of -195 mV at a sweep rate of 100 mVs^{-1}.

This agrees well with the value found for transfer of the $TCNQ^-$ radical anion in Chapter 3. It seems possible then that some process has led , for cell 6.1 , y = 6.25 , to the production of $TCNQ^-$ in the organic phase. There are two mechanisms which might be put forward for this process , one homo- and one heterogeneous.

A homogeneous process would involve transfer of the $[Ru(bpy)_3]^{2+}$ ion from aqueous to organic phase as the potential was swept negative. Once in the organic phase this ion would be oxidised by TCNQ to the $[Ru(bpy)_3]^{3+}$ ion. This mechanism is unlikely on a number of grounds. Firstly , on the basis of known electrode potentials , this reaction should be endothermic. The UV-Vis. spectrum of a mixture of $[Ru(bpy)_3][BF_4]_2$ and TCNQ in 1,2-DCE was found to correspond to the superimposed spectra of the two compounds , which leaves as untenable the hypothesis that these two react in 1,2-DCE.

It seems more likely then that a heterogeneous mechanism is at work. If there was a wave corresponding to electron transfer between TCNQ and $[Ru(bpy)_3]^{2+}$ which occurred at similar potentials to ion transfer, this would result in a net decrease in observed current densities, and thus in the apparent diffusion coefficient for the ion in the presence of TCNQ. Unfortunately the difference found for this quantity is not significant given that control of the cell temperature was not rigorous.

The electrode potentials reported in section 6.3. for TCNQ and the $[Ru(bpy)_3]^{2+}$ ion allow the free energy of reaction between these two species in 1,2-DCE to be calculated to be $+108kJmol^{-1}$. The free energies of transfer of the oxidised and reduced forms of the ruthenium complex are known and so a thermodynamic cycle may be constructed for the heterogeneous electron transfer reaction;

Figure 6.4.1. Thermodynamic Cycle for the Heterogeneous Oxidation of $[Ru(bpy)_3]^{2+}$ by TCNQ.

$$[Ru(bpy)_3]^{2+}{}_{DCE} + TCNQ_{DCE} \overset{\Delta G_{HOM}}{\rightleftharpoons} [Ru(bpy)_3]^{3+}{}_{DCE} + TCNQ^-_{DCE}$$

$$\Delta G^{DCE \to H2O}_{tr,RuII} \qquad -\Delta G^{DCE \to H2O}_{tr,RuIII}$$

$$[Ru(bpy)_3]^{2+}{}_{H2O} + TCNQ_{DCE} \overset{\Delta G_{HET}}{\rightleftharpoons} [Ru(bpy)_3]^{3+}{}_{H2O} + TCNQ^-_{DCE}$$
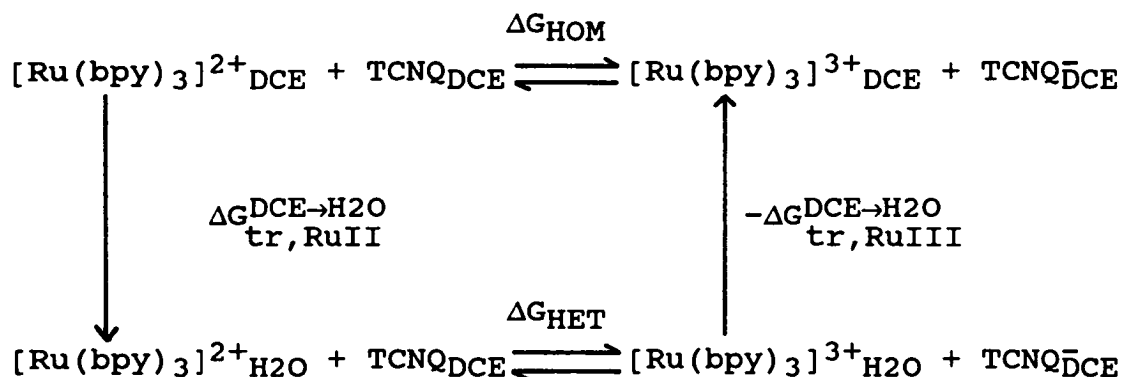
It can be easily seen then that the free energy of heterogeneous reaction is given by

$$\Delta G_{HET} = \Delta G_{HOM} + \Delta G^{DCE \to H2O}_{tr,RuII} - \Delta G^{DCE \to H2O}_{tr,RuIII} \qquad \text{Eqn. 6.4.2.}$$

using the values determined here and in Chapter 3 for ΔG_{HOM} , $\Delta G^{DCE \to H2O}_{tr,RuII}$ and $\Delta G^{DCE \to H2O}_{tr,RuIII}$ of 108 , 17.3 and -35.0 $kJmol^{-1}$. This yields a value for ΔG_{HET} of 160.3 $kJmol^{-1}$ and thus a value of $\Delta^O_w \varphi^0_{HET}$ of 1660 mV.

This potential is of course well outside the potential window available for cell 6.1. Neither is this the only argument against the occurence of a heterogeneous reaction. Such a process should produce the $[Ru(bpy)_3]^{3+}$ ion in the aqueous phase. The transfer of this species should be observed in figure 6.3.6. at around -120mV , but no such peak may be discerned.

The peak at -190mV is not present in the cyclic voltammogram for cell 6.1 with x = 0 , y = 6.25 , and so clearly the ruthenium complex plays some part in its generation , but the exact mechanism is unclear. $TCNQ^-$ might result from a reaction at the platinum counter electrode, but this is distant from the interface by some 15mm, and the peak at -190mV is present in even the first scan.

Section 6.4.2.   Discussion of the Photoelectrochemical Behaviour of Cell 6.1.

The photocurrent generated through illumination of cell 6.1 corresponds to the transfer of negative charge from the aqueous phase to the organic , or of positive charge in the opposite direction. This is consistent with the assignment of the observed signal to PET , the transfer of an anion from the aqueous phase or a cation from the organic phase. It is certain that the signal does not arise from a photoinduced potential for three reasons. The interfacial potential is controlled through a potentiostat , and should thus be invulnerable to potential shifts. Furthermore the signal is extinguished by the presence of oxygen , which does not affect the amount of energy absorbed by the system and also the signal is at a maximum in the middle of the potential window , where any shift in potential would have the least effect on the current passed.

Figures 6.3.11. and 6.3.12. show clearly that the signal increases with the concentration both of the sensitiser and the quencher. Figure 6.3.11. shows a linear relationship , as expected whilst figure 6.3.12. shows a more complex pattern. It appears that the signal quickly comes to a maximum as the concentration of TCNQ is increased. This might be explained by the low steady state concentration of the excited $[Ru(bpy)_3]^{2+*}$ ion at the interface. Because this concentration is low , almost any concentration of TCNQ in the organic phase should constitute an excess , rendering the process *pseudo* first order with respect to the excited $[Ru(bpy)_3]^{2+*}$ ion.

If the signal is to be assigned as an ion transfer current following electron transfer then some interfacial reaction must be postulated which gives rise either to a hydrophilic cation in the organic phase or a hydrophobic anion in the aqueous phase. It could be argued that there

160

was partition of the TCNQ into the aqueous phase , and that this was reduced in a homogeneous reaction with the excited $[Ru(bpy)_3]^{2+*}$ ion. In this case however , there would be no mechanism to prevent the subsequent highly exothermic back reaction.

It is postulated then that the photocurrent for cell 6.1 , y > 0 arises from photoinitiated electron transfer across the interface between water and 1,2-DCE , according to the following scheme.

Figure 6.4.2. Scheme to Account for the Photocurrent in Cell 6.1.

Aqueous

$$h\nu$$
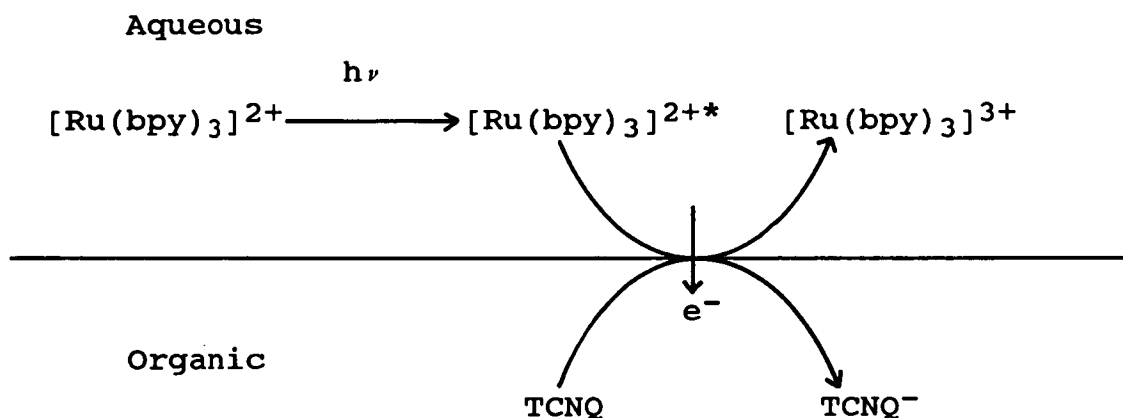
$[Ru(bpy)_3]^{2+} \longrightarrow [Ru(bpy)_3]^{2+*} \qquad [Ru(bpy)_3]^{3+}$$

Organic

e^-

TCNQ   TCNQ$^-$

It can be seen from figure 6.4.2. that the products of the supposed PET reaction are TCNQ$^-$ and $[Ru(bpy)_3]^{3+}$. The TCNQ$^{0/-1}$ couple was found to be reversible in water saturated 1,2-DCE and so it can be supposed that TCNQ$^-$ formed in a photoreaction will also be stable. In order that the signal measured should correspond solely to electron transfer , it must be certain that neither of the two species formed will cross the interface. The photocurrent measurements reported here were carried out at interfacial potentials of between 125 and 325 mV. This range lies well positive of the transfer potential of the $[Ru(bpy)_3]^{3+}$ ion of -124 mV. Although it cannot be certain

that the transfer potential for TCNQ⁻ lies in this potential range , it seems from the results presented in Chapter 3 that this value is around -150 mV. The conclusion is then that the products of the PET step will remain in their separate phases.

This is probably also the reason why a net photoreaction can be observed in this system. the measurements have been carried out at an interfacial potential for which the presence of the initial photoproducts at the interface is energetically unfavourable. This ensures that back reaction between the TCNQ⁻ and $[Ru(bpy)_3]^{3+}$ ions is hindered to some extent , thus allowing a net reaction to take place.

A thermodynamic cycle may be constructed for the proposed photoinitiated heterogeneous process similar to that shown in figure 6.4.1. for heterogeneous electron transfer between the ground state species.

Figure 6.4.3.   Thermodynamic Cycle for Photoinitiated Electron Transfer.

$$[Ru(bpy)_3]^{2+*}_{DCE} + TCNQ_{DCE} \underset{\Delta G_{HOM}}{\rightleftarrows} [Ru(bpy)_3]^{3+*}_{DCE} + TCNQ^-_{DCE}$$

$$\Delta G^{DCE \to H2O}_{tr,Ru(II)*} \qquad -\Delta G^{DCE \to H2O}_{tr,Ru(III)}$$

$$[Ru(bpy)_3]^{2+*}_{H2O} + TCNQ_{DCE} \underset{\Delta G_{HET}}{\rightleftarrows} [Ru(bpy)_3]^{3+}_{H2O} + TCNQ^-_{DCE}$$

Again it may be seen that;

$$\Delta G_{HET} = \Delta G_{HOM} + \Delta G^{DCE \to H2O}_{tr,Ru(II)*} - \Delta G^{DCE \to H2O}_{tr,Ru(III)} \quad \text{Equation 6.4.3.}$$

Assuming, for want of any better figure, that the free energy of transfer of the excited ruthenium species is the same as that of the ground state ion and that the

excited state is 2V [99] easier to oxidise than the ground state in 1,2-DCE then ΔG_{HOM} is $-84.9 kJmol^{-1}$ and ΔG_{HET} is $-32.6 kJmol^{-1}$. This leads in turn to a value of $\Delta_O^W \varphi_{HOM}^O$ of $-338mV$. All these figures are of course approximate but it would appear then that the heterogeneous reaction postulated in figure 6.4.3. should be spontaneous over the whole potential window for cell 6.1.

Figure 6.3.15. shows the variation of the photocurrent with $\Delta_W^O \varphi$. The observed pattern is not readily explicable but may simply demonstrate the sensitivity of the PET signal to the ion transfer currents which are incipient as the ends of the potential window are approached.

Figure 6.3.16. backs up the assignment of the process reported here as interfacial. Phosphatidylcholine is known to adsorb strongly at the water/1,2-DCE interface [98]. this figure shows clearly that the presence of this lipid in solution leads to a reduction in the photocurrent recorded. This diminution of the signal appears to level out as higher concentrations are reached. This phenomenon may well be due to the restriction of access of excited $[Ru(bpy)_3]^{2+*}$ ions to TCNQ molecules in the organic phase in the presence of an adsorbed monolayer at the interface.

Section 6.5.   Conclusion.

The phenomenon of photoinitiated electron transfer at the interface between two immiscible electrolyte solutions has , in all probability been demonstrated. There now exists the opportunity for a great deal of work to characterise this effect more fully, both from the practical and theoretical aspects. Practical work could start with the use of different sensitisers and quenchers in systems similar to these. Quenchers which might prove useful would be such substances as tetracyanoethene and tertrachlorobenzodiquinone. Both these species have facile

, reversible reductive couples. A more hydrophilic sensitiser ion than $[Ru(bpy)_3]^{2+}$ would provide a greater window of polarisation , and synthesis of such species should be considered. The system reported here will no doubt appear rustic should any further work in this field be carried out.

References.

97.   V.A. Starodubova , G.G. Blagopoluchnaya and V.I.
Titov, Izv. Sib. Otd. Akad. Nauk SSSR, Ser. Khim. Nauk
5(1977)78.

98.   D.J. Schiffrin and H.H. Girault in Charge Field Eff.
Biosyst., Abacus Press, (1984)171.

99. P.D. Rillema, G. Allen, T.J. Meyer and D. Conrad,
Inorg. Chem., 22(1983)1283.

*"The hardest bones, containing the richest marrow, can be
conquered only by a united crunching of all the teeth of
all dogs. That, of course, is only a figure of speech and
exaggerated; if all teeth were but ready they would not
need even to bite, the bones would crack themselves and
the marrow would be freely accessible even to the feeblest
of dogs. "*

Franz Kafka "Investigations of a Dog"

EPILOGUE

It has been shown that the ITIES is a fruitful hunting ground for the photoelectrochemist in search of novel phenomena. There exists still a vast and largely untapped potential for experiment in this field. Perhaps the most obvious step towards increasing the efficiency of PET reactions at the ITIES would be to work with sensitisers and quenchers which were capable of being adsorbed at the interface, and thus brought into closer association with one another. Surfactant derivatives of the basic 2,2′-bipyridyl ligand are known and these would seem to represent suitable first building blocks in the construction of the edifice to which this field could amount.

There are also a number of other experiments which could be attempted, less certain of success, but potentially more rewarding. Intramolecular PET reactions between metal centres have been recognised spectroscopically for some time. The possibility arises then that a suitable amphiphilic molecule adsorbed at the ITIES could give rise to a measureable electrochemical signal as a result of intramolecular photoinitiated electron transfer. Such a molecule would require careful design, taking into account spectroscopic, redox and surfactant factors.

The design of any practical photogalvanic device based on immiscible electrolytes is still in the distant future. The realisation of such a contrivance would require sensitisers and quenchers stable to extended periods of irradiation. Even 1,2-DCE, the organic solvent of choice at the moment, is not stable to prolonged exposure to visible light. Such problems have not proved insurmountable in other fields.

166

APPENDIX ONE

Computer Programs.

The following programs were written and run on the Edinburgh Multi-Access System.

Program "Marcel".

This program was written to evaluate Equation 2.5.4. as a function of time.

```
        PROGRAM MARCEL
C       Prog to model photoinitiated ion transfer across ITIES
C       With kinetic control of transfer k=KPRIME
C       And separate the factors determining current

        IMPLICIT DOUBLE PRECISION (A-H,K,O-Z)

C       Set up data files

        CHARACTER*7 XFILE
        CHARACTER*2 XNUM

C       Name data files

        CALLEMAS3PROMPT('TWO DIGIT ID FOR CURRENT DATAFILE(XDATA)IS  ')
        READ(5,*)NUM
        WRITE(XNUM,6000)NUM
        XFILE='XDATA'
        XFILE(6:7)=XNUM
        OPEN(10,FILE=XFILE,FILETYPE='C')


C       Assignment of variables

        F=96485
        CONC=2.4E-6
        DIFCO=1.E-5
        EPSILON=1.38E7
        TENSITY=9.05E-10
        KPRIME=1
        CALLEMAS3PROMPT('RATE CONSTANT FOR EXP DECAY IS?...')
          READ(5,*)K
        CALLEMAS3PROMPT('QUANTUM YIELD IS.....?')
          READ(5,*)PHI
        ALPHA=EPSILON*CONC
        BETA=K-DIFCO*ALPHA**2
        A=PHI*TENSITY*EPSILON*CONC
        SPLAT=((KPRIME**2)/DIFCO)-K
        FACT1=(F*A*DIFCO*KPRIME)/(KPRIME-(DIFCO*ALPHA))
        TIME=0
```

```
C       Calc of current density over 500 seconds
C       Evn. of function in five sections

        DO 10 COUNT=0,300,1
         TIME=COUNT
         FACT2=(SQRT(K/DIFCO))*ERF(SQRT(K*TIME))
         X=ALPHA*(SQRT(DIFCO*TIME))
         1F (X.GT.2) THEN
         SER1=2*(X**2)
         SER2=1/1.7726*X
         SER3=1/SER1
         SER4=3/((SER1**2))
         SER5=15/((SER1**3))
         SERIES=SER2*(1-SER3+SER4-SER5)
         FACT3=EXP(-K*TIME)*SERIES
         ELSE
         FACT3=(EXP(-BETA*TIME))*(1-(ERF(ALPHA*(SQRT(DIFCO*TIME)))))
         ENDIF
         X=(KPRIME**2)*(TIME/DIFCO)
         IF (X.GT.2) THEN
         SER1=2*(X**2)
         SER2=1/(1.7726*X)
         SER3=1/SER1
         SER4=3/((SER1**2))
         SER5=15/((SER1**3))
         SERIES=SER2*(1-SER3+SER4-SER5)
         FACT4=EXP(-K*TIME)*SERIES
         ELSE
         FACT4=EXP(SPLAT*TIME)*(1-(ERF(KPRIME**2)*((TIME/DIFCO))))
         ENDIF

C       Now calculate currents

         FACT5A=((-ALPHA/BETA)*(1-FACT3))
         FACT5B=((KPRIME/(SPLAT*DIFCO))*(1-FACT4))
         FACT5C=((1/BETA)+(1/SPLAT))*FACT2
         CURRENTL=FACT1*(FACT5A-FACT5B+FACT5C)
         CURRENT=CURRENTL*1E9
         FACT6=-FACT1*(1/BETA)*(ALPHA-FACT2-(ALPHA*FACT3))
         FACT7=FACT1*(1/SPLAT)*(FACT2-((KPRIME/DIFCO)*FACT4))
C       Send data to data files
         WRITE (10,*)TIME,CURRENT
10      CONTINUE
        PRINT*,'ION TRANSFER WITH KINETIC CONTROL COMPLETE'
        PRINT*,'TIME vs.CURRENT DATA IN FILE ',XFILE
        CLOSE(10)
 6000   FORMAT(I2)
        END
```

Program "Jeanpaul".

This program was written to evaluate Equation 2.5.5. as a function of concentration.

```
      PROGRAM JEANPAUL
C     Limiting TPB type photocurr as function of conc

      IMPLICIT DOUBLE PRECISION (A-H,K,O-Z)

C     Set up data files

      CHARACTER*7 ZFILE
      CHARACTER*2 ZNUM

C     Name data files

      CALLEMAS3PROMPT('TWO DIGIT ID FOR  DATAFILE(ZDATA)IS  ')
      READ(5,*)NUM
      WRITE(ZNUM,6000)NUM
      ZFILE='ZDATA'
      ZFILE(6:7)=ZNUM
      OPEN(10,FILE=ZFILE,FILETYPE='C')

C     Assignment of variables

      F=96485
      DIFCO=1.E-5
      EPSILON=1.38E7
      TENSITY=9.05E-10
      KPRIME=1
      PHI=2.54E-3
      CALL EMAS3PROMPT('K IS ?  ')
      READ(5,*)K
      DO 10 COUNT=5E-8,3E-6,5E-8
       CONC=COUNT
       ALPHA=EPSILON*CONC
       A=PHI*TENSITY*EPSILON*CONC
       FACT1=KPRIME/(KPRIME+SQRT(K*DIFCO))
       FACT2=F*A/(ALPHA+SQRT(K/DIFCO))
       FACT3=FACT2*FACT1
       CURRENT=FACT3*1E9
       CONCM=CONC*1E6
       WRITE (10,*)CONCM,CURRENT
10    CONTINUE
      PRINT*,'DATA IN FILE ',ZFILE
      CLOSE(10)
6000  FORMAT(I2)
      END
```

APPENDIX TWO

Synthetic Methods.

The preparation of LiTPFB was based on the work of Massey and Park [100]. Bromopentafluorobenzene (Aldrich 6ml , 48mmol) was dissolved in dry pentane (150ml) placed in a three necked flask equiped with a thermocouple probe , gas inlet , pressure equalised dropping funnel and stirrer bar. The flask contents were then deaerated by bubbling with oxygen free nitrogen and cooled to 198K using a dry ice/methanol slush bath.

2.5moldm^{-3} butyllithium in hexanes (19.2ml , 48mmol) was transfered by syringe to the dropping funnel through a rubber septum , and added dropwise to the reaction vessel. Vigorous stirring was maintained throughout the reaction.The resulting suspension of pentafluorophenyl-lithium was stirred for a further 10 minutes.

1.0 moldm^{-3} boron trichloride in hexanes (12ml , 12mmol) was transfered to the cleaned dropping funnel and added dropwise over fifteen minutes. Forty minutes after this addition was complete , the temperature of the vessel was allowed slowly to rise to that of the laboratory. Care must be taken at this stage as any excess organometallic reagent can decompose violently if the the vessel warms too quickly , resulting in a lowered yield.

Once at room temperature the reaction liquor was filtered to yield an ochre powder. This solid was washed with dichloromethane (100ml) wich was then filtered and evaporated to yield a yellow oil. Trituration of this oil with hexane yielded an ivory powder which was redisolved in dichloromethane. Addition of excess hexane precipitated the white lithium tetrakis(pentafluorophenyl)borate.

In general , salts not commercially available were

prepared by direct metathesis. Equimolar aqueous solutions were mixed , the solid collected by vacuum filtration and recrystallised twice from an acetone/water mixture. This was achieved by dissolving the wet solid in the minimum volume of boiling acetone and adding hot deionised water untill the solution just became permanently cloudy. This saturated solution was then allowed to cool to room temperature thence placed in a freezer prior to isolation of the crystalline material by filtration. This material was dried under vacuum. Salts of the TPBCl anion were prepared in a similar manner ,initially substituting a 2:1 mixture of methanol and water as the solvent.

$[Ru(bpy)_3][Cl]_2$ was prepared by literature methods [101]. $[Ru(bpy)_3][SO_4]_2$ was prepared by metathesis from $[Ru(bpy)_3][BF_4]_2$ and $[TBA]_2SO_4$ in acetone. $[TBA]_2SO_4$ was in turn prepared by the neutralisation of TBAOH with H_2SO_4 followed by the removal of the water by heating under vacuum. $[Ru(bpy)_3][TPFB]_2$, which could only be recrystallised by slow evaporation from ethanol under vacuum, was prepared by metathesis from the chloride and an aqueous solution of LiTPFB.

$[Ru(bpy)_3]_2[SO_4]_3$ was prepared by chemical oxidation of $[Ru(bpy)_3]SO_4$. Chlorine gas, generated through the action of concentrated HCl on potassium permanganate was bubbled through a concentrated solution of $[Ru(bpy)_3]SO_4$ in 10% sulphuric acid. Once the blue colour characteristic of the Ru(III) species had developed, excess Na_2SO_4 was added and this solution transferred to a freezer and left overnight. This procedure afforded small greenish-blue crystals which were isolated by filtration and dried in *in vacuo*.

Viologen bromides were synthesised according to the following general scheme. 4,4-dipyridyl (1g) was dissolved in dimethylformamide (DMF) and a one and a half fold excess of the appropriate alkylbromide added. This solution was then refluxed for twenty hours and cooled to

room temperature. The resulting crystalline precipitate was then recrystallised from DMF. The TPFB$^-$ salts of viologens were prepared by metathesis from equimolar solutions of LiTPFB and the appropriate viologen bromide. The resulting precipitate was collected and recrystallised from an ethanol/water mixture.

All compounds synthesised gave satisfactory elemental analyses with the exception of LiTPFB , all other salts of the TPFB$^-$ ion gave excellent analyses. $[Ru(bpy)_3]_2[SO_4]_3$ was not submitted for elemental analyses, its identity being assured through UV-Vis. spectroscopy.

Chemicals Used.

BTPPACl (Aldrich 99%), TBABr (Aldrich 99%), KTPBCl (Lancaster Synthesis 99%), TBAOH (Aldrich 40% (aq)), H_2SO_4 (BDH Analar), $RuCl_3.3H_2O$ (Johnston Mathey), 2,2'-bipyridyl (Aldrich 99%), 4,4'-bipyridyl (Aldrich 99%), Dodecyl bromide (Aldrich 99%), Heptadecylbromide (Aldrich 99%), Bromopentafluorophenylbenzene (Aldrich 99%), Butyllithium 2.5M in hexanes (Aldrich), Boron Trichloride 1.0M in hexanes (Aldrich).

References.

100. A.G. Massey and A.J. Park, J. Organometal. Chem., 2(1964)245.
101. R.A. Palmer and T.S. Piper, Inorg. Chem., 5(1966)864.

Courses Attended.

Departmental Course in Scientific German.

Departmental Colloquia.

Physical Chemistry Thursday Evening Seminars.

Occasional Inorganic Chemistry Friday Meetings.

Physical Postgraduate Lectures 1989-91.

Spectroscopic Techniques, fourth year course by L.J.Yellowlees.

Butler Meetings 1989 and 1990.

University of Strathclyde Inorganic Chemistry Conferences 1989 and 1990.

Durham University Inoganic Exchange 1990.

Photochemical transfer of tetraaryl ions across the interface between two immiscible electrolyte solutions

Zdenek Samec *, Alan R. Brown, Lesley J. Yellowlees and Hubert H. Girault **

Department of Chemistry, University of Edinburgh, West Mains Road, Edinburgh EH9 3JJ, Scotland (Great Britain)

(Received 2 March 1990)

ABSTRACT

Illumination of solutions of tetraarylborate and tetraarylarsonium ions in 1,2-dichloroethane in contact with an aqueous electrolyte solution leads to the onset of a photocurrent at the interface between the two immiscible electrolyte solutions. These photocurrents have been attributed to ion transfer reactions. Analysis of the data shows that the transferring ion is an intermediate in the photochemical decomposition of the tetraarylborate/arsonium ions. The present communication demonstrates how measurement of photocurrents at liquid/liquid interfaces can be used to measure the lifetimes of intermediates in photochemical reactions.

INTRODUCTION

Photoinduced charge transfer involving an electron acceptor A and an electron donor D has attracted a great deal of interest as a basis for solar energy conversion [1]. Much attention has been focussed on the stabilisation of the product A^-D^+ in micelles [2], vesicles [3], microemulsions [4], zeolite cages [5] and by charge separation in thin film systems [6]. We have been interested in using the Interface between Two Immiscible Electrolyte Solutions (ITIES) for this purpose [7,8].

At the ITIES, the primary electrochemical step might be

$$D(o) + A(w) \xrightarrow{h\nu} D^+(o) + A^-(w) \tag{1}$$

where o and w represent the organic and aqueous electrolyte solutions. The rate of reaction (1) can be controlled by the electrical potential difference across the ITIES,

---

* SERC Visiting Fellow from J. Heyrovsky Institute of Physical Chemistry and Electrochemistry, Czechoslovak Academy of Sciences, Dolejškova 3, 18223 Prague 8, Czechoslovakia.
** To whom correspondence should be addressed.

which is applied from an external voltage source [9], or arises from the equilibrium partition of a suitable salt [10]. These techniques are known as electrolysis at the ITIES [11] and phase transfer catalysis [12], respectively.
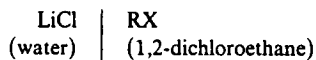
A related problem is obviously the photosensitivity of other components of the the electrolyte solutions, which may cause parallel photochemical or photoelectro-chemical processes. Notably, aromatic ions like tetraarylborates $[BR_4]^-$ or tetraaryl arsonium $[AsR_4]^+$ are often present in these types of systems. Their role is to ensure a good conductivity and the establishment of excess charge in the organic solvent phase.

We have shown that the irradiation of the ITIES in the presence of tetraphenyl-borate $[BPh_4]^-$ or tetraphenylarsonium $[AsPh_4]^+$ ions can give rise to a photocurrent, which is closely related to their excited states [13]. In the present study we are concerned with the mechanism and quantitative interpretation of the process. In particular, we shall discuss the possibility of photoion transfer across the ITIES,

$$S^\pm(o) \xrightarrow{h\nu} S^\pm(w) \qquad (2)$$

EXPERIMENTAL

Four types of systems were studied by cyclic voltammetry, absorption and emission spectroscopy and photocurrent transient measurements at a constant interfacial potential. These systems were:

$$\begin{array}{c|c} \text{LiCl} & \text{RX} \\ \text{(water)} & \text{(1,2-dichloroethane)} \end{array}$$

where RX = tetrabutylammonium tetraphenylborate (TBATPB), tetrabutylam-monium carboranebromide (TBACBB) (with $CBB^- = 7,8,9,10,11,12$-hexabromo-hexahydro-1-carba-closo-undecaborate$(1 -))$, tetrabutylammonium tetrakis(4-chlorophenyl) borate (TBATPBCl) and tetraphenylarsonium carboranebromide (TPAsCBB).

The system used for measuring the voltammetric and and photocurrent transients is shown in block form in Fig. 1. The interface between water and 1,2-dichloro-ethane (area 2.5 cm^2) was formed in an all-glass four-electrode cell with the organic solvent phase placed in its bottom part. The potential $E = \phi(Ag) - \phi(Ag')$ of the cell was controlled by means of a home built four electrode potentiostat [9] and a voltage ramp generator (Hitek PPR1, UK). The reference electrodes RE1 and RE2 were shielded against light by black PVC tubing [8]. The potential E will be expressed relative to the zero-charge potential E_{pzc}, which was determined by means of electrocapillary measurements [14,15]. Electrical current associated with the transfer of positive charge from the aqueous to the organic solvent phase is conventionally regarded as positive.

The light from a 150W xenon arc source (Applied Photophysics, Model 4060, UK) was reflected by a mirror at 45° and directed onto the cell; the top of which
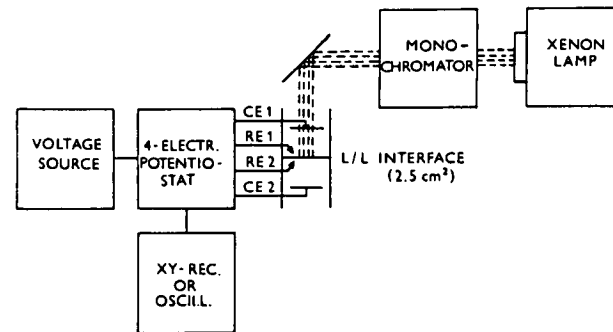

Fig. 1. Block scheme of apparatus.

was left open. Monochromatic light was obtained from a monochromator (Applied Photophysics) placed between the xenon lamp and the mirror. The incident intensity of the monochromatic light upon reflection by the mirror was measured by means of a calibrated photodiode detector (Macam Photometrics, model SD101UV, UK). Absorption spectra were measured on a UV–Vis–NIR spectrometer (Perkin Elmer, Lambda 9) and emission spectra on a luminescence spectrometer (Perkin Elmer, LS-5). Time resolved fluorescence measurements were carried out using a Nd : YAG (Spectron SL801) pumped dye laser (Quanta-Ray PDL-2) with frequency doubler (Quanta-Ray EWX-1c), combined with oscilloscope (Tektronix 2445A (150MHz)).

Reagent grade chemicals LiCl (BDH), tetrabutyl ammonium chloride (Fluka AG), tetraphenylarsonium chloride (Fluka AG) and 1,2-dichloroethane (BDH) were used as received. Water was deionised and doubly distilled. TBATPB, TBACBB, TBATPBCl and TPAsCBB were precipitated from TBACl and KTPBCl (Lancaster Synthesis), NaTPB (Aldrich) or CsCBB. The products were recrystallised from acetone or a water + acetone mixture. The TPAsCBB salt was prepared according to the procedure [16] by K. Base from the Institute of Inorganic Chemistry, Czechoslovak Academy of Science, and its generous gift is gratefully acknowledged.

All measurements were performed at ambient temperature (20 ± 2°C) with air saturated solutions, except where otherwise stated.

All the calculations, data fitting and graphic displays were carried out on the mainframe computer of the Edinburgh University Computing Service.

RESULTS

Cyclic voltammetry was used to measure dark currents corresponding to the charging of the ITIES and the transfer of the base electrolyte ions (Li$^+$, Cl$^-$, R$^+$, X$^-$). Since ion transfer rates are high and the apparent rate constants are all about 10^{-2} cm s^{-1} [17], the potential range available for the electrochemical polarisation
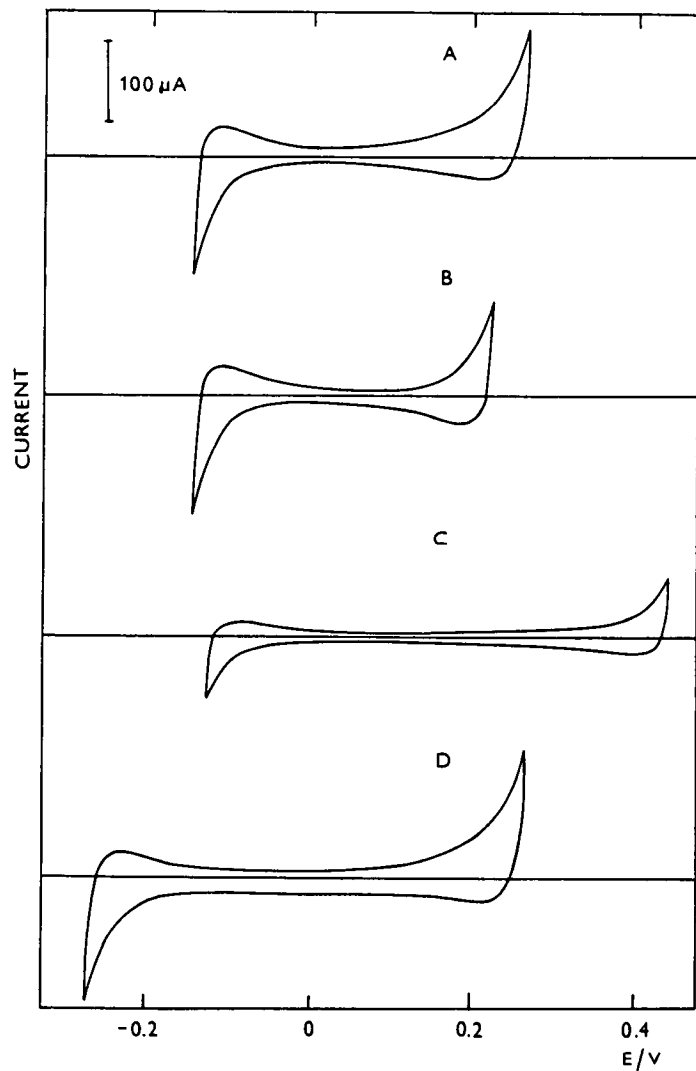
Fig. 2. Cyclic voltammograms of the interface between 0.01 M LiCl in water and 0.01 M TBACBB (A), 0.01 M TBATPB (B), 0.01 M TBATPBCl (C) or 0.01 M TPAsCBB (D) in 1,2-dichloroethane. Sweep rate: 0.1 V s^{-1}. Potential E relative to the potential of zero charge.
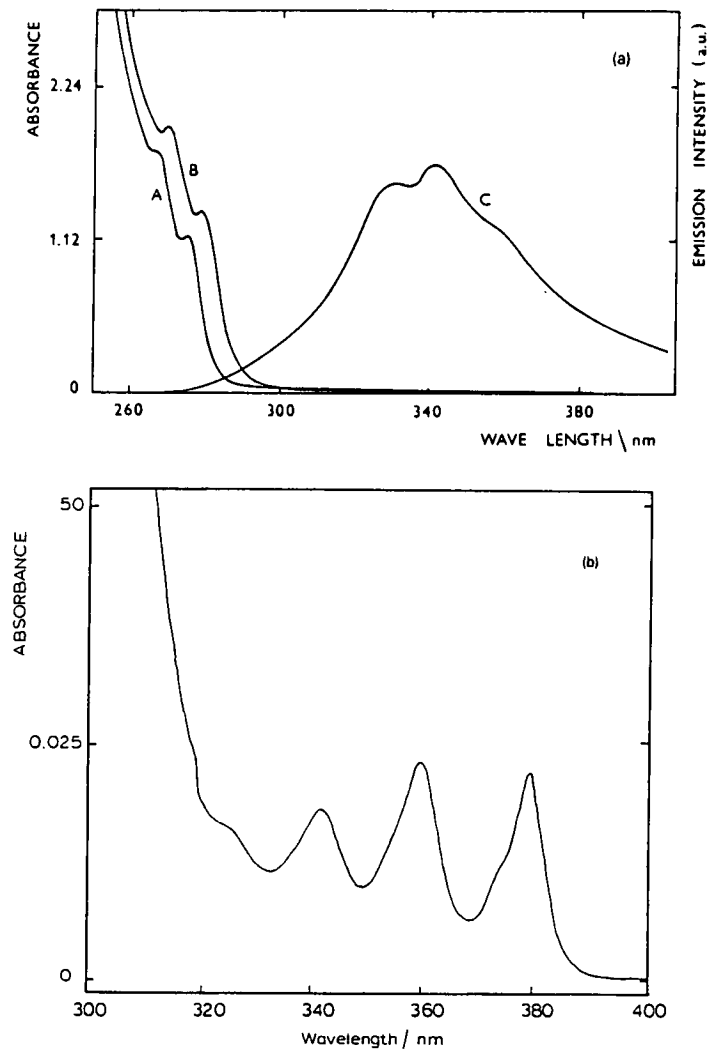

Fig. 3. (a) Absorption spectra of 5×10^{-4} M TBATPB (A) or TBATPBCl (B) in 1,2-dichloroethane and emission spectrum of 5×10^{-4} M TBATPB (C) at $\lambda = 270$ nm. Optical cell length = 1 cm. (b) Absorption spectrum of 8×10^{-4} M TBATPB in iodoethane.

of the ITIES depends mainly on the Gibbs transfer energies of the base electrolyte ions [11]. The change in the potential limits (Fig. 2) reflects the increasing hydrophobic character of the organic anions TPB⁻ < CBB⁻ < TPBCl⁻ or cations TBA⁺ < TPAs⁺.

Absorption and emission spectra of the tetraphenylborate ion are shown in Fig. 3. Both tetraphenylborate and tetraphenylarsonium ions absorb strongly in the UV region. The intense absorption bands clearly arise from symmetry and spin allowed transitions, namely $S_n \leftarrow S_0$ (ground state to a singlet excited state). Excitation to a state S_n may be followed by either internal conversion to a lower energy singlet state or intersystem crossing to a triplet state, e.g. T_1. Return to the ground state from the singlet state may or may not be forbidden on symmetry grounds and $T_1 \rightarrow S_0$ will be forbidden on the grounds of spin multiplicity. The position of the triplet state of the the TPB⁻ ion was determined from absorption measurements in iodoethane where
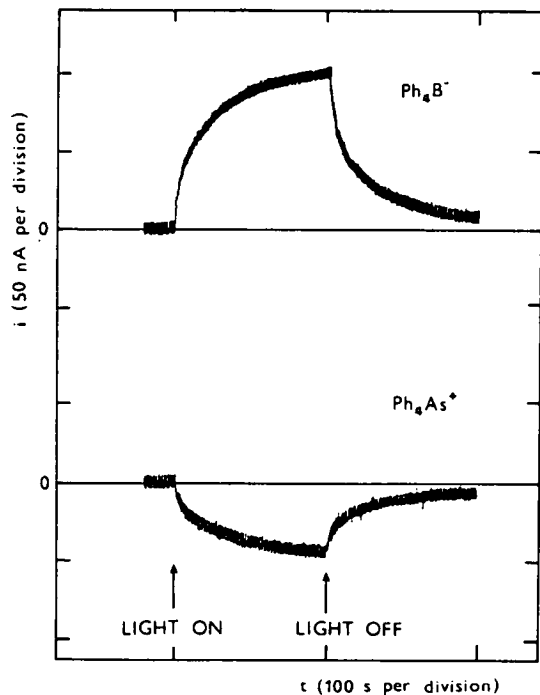

Fig. 4. Photocurrent transients for the interface between 0.01 M LiCl in water and 0.01 M TBATPB ($E = 0$ V) or 0.01 M TPAsCBB ($E = -0.1$ V) in 1,2-dichloroethane irradiated by monochromatic light at $\lambda = 270$ nm.
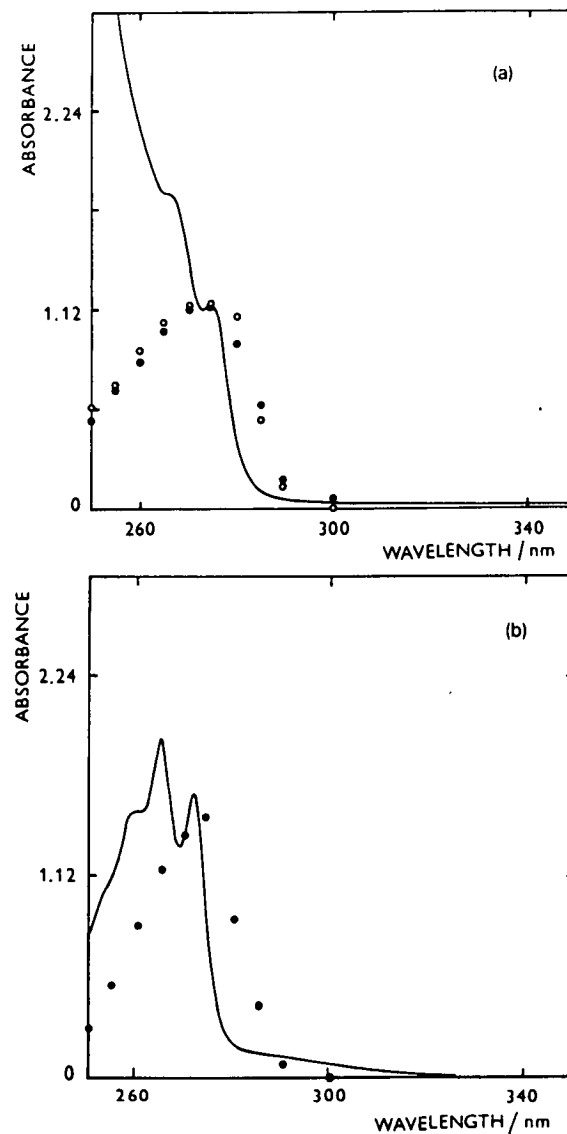

Fig. 5. Action spectra (○, ●) for TPB⁻ (a) and TPAs⁺ (b) showing the variation of the limiting photocurrent (in arbitrary units) with wavelength of the incident light at the interface between 0.01 M LiCl in water and 0.01 M TBATPB or TPAsCBB in 1,2-dichloroethane, bandwidth: 14 mm (●), 7 mm (○). Full lines: absorbance in the solution of 5×10^{-4} M TBATPB or TPAsCBB in 1,2-dichloroethane. Optical cell length = 1 cm.

the external heavy atom effect [18] allows direct population of T_1 from S_0. Figure 3b shows the $T_1 \leftarrow S_0$ transition at 378.5 nm. The shorter wavelength bands correspond to transitions to higher vibrational levels within the T_1 manifold.

Laser spectroscopy at $\lambda = 270$–280 nm was used to estimate the lifetimes of the singlet excited states of tetraaryl borates from the fluorescence point to the population of a short-lived excited state S_1 ($\tau < 10$ ns) at such energies of excitation. Attempts to measure directly the lifetime of the triplet excited state of the TPB^- ion by means of laser flash photolysis techniques have been unsuccessful because triplet–triplet transitions were not observed. Since tetraphenylmethane, which is isoelectronic with TPB^-, behaves spectroscopically as four independent benzene rings [19] this result is not unexpected as the first triplet–triplet transition of benzene is obscured by the first singlet–singlet transition [20].

The irradiation of the ITIES results in a slow rise-time photocurrent, which is demonstrated in Fig. 4. An absorbing anion (TPB^-, $TPBCl^-$) or cation ($TPAs^+$) gives rise to a positive or negative photocurrent respectively. No photocurrent was detected, however, for non-absorbing TBA^+ and CBB^- ions. In either case a limiting value is reached in about 2 min.

Four features should be noted:

(i) Action spectra for TPB^- or $TPAs^+$ ions showing the variation of the limiting photocurrent with the wavelength of the incident light follow the $S_1 \leftarrow S_0$ transition
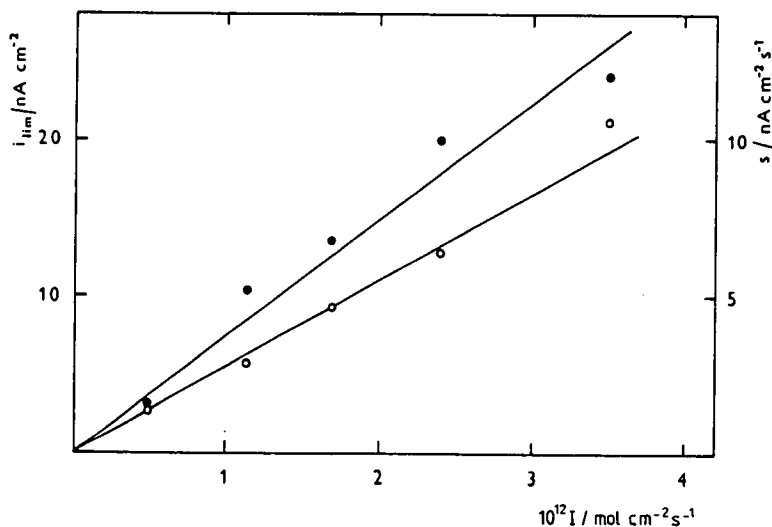

Fig. 7. Variation of the initial slope s of photocurrent transients with potential E for the interface between 0.01 M LiCl and 0.01 M TBATPB ($\bullet$), 0.01 M TBATPBCl (o) or 0.01 M TPAsCBB ($\square$) irradiated by the white light from the Xe lamp.

(Fig. 5). The action spectrum is red-shifted, a feature which may be due to the specific adsorption of these ions at the ITIES.

(ii) At a constant irradiation wavelength both the initial slope $s = (i/t)$ and the limiting current i_{lim} are proportional to the light intensity I (Fig. 6).

(iii) When the potential difference across the ITIES is changed, the slope s increases exponentially and reaches a limit at extreme positive or negative potentials for organic anions or cations, respectively (Fig. 7). In contrast, the limiting current is practically independant of the applied potential (Fig. 8).

(iv) Both s and i_{lim} increase with increasing concentration of absorbing ion (Fig. 9), but in the latter case a non-linear relationship was found (Fig. 9b). In addition the photocurrent for TPB^- anion did not change when the concentration of the aqueous supporting electrolyte, LiCl, was increased to 0.1 mol dm^{-3}, or LiCl was replaced by HCl, or when argon was bubbled through both phases to remove the oxygen prior to measurements.

Fig. 6. Limiting photocurrent i_{lim} ($\bullet$) and the initial slope s (o) of the transient is the monochromatic light intensity I at $\lambda = 270$ nm and $E = 0$ V, for the interface between 0.01 M LiCl in water and 0.01 M TBATPB in 1,2-dichloroethane.
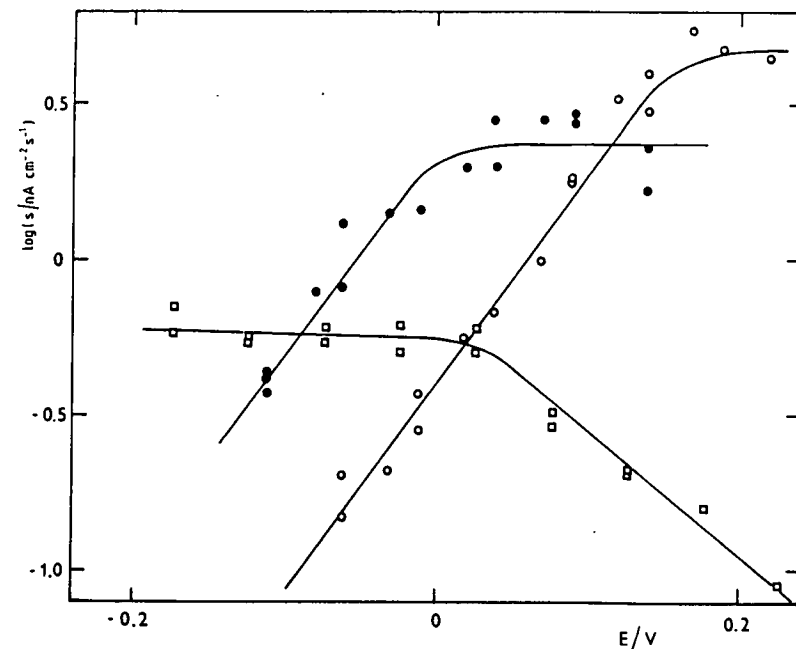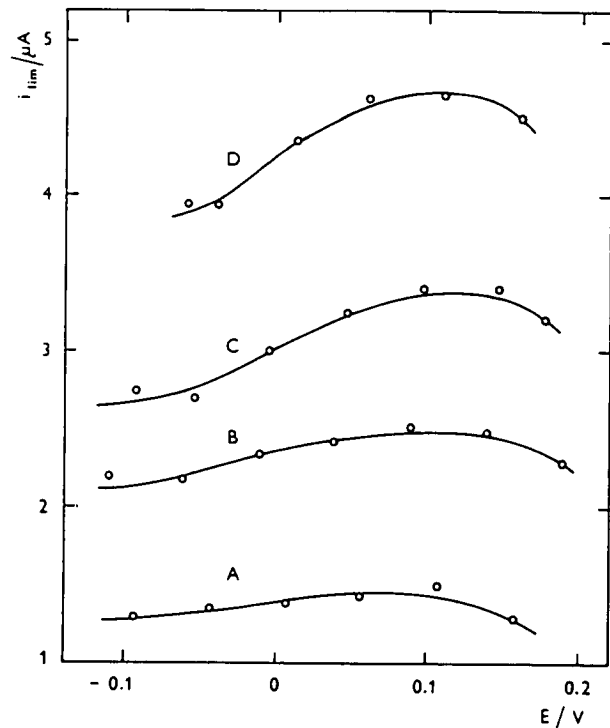
Fig. 8. Variation of the limiting photocurrent i_{lim} with the potential E for the interface between 0.01 M LiCl in water and 0.002 M (A), 0.01 M (B), 0.02 M (C) or 0.05 (D) TBATPB in 1,2-dichloroethane, irradiated by the white light from the Xe lamp.

DISCUSSION

The observed photocurrent corresponds to the slow transfer of an ionic species, from the organic to the aqueous phase, carrying the same charge as the absorbing species. The simplest mechanism to explain the photocurrent would assume the formation of the excited state of the ion followed by the transfer of that excited ion across the ITIES. The geometry and electronic density distribution of the excited ion might well be distorted relative to the corresponding ground state ion. This would result in the excited ion being more polar and indeed more polarisable than the ground state ion and therefore more hydrophilic. The fast decay $S_1 \rightarrow S_0$ probably does not permit transport of ions in S_1 across the interface. Although there
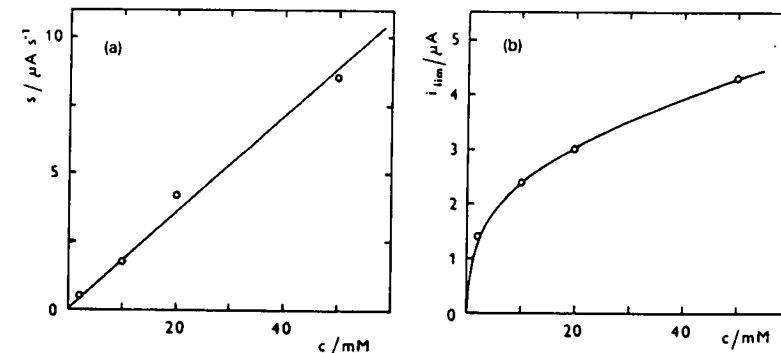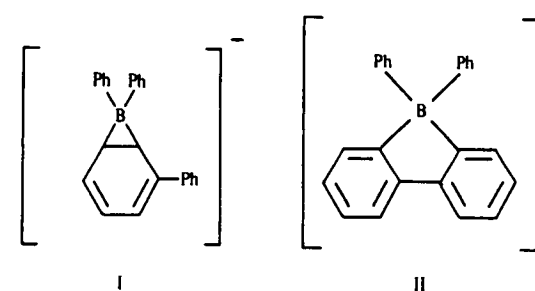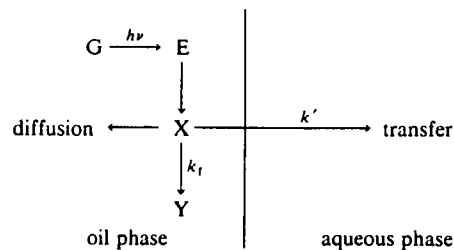

Fig. 9. Variation of the initial slope s (a) and the limiting photocurrent i_{lim} (b) with the concentration of TBATPB in 1,2-dichloroethane. Aqueous phase: 0.01 M LiCl. Irradiation by the white light from the Xe lamp.

is no information on the lifetime of the T_1 excited state of these ions, it is not inconceivable that they could be as long as several hundred nanoseconds. If the diffusion coefficient of TPB$^-$ is 5×10^{-6} cm^2 s^{-1} in either phase, then the average pathlength is about 15 nm, which is more than sufficient to cross the liquid/liquid interface, proposed to consist of a mixed solvent layer not exceeding $= 1$ nm [11].

We need also to consider another transferring ion with the same charge as the absorbing ion which could result from a photochemical reaction yielding a species more hydrophilic than the parent ion. In the case of the TPB$^-$ ion, the formation of a stable bridged borate(I) has been indicated by NMR spectroscopy [21] and Williams et al. [22] have suggested (II) as a likely intermediate in the photolysis of this ion. It can be seen from the structures of species(I) and (II) that the high symmetry of the TPB$^-$ ion has been lost. In the presence of dioxygen, species (I) reacts to give final products biphenyl and Ph$_2$BO$^-$ and consequently a polar ion is formed. The analyses of the photoproducts of TPAs$^+$ and TPBCl$^-$ have not been investigated but the photochemical properties of these ions may be similar.

On the basis of these arguments. we propose the following reaction scheme for the observed photocurrents.

$$G \xrightarrow{h\nu} E$$

$$\text{diffusion} \longleftarrow X \xrightarrow{k'} \text{transfer}$$

$$\downarrow k_f$$

$$Y$$

oil phase | aqueous phase

Where G represents the ground state ion. E the primary excited state, X the transferring species i.e. triplet state ion or photochemical intermediate, Y the final photoproduct and k' the heterogeneous transfer rate constant for X.

In this model the concentrations c_G, c_E, and c_X of the respective species are governed by the following equations.
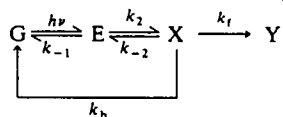
$$c_G(x, t) = G_0 = \text{constant} \tag{3}$$

$$c_E(x, t) = A \exp(-ax) \tag{4}$$

$$\frac{\partial c_X(x, t)}{\partial t} = D \frac{\partial^2 c_X(x, t)}{\partial x^2} + A \exp(-ax) - k c_X(x, t) \tag{5}$$

where x is the distance from the interface, A is the pre-exponential factor stemming from the Beer–Lambert law given by $\phi \epsilon G_0 I$ with ϕ being the quantum efficiency for the generation of E, I is the incident light intensity at the interface, ϵ is the extinction coefficient of G, and k is the decay rate constant for X.

The constant a in eqn. (5) is also derived from the Beer–Lambert Law and is given by ln $10\epsilon G_0$. By assuming a steady state concentration of the primary excited state E in the photochemical process

$$G \underset{k_{-1}}{\overset{h\nu}{\rightleftharpoons}} E \underset{k_{-2}}{\overset{k_2}{\rightleftharpoons}} X \xrightarrow{k_f} Y$$

$$\underset{k_b}{\underbrace{\qquad\qquad}}$$

then the quantum efficiency ϕ and the decay rate constant k are given by $k_2/(k_2 + k_{-1})$ and $k_f + k_b + k_{-1}k_{-2}/(k_{-1} + k_2)$ respectively.

Equation (5) can also be solved as described in the Appendix. The resulting expression for the photocurrent density is given in eqn. (6).

$$I_{(t)} = \frac{nFADk'}{k' - Da} \Big[-(a/B)\big[1 - \exp(-Bt) \, \mathrm{erfc}\big(a(Dt)^{1/2}\big)\big]$$

$$- (k'/CD)\big[1 - \exp(Ct) \, \mathrm{erfc}\big(k'(t/D)^{1/2}\big)\big]$$

$$+ (k/D)^{1/2}[B^{-1} + C^{-1}] \, \mathrm{erf}(kt)^{1/2}\Big] \tag{6}$$

where B is equal to $k - Da^2$ and C is equal to $(k'^2/D) - k$.
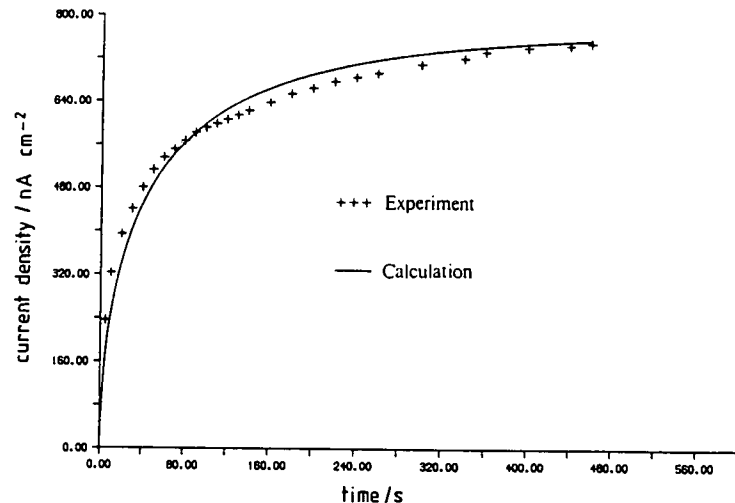

Fig. 10. Photocurrent–time transients for 9.94 mM TBATPB.

In eqn. (6), n is the stoichiometric charge of G and F is the Faraday constant. The important features of eqn. (6) are the slope, s, at the origin, given in equation (7) and the plateau current density, $i_{\lim}$, given in eqn. (8).

$$s = nFAk' \tag{7}$$

$$i_{\lim} = nFAk' / \big[(a + (k/D)^{1/2}\big(k' + (kD)^{1/2}\big)\big] \tag{8}$$

Equation (7) implies that the slope, s, is proportional to the light intensity, I_0, and the concentration of G. Both these relationships are corroborated by experiment, see Figs. 6 and 9. Moreover the limiting current is also proportional to the light intensity, see Fig. 6, but not to the concentration of G since parameters A and a are both proportional to the concentration. Equations (6), (7) and (8) have been used to optimise the experimental parameters of the proposed scheme. The initial slope s in Fig. 6 gives a heterogeneous rate constant k' of 1.4×10^{-3} cm s^{-1}, assuming the quantum yield to be unity. Subsequent optimisation allowed us to derive values of 5×10^{-3} cm s^{-1}, 3.5×10^{-3} s^{-1} and 0.22 for k', k and ϕ. Figure 10 demonstrates the closeness of fit between experimental data and the curve calculated using these values in eqn. (6). The quantum yield derived is in good agreement with literature data for the TPB$^-$ system in water where the quantum yield for the final photoproducts is 0.2 [22]. The value of the heterogeneous rate constant is reasonable for a slow charge transfer reaction at an ITIES exhibiting Butler–Volmer behaviour [11,17].
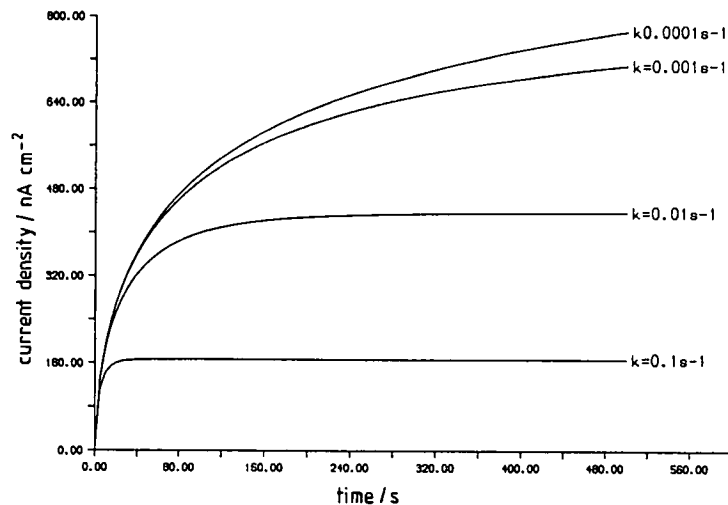
Fig. 11. Variation of photocurrent–time transient with k. $k' = 0.005$ cm s^{-1}.

Fig. 12. Variation of photocurrent–time transient with k'. $k = 3.5 \times 10^{-3}$ s^{-1}.

It can be seen from Fig. 11 that the time taken for the photocurrent to reach a steady state value depends on k but is independent of the ion transfer rate constant, k' (Fig. 12).

The theoretical model suggests that the observed photocurrent cannot be accounted for in terms of triplet state ion transfer as the maximum lifetime of collisionally quenched species in solution will not exceed the millisecond timescale which leads to a value of at least 10^3 s^{-1} for k. Fast decay of E to G observed by laser spectroscopy ($k = 10^8$ s^{-1}) and the value of the quantum yield derived imply that while the conversion of E to X is also fast, i.e. $k_2 = 3 \times 10^7$ s^{-1}, one of the decay processes X → E, X → G or X → Y must be rather slow as $k = k_f + k_b + 0.8k_{-2} = 3.5 \times 10^{-3}$ s^{-1}. We can conclude therefore that the photocurrents observed stem from the transfer of a long lived intermediate which may take the form of species (I) or (II). The model also shows that the photocurrent is not due to the transfer of the final photoproduct as in the work of Kuzmin and co-workers [23,24]. Indeed photoproduct transfer would be equivalent in our model to having $k = 0$ and therefore the plateau current equal to nFA/a.

The differential equation (6) used in the present work is rather similar to that describing the photosensitization of titanium(IV) oxide with tris(2,2′-bipyridine) ruthenium(II) as described by Hamnett et al. [25,26]. In that case however the mass transport involved is that of a triplet state ion and not an ionic intermediate of a photoreaction.
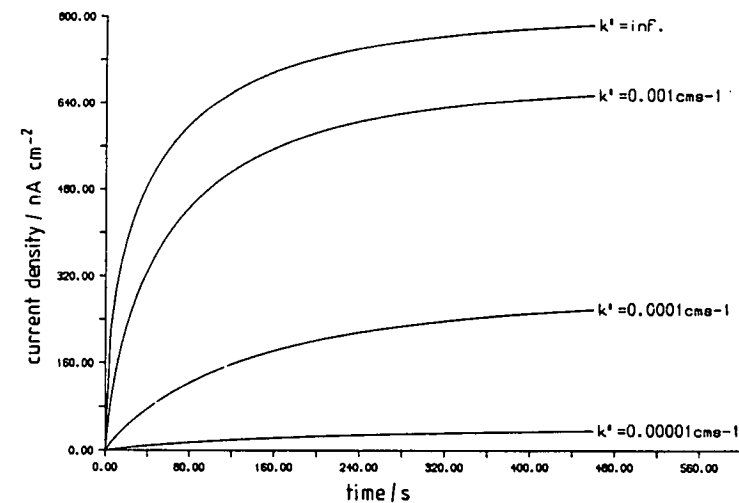
CONCLUSIONS

The present work shows that the electrochemical measurement of photocurrents generated by the transfer of ionic intermediates across the ITIES may be used to measure the lifetime of these intermediates. The method described here can then be used for the kinetic study of photochemical processes in which changes of solvation energy are induced.

It can also be concluded from this work that care must be taken in the selection of supporting electrolyte and counter-ions in systems containing an oil–water interface, for instance the simple liquid/liquid interface and also microemulsion and vesicle systems, when these systems are to be employed in photochemical studies. Clearly the ions chosen for these tasks should not themselves be photochemically active under the conditions used.

This study extends the range of photochemical processes which may be studied in heterogeneous media, and points the way towards the study of ion transfer kinetics at constant interfacial potential by photogeneration of ions in this region, a process stepping beyond the limitations imposed by the charging of the double layer encountered in potential step experiments. This technique would be equivalent to photoinduced chronoamperometry, a new technique which will be presented at a later stage.

The ion selective electrode field is another for which our results with the tetraphenylborate anion have important implications. TPB$^-$ is often used as a

hydrophobic counter ion to solubilize in a PVC membrane, the cationic species to which the electrode is responsive. It can be inferred from the present investigation that UV irradiation will cause the borate anion to transfer from the polymer membrane to the adjacent aqueous phase, which will, in turn, lead to a decrease in the concentration of the target cationic species and therefore to a deterioration of the ion selective electrode performance.

APPENDIX

Equation (5) can be solved by use of the Laplace transform with the following boundary condition

$$I = nFD\left(\frac{\partial c_X}{\partial x}\right)_{x=0} = nFk'c_X(0, t) \tag{A1}$$

$$\lim_{x \to \infty} c_X(x, t) = c_X(x, 0) = 0 \tag{A2}$$

The distance dependance for the Laplace transform for time is then given by

$$\bar{c}_X(x, u) = \frac{A}{u(u+B)} \exp(-ax) - \frac{A(k' + Da)\exp\left(-x\sqrt{\frac{u+k}{D}}\right)}{u(u+B)\left[k' + (D(u+k))^{1/2}\right]} \tag{A3}$$

The Laplace transform for the current density, $\bar{I}$, is obtained from

$$\bar{I}_{(u)} = nFD\left(\frac{\partial \bar{c}_X}{\partial x}\right)_{x=0} = \frac{-nFAD}{u(u+B)}\left[a - \frac{Da + k'}{k' + (D(u+k))^{1/2}}\left(\frac{u+k}{D}\right)^{1/2}\right] \tag{A4}$$

Using the following identity (26)

$$L^{-1}\left[1/\left((a + (p+k)^{1/2})(p+c)\right)\right]$$

$$= \frac{1}{a^2 + c - k}\left[a\exp(-ct) - (k-c)^{1/2}\exp(-ct)\,\text{erf}\left[(k-c)t\right]^{1/2}\right.$$

$$\left. - a\exp(-kt + a^2 t)\,\text{erfc}\left(a(t)^{1/2}\right)\right] \tag{A5}$$

the current density can be obtained by deconvolution of eqn. (A4). The result is given by eqn. (6).

ACKNOWLEDGEMENTS

REFERENCES

1 J.R. Bolton, Science, 202 (1978) 105.
2 S.A. Alkaitis, G. Beck and M. Gratzel, J. Am. Chem. Soc., 97 (1975) 5723.
3 W.E. Ford, J.W. Otvos and M. Calvin, Nature (London), 274 (1978) 507.
4 (a) C.E. Jones, C.A. Jones and R.A. Mackay, J. Phys. Chem., 83 (1979) 805. (b) I. Wilner, W.E. Ford, J.W. Otvos and M. Calvin, Nature (London), 280 (1979) 823.
5 P.K. Dutla and J.A. Incavo, J. Phys. Chem., 92 (1987) 4443.
6 C.L. Renschler and L.R. Faulkner, Faraday Discuss. Chem. Soc., 70 (1980) 311.
7 F.L. Thomson, L.J. Yellowlees and H.H. Girault, J. Chem. Soc., (1988) 1547.
8 V. Marecek, A.H. De Armond and M.K. De Armond, J. Am. Chem. Soc., 111 (1989) 2561.
9 Z. Samec, V. Marecek and J. Weber, J. Electroanal. Chem., 100 (1979) 841.
10 V.J. Cunane, D.J. Schiffrin, C. Beltran, G. Geblewicz and T. Solomon, J. Electroanal. Chem., 247 (1988) 203.
11 H.H. Girault and D.J. Schiffrin in A.J. Bard (Ed.), Electroanalytical Chemistry, Vol. 15, Marcel Dekker, New York, 1989, p. 1.
12 C.M. Starks and C. Liotta, Phase Transfer Catalysis Principles and Techniques, Academic Press, New York, 1978.
13 Z. Samec, A.R. Brown, L.Y. Yellowlees, H.H. Girault and K. Base, J. Electroanal. Chem., 259 (1989), 309.
14 Z. Samec, V. Marecek, K. Holub, S. Racinsky and P. Hajkova, J. Electroanal. Chem., 225 (1987) 65.
15 H.H. Girault and D.J. Schiffrin, J. Electroanal. Chem., 195 (1985) 213.
16 T. Jelinek, J. Plesek, S. Hermanek and B. Stilber, Collect. Czech., Chem. Commun., 51 (1986), 819.
17 Z. Samec and V. Marecek, J. Electroanal. Chem., 200 (1986) 17.
18 M. Kasha, J. Chem. Phys., 20 (1952) 71.
19 I. Novak and A. Potts, J. Organomet. Chem., 262 (1984) 17.
20 T.S. Godfrey and G. Porter, Trans. Faraday Soc., 62 (1966) 7.
21 J.D. Wilkey and G.B. Schuster, Org. Chem., 52 (1987) 2117.
22 J.L.R. Williams, J.C. Doty, P.J. Girsdale, R. Searle, T.H. Regan, G.P. Happ and D.P. Maier, J. Am. Chem. Soc., 89 (1967) 5153.
23 N.K. Zaitsev, N.I. Kulakov and M.G. Kuzmin, Elektrokhimiya, 21 (1985) 1293.
24 N.K. Zaitsev, O.F. Gorelik, N.A. Kotov, V.L. Shapovalov and M.G. Kuzmin, Elektrokhimiya, 24 (1988) 1346.
25 A. Hamnett, M.P. Dare-Edwards, R.D. Wright, K.R. Seddon and J.B. Goodenough, J. Phys. Chem., 83 (1979) 3280.
26 J. Brocas, R. Dewitt and A. Kirsch-de-Mesmaeker, J. Phys. Chem., 86 (1982) 3492.
27 K. Holub, private communication, 1989.